ABSTRACT

Title of Dissertation: BILAYER MEMBRANE ELECTROSTATICS AND CHARGE-REGULATED MEMBRANE-NANOPARTICLE INTERACTIONS

Shayandev Sinha

Dissertation directed by: Dr. Siddhartha Das
Department of Mechanical Engineering

Nanoparticle (NP) driven targeted drug delivery and NP driven imaging of cells, tumors etc. have been one of the most investigated areas in interfacial and biomedical engineering in recent years involving a massive amount interdisciplinary efforts cutting across disciplines like physics, chemistry, material science, biology, pharmaceutics, and engineering. Drug delivery or imaging with the NPs invariably require the NPs to first adhere to the surface of a cell, which is bound by a cell membrane (also known as plasma membrane or PM). All of these processes occur in an electrolyte medium as the fluids present inside and outside the cell have ions inside them. There have been significant amount of studies on adhesion of nanoparticles but until today, there has been very less number of investigations on the role of the ionic environment on such systems of adhesion. The ions present in the intracellular and the extracellular space produce an electric double layer (EDL) on both sides of the PM. The PM is also a semipermeable membrane i.e it does not let all kinds of ions to pass through it. The moieties that it lets to pass through it is completely dependent on the ion channels present across it and such semi-permeable action dictates the ion distribution around the PM, which in turn would regulate the NP-PM interactions.

The main aim of this dissertation is to look into the influence of this ionic environment and the role that it can play on adhesion of NPs. In order to look deeply we first look into the electrostatics of the PMs. We develop a continuum model to investigate the role of the ionic environment or the EDL on the electrostatics present across the membrane. This investigation led us to a very important aspect of membrane electrostatics. We found out charge-inversion (CI) like characteristics on the cytosol side (fluids present inside the cell) of the membrane. There has been no previous reports of such CI like characteristics in either the PM electrostatics or more importantly, in a system consisting of only monovalent electrolyte ions (as is the case we consider). In the next step, we looked into the role of the the surface charge density of the membrane and the concentration of the ions in influencing this PM electrostatics. This led to more interesting results. We found out that for biologically relevant conditions and for standard membrane surface charges, there is a possibility of having the location of CI on the surface of the membrane itself. This is a most remarkable result establishing a positive zeta potential on the surface of the negatively charged PM and we explored the phase-space where such situation of opposite signs of membrane zeta potential and membrane surface charge persists.

This electrostatics definitely influences various measurable properties of the membrane. One such very important measurable property of a membrane is the membrane capacitance. It has been widely reported that the ionic environment does not influence the capacitance much. However, with exploration of this phase-space through our continuum simulations we were able to pinpoint a domain where the capacitance can be influenced by as much as 15%. This also stems from the fact that the electrostatics of the system is itself very interesting to study under various conditions.

We then move on to explore the effect of this electrostatics on the adhesion of NP on

the membranes. Most of these adhesive processes occur through the receptor-ligand (R-L) mechanism. Therefore, until and unless a ligand is able to physically influence a receptor and can get bonded to it, the process of adhesion will never begin. The electrostatics can cause a hindrance to this phenomenon. The main reason is the electrostatic osmotic or disjoining pressure, which causes a repulsion between the ligand-bearing NP and the receptor-bearing cell membrane, and forbids the NP to come to significant proximity of the PM for ensuring that the ligands start to interact with the receptors. Through our analysis, we calculated such repulsion and calculated the distance up to which this repulsion remains strong and can overcome the influence of other attractive effects (e.g., van der Waals forces or thermal forces) that drive the NP closer to the PM. We hypothesize that if the length of the ligand-receptor complex is not larger than this distance up to which the electrostatic repulsion effects remain dominant then the process of adhesion will not even begin.

Next, we study what is the role of this ionic environment for the case where the NP adhere to the PMs non-specifically. Such non-specific adhesion (NSA) refers to the adhesion of the NP to the PM by actual physical attachment without involving R-L interactions. Understanding such NSA is vital to gauge the side effects of the NP-based drug delivery – the dug carrying NP will invariably adhere (non-specifically) to the healthy cells causing damages to the healthy cells. Therefore the current practice necessitates uses of those NPs that demonstrate least cytotoxicity post adhesion and internalization in healthy cells. We show that when metallic NPs non-specifically adhere to the PMs, the resulting destruction of the surface charge effects of PMs would lead to a favorable energy change, which in turn drives the NP NSA to even stiffer membranes (e.g., cell membranes rich in cholesterol).

Subsequently, we show that one can use biomimetic NPs (namely NPs encapsulated in PM-derived lipid bilayers) to ensure that electrostatic interactions between the biomimetic NPs and the PM can usher in the most coveted scenario where one can simultaneously ensure the promotion of specific adhesion and prevention of NSA.

Finally we address the future directions of this work and how this work can start the discussion about the role of other kinds on nanoparticles in drug delivery and therapy.

BILAYER MEMBRANE ELECTROSTATICS AND CHARGE-REGULATED MEMBRANE-NANOPARTICLE INTERACTIONS

by

Shayandev Sinha

Dissertation submitted to the Faculty of the Graduate School of the
University of Maryland, College Park in partial fulfillment
of the requirements for the degree of
Doctor of Philosophy
2018

Advisory Committee:
Assistant Professor Siddhartha Das, Chair/Advisor
Associate Professor Amir Riaz
Assistant Professor Ryan Sochol
Professor Abhijit Dasgupta
Associate Professor Liangbing Hu, Dean's Representative

Table of Contents

List of Tables

List of Figures

Chapter 1: Introduction

In this chapter, brief descriptions are first provided to introduce the fundamental problem on membrane nanoparticle adhesion systems. It discusses the scope and directions of the thesis. A breakup of the thesis is also provided.

Every living cell is covered by a membrane called the plasma membrane. Even inside the cell there are many cell organelles that remain covered by the plasma membrane. Thus plasma membrane is present everywhere in this living world in both plants and animals. The structure of a plasma membrane is very interesting. It is composed of two lipid layers that are sandwiched with on another. The lipid molecules have hydrophobic and hydrophilic tails. The hydrophilic tails points outwards as the plasma membrane survives in a liquid medium which contains a huge amount of water. The hydrophobic ends are present and the ends of each layer face one another. There are theories suggesting that is it a self assembled layer.

Proteins are an integral part of the plasma membrane. They are present on both sides of the lipid bilayer. On the outer side there are a series of proteins that mainly functions and facilitates the entry and exit of various particles and ions through the membrane. There are also some proteins that help the cell in chemotaxis, environment sensing etc. There are another set of proteins present inside the plasma membrane. These helps the membrane to hold itself by their attachment to microtubules. There are also

some proteins that go through the bilayer itself. These are called transmembrane proteins. Many such transmembrane systems function as ion channels and channels for transport of other entities through the cell.

These thesis mainly focuses on the bilayer itself and its surface charges. The lipid tails are charged and overall they represent a surface charge on its structure. We are mainly concerned with those proteins on the lipid bilayer which act as receptors that facilitate the whole process of endocytosis. These receptors always remain on the external side of the plasma membrane. Various entities are allowed access inside the cell by these proteins. Particularly for the case of nanoparticles (NPs), these receptors bind to the ligands present on the surface of the NPs. This triggers the whole adhesion between the NP and the cell. The process described above is the classical picture of adhesion on NPs and in this thesis we mention it as specific adhesion.

Adhesion might even happen without ligand receptor binding. In that case the surface interactions of the NP and the lipid bilayer itself effects the adhesion. This kind of adhesion has been deeply addressed in this thesis and has been mentioned as non-specific adhesion (NSA). NSA is the typical cause for unwanted entry of NPs into various cells as there is no receptor-ligand (R-L) binding happening to facilitate the process. In nanoparticle driven drug delivery this is the one of the main cause of entry of nanoparticles even to healthy cells inside a tissue that are present around the diseased cells. While treating the disease even the healthy cells get affected by the drugs released by the nanoparticles. This leads to toxicity inside the healthy cells known as cytotoxicity. One of the greatest bottlenecks of nanoparticle driven drug delivery is this cytotoxicity that kills the healthy cells too.

1.1 Aim and scope of the thesis

There has been a significant amount of theoretical studies on the mechanics of NP adhesion on cell membranes. a good amount of literature has been cited in all the subsequent chapters. All of them deeply focused on membrane deformation, bending and the ligand-receptor interactions as the main factors for NP adhesion. None of those theories incorporates the role of the ionic environment around the membrane itself.

Cells cannot survive without an ionic environment either in-vitro or in-vivo. SO every such NP adhesion or other kind of adhesion always happens inside an liquid medium which has a huge concentration of ions mainly due to the various kind of salts present both outside and inside the cell. The plasma membrane is known to be semi-permeable. It allows only certain kinds of ions and entities to pass through it and enter the cell. Thus this creates a change in the ionic concentration of the fluid around itself.

This thesis tries to investigate the role of this ionic environment around the cell membrane on the process of NP adhesion. It significantly focuses on modeling this ionic environment and its role on NP adhesion. The surface charges on the lipid bilayer leads to the formation of an Electric Double Layer (EDL) around it self. We carefully consider the structure of this EDL in our calculations. We find the electrostatic potential of this EDL in various configurations of the lipid bilayer. We then calculate osmotic pressure due to this EDL on the bilayer and on the NPs. This has lead us to understand the effects of this EDL on the process of adhesion which is very significant.

Many chapters consider a 1-D NP. The literature is full of articles that consider spherical NPs for various calculations. But it is now known from very recent literature (2015 onwards) that 1D NPs show better binding and better yield in adhesion and NP

driven drug delivery than spherical NPs. Thus we wanted to explore the effects of such 1-D disc like NPs in this thesis. Before us there has been only one study of another kind of 1-D nanoparticle- a cylindrical NP adhesion on cell membrane.

1.2 Structure and organization of the thesis

In Chapter 2 we first try to understand the structure and the electrostatic potential of EDL around the membrane. We try to understand how would these potential distribution look like in two conditions of permeability of ions. We get distinctly different potential distributions for fully permeable and semi permeable conditions of the lipid bilayer. The main parameters in the problem are the surface charge of the bilayer and the concentration of the salt in the ionic environment. We discover a very interesting behavior in the system called *Charge Inversion*. Then we explore the location of this charge inversion- that is where does the potential distribution flips signs. We were able to find out a phase space where this inversion happens on the lipid bilayer itself.

In Chapter 3 we explore the possibility of these phenomenon on the capacitance of the membrane. Typically experimentalists measure the membrane capacitance and by using capacitance correlations back calculate the membrane surface charges and other properties. This stems from the fact that the capacitance of the EDL on both sides of the lipid bilayer are in series with the membrane itself and the contributions of the EDL capacitance is very less on the capacitance of the system. But if one carefully takes into account the EDL distribution this is not the case. The capacitances of the EDL on both sides of the membrane have significant contributions to the overall capacitance of the system. What they do specifically is that they decrease the overall capacitance of the

system. We provide a phase space of where this EDL effects can show a 20 % decrease in the overall capacitance measurement when compared to the capacitance of the membrane.

Chapter 4 deals with the problem of attraction of a gold NP towards a lipid bilayer. Due the EDL distribution each particle inserts a pressure on the system which is electrostatic in nature. The EDL exhibits a negative potential on the NP surface. The membrane is itself negatively charged. Thus there is an electrostatic repulsion between them. When it comes very close then it also feels a van der Waal's attraction to the membrane. Thermal fluctuations of such a nanoscale system are present throughout the system. We try to understand the role of these counteracting forces on the NP adhesion process. We define a non-dimensional parameter that is the ratio of these repulsive and attractive forces. Where this ratio becomes 1, we call that a favorable condition for adhesion. With this we have been able to detect a length scale of the adhesion process- that is if the NP can come within this distance then only adhesion will be feasible. The NP has to physically be in this distance in order to initiate R-L binding. Thus the length of the R-L complex is also important. If the R-L complex is shorter than this critical length adhesion will not be feasible.

There is a parameter space in chapter 4 that shows that their will be cases when there will only be attraction between the NP and the lipid bilayer. In those cases repulsion is very weak. This is the domain of NSA mentioned earlier. Chapter 5 provides a full scale theory that takes into account membrane deformations into account and takes the assumption that NSA has happened. We explore how the adhesion gets affected by salt concentration of the ionic environment. We come to a remarkable conclusion. We find

out that tweaking the concentration of the salt solution can lead to NSA on stiffer membranes. Stiffer membranes are present due to many physiological symptoms and diseases. Presence of excess cholesterol is one such system where membrane stiffening happens. Drug delivery by normal methods become tougher due to the membrane stiffness. NSA can provide a new route to deliver drugs to such cells. NSA thus can be good too.

In Chapter 6 we address the problem of how to stop NSA. Our solution in this thesis is to coat the NP with the lipid bilayer (LB) itself. This was motivated by numerous experiments in literature showing promise of increased targeted drug delivery by this LB coated NPs. We found out that the electrostatics of the system significantly changes from the case of bare gold NPs. This is the main cause for such targeted drug delivery. The repulsion parameter mentioned in chapter 4 shows a different nature in this case. The parameter space where previously NSA could happen gets destroyed in this case. Thus this system completely resists NSA and promotes specific adhesion.

We discuss about the future and the directions from this work in Chapter 7. This work can be the precursor for studying various other systems and nanoparticles that are being used or will be designed for carrying cargo, drug delivery and advanced therapies.

Chapter 2: Electrostatics of permeable and semi-permeable bilayer membranes

In this chapter we discuss the electrostatics of the eletric double layer present around the lipid bilayer. We explore the effects of surface charges and ionic conditions on the membrane electrostatics.[1]

Semi-permeable membranes are ubiquitous in biology and technology [1–10]. The most common example is the biological plasma membrane surrounding the biological cells. These membranes are typically impermeable to ions due to their phospholipid bilayer architecture. However, they become semi-permeable and allow selective transport of typically small ions with the opening up of the ion channels that are composed of the membrane proteins [11, 12]. Such ion-exchange controls signal transduction [13, 14] that is key to the survival and functioning of the cells. An equally important issue is how such membrane semi-permeability leads to an equilibrium ion distribution on the two sides of the membrane [i.e., the cell side or the cytosol side (CS) and the cell-exterior or the electrolyte side (ES)] [1, 15]. Membrane semi-permeability dictates that this equilibrium leads to an unequal ion distribution on the two sides of the membrane – the resulting gradient in ion concentration leads to a large osmotic pressure that the membrane has

[1]Contents of this chapter have been published as: *1. S. Sinha, H. Jing, and S. Das, Journal of Membrane Science, 533, 364-377 (2017); 2. S. Sinha, H. Jing and S. Das, Applied Physics Letters, 111, 063702 (2017)*

to withstand [16, 17]. More importantly, this gradient leads to the development of the well known *membrane potential* across the membrane that has massive implications in several biophysical phenomena, such as ATP synthesis by the mitochondrial cells [18], regulation of intracellular Ca^{2+} ions [19, 20], control of the arterial diameter [19], apoptosis in cancer cells [21], regulation of cell-antibody interactions [81], etc. This entire scenario of semi-permeable membrane electrostatics has been classically identified as the Donnan equilibrium [1]. Of course, in addition to the plasma membranes, semi-permeable membranes and the corresponding semi-permeability-driven electrostatics have been extensively applied in a myriad of applications in dialysis [23], water filtration [24], synthetic vesicles [5], sustainable power generation [25], development of fuel cells [26] and cell-based medicines [27], etc.

Classically, the Poisson-Boltzmann (PB) approach [17, 28–42] or a more involved integral-equation formalism [42–46] have been employed to model the electric double layer or the EDL electrostatics and resulting the ion distribution for both fully permeable and semi-permeable membranes. In other words, these studies probe the Donnan equilibrium of a charged membrane under the framework that considers the development of a charged-membrane-induced EDL. The most important results have been (a) symmetric ion distribution for permeable membranes [38], (b) asymmetric ion distribution and the consequent membrane-potential development for semi-permeable membranes [34], (c) finite osmotic interaction force between a semi-permeable membrane and other entities [17, 34, 36], and (d) alteration of the membrane potential as a function of the non-uniformity in the dielectric constants across the media [47], ion-ion interactions [48, 49], presence of zwitterions and other moieties in the lipid bilayer [50], presence of ions of varying nature and valence in the electrolyte [51, 52], etc. In addition to the continuum approaches, there have

been extensive atomistic simulation based investigations that explicitly model the lipid bilayers and elucidate the specific ion distribution across the bilayer membrane and the corresponding membrane potential [53–61]. In none of these above studies, there has been any report of a Charge-Inversion-like electrostatics associated with the membrane EDL electrostatics – in this paper, we shall report such an electrostatic effect characterized by the change of sign of the EDL potential within the EDL itself.

In this chapter, we employ the PB approach to study the electrostatics and the disjoining pressure of a semipermeable, negatively-charged membrane. Considering parameters similar to those of the negatively-charged plasma membrane, we probe two facets that to the best of our knowledge have not yet been investigated in the context of the membrane EDL electrostatics. Firstly, we study the case where this negatively-charged membrane is permeable to positive ions but impermeable to negative ions of a given salt. Secondly, we study the influence of an external permeable salt (i.e., a salt such that the membrane is permeable to both the cations and anions of that salt) in the membrane electrostatics. There are two key findings of this study. Firstly, and most remarkably, we witness a charge-inversion-like (CI-like) electrostatics on the cytosol side of the negatively-charged membrane for the case when it is permeable to positive ions but impermeable to negative ions. This CI-like electrostatics is characterized by the switching of the electrostatic potential from a negative value (at the membrane-cytosol interface) to a positive value (deep within the cytosol). The principle of the development of such a CI-like electrostatics and its relevance in the context of the classical understanding of electrostatics of the semi-permeable membrane has been illustrated in Fig. 1. Typically, for an uncharged semi-permeable membrane, the nature of the membrane permeability dictates the sign and the magnitude of the membrane potential. This membrane potential refers to the

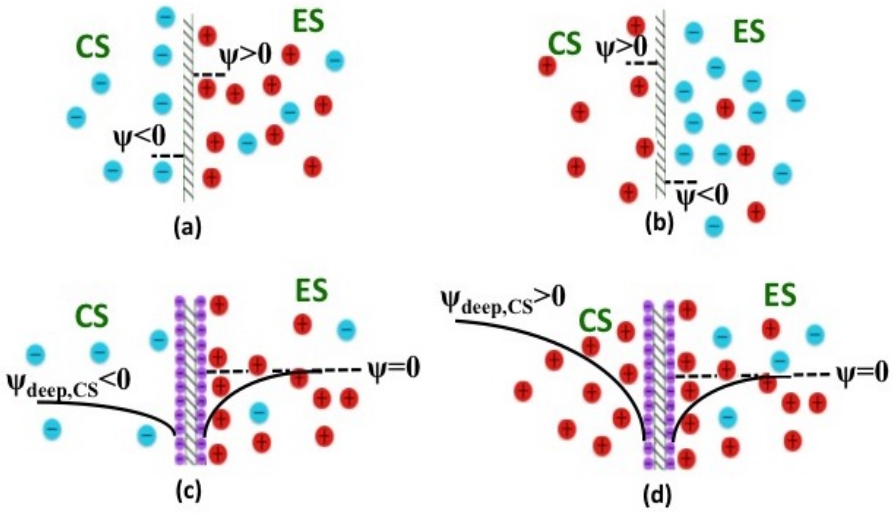

Figure 2.1: (a) Case of an uncharged semi-permeable membrane permeable to negative ions but impermeable to positive ions – the result is an accumulation of negative ions in the cytosol side (CS) and more number of positive ions than negative ions in the electrolyte side (ES). (b) Case of an uncharged semi-permeable membrane permeable to positive ions but impermeable to negative ions – the result is an accumulation of positive ions in the cytosol side (CS) and more number of negative ions than positive ions in the electrolyte side (ES). As a result the electrostatic potential in the immediate vicinity of the membrane in the CS is positive, whereas the electrostatic potential in the immediate vicinity of the membrane in the ES is negative. Here the electrostatic potential in the immediate vicinity of the membrane is considered, since that is what is needed to characterize the membrane potential. (c) Case of a negatively-charged semi-permeable membrane permeable to negative ions but impermeable to positive ions – the result is an EDL consisting of both coions and counterions in the ES ensuring $\psi = 0$ deep within the ES and a coion-only EDL in the CS. (d) Case of a negatively-charged semi-permeable membrane permeable to positive ions but impermeable to negative ions – the result is an EDL in the ES leading to $\psi = 0$ deep in the ES and a *counterion-only* EDL in the CS. Therefore, one witnesses the *Charge Inversion like electrostatics* in the CS.

difference in the values of the electrostatic potential (in the immediate vicinity of the membrane) on the two sides of the membrane. For example, consider the case of an uncharged semi-permeable membrane that is permeable only to negative ions but impermeable to positive ions. Let us consider that such a membrane separates the electrolyte (containing a salt CB that furnishes C^+ cation and B^- anion) from the cytosol. Given the nature of the membrane semi-permeability, B^- ions will diffuse to the cytosol side (CS) from the electrolyte side (ES). As a consequence, there will be an accumulation of anions in the immediate vicinity of the membrane in the CS. On the other hand, there will be more C^+ ions than B^- ions in the immediate vicinity of the membrane in the ES. As a result, while the net charge neutrality of this entire cytosol-membrane-electrolyte system is still maintained, there will be negative potential in the CS in the immediate vicinity of the membrane and a positive potential in the ES in the immediate vicinity of the membrane. This has been depicted in Fig. 1(a). Next consider a situation when the membrane is uncharged and permeable to only positive ions and impermeable to negative ions and separates an electrolyte (containing a salt AD that furnishes A^+ cation and D^- anion) from the cytosol. In this case, A^+ ions will diffuse to the cytosol side (CS) from the electrolyte side (ES) – therefore, there will be an accumulation of cations in the immediate vicinity of the membrane in the CS, while there will be more D^- ions than A^+ ions in the immediate vicinity of the membrane in the ES. Consequently, one will witness $\psi > 0$ and $\psi < 0$ in the CS and ES, respectively in the immediate vicinity of the membrane. In both these cases [Figs. 1(a,b)] the membrane potential is the difference in the values of the electrostatic potential in the immediate vicinity of the membrane on the two sides of the membrane – as evident from Figs. 1(a,b), this potential jump from the CS to the ES is $\Delta\psi > 0$ ($\Delta\psi < 0$) for the semi-permeable membrane permeable to the negative

(positive) ions and impermeable to the positive (negative) ions.

Unlike the case of this uncharged membrane, when the membrane is charged, an EDL indeed develops. For example, for a negatively-charged membrane that is permeable to negative ions and impermeable to positive ions of a given salt, EDLs develop on both the ES and the CS – however, the EDL on the ES consists of both coions and counterions, while the EDL in the CS consists of only coions [see Fig. 1(c)]. This is a most intriguing situation, where we find that the cytosol contains only anions despite being in contact with the negatively-charged membrane. Physically, such a situation becomes possible when the diffusive flux of the anions, on account of large concentration gradient across the membrane, overcomes the retarding electrical flux. Also, as will be illustrated later, such an ion distribution does not violate the charge neutrality condition, stemming from the fact that net charge density of the ions within the cytosol is still positive (as discussed in details during the explanation of Figs. 3 and 4). More importantly, in a very recent study, Madura and Vinogradova [67] established the possibility of a very similar situation, where a solvent, containing only cations, can be in contact with a positively-charged semi-permeable membrane that allows exchange of cations. The most remarkable case, however, that we study here is the case of the negatively-charged membrane permeable to positive ions and impermeable to negative ions [see Fig. 1(d)] of a salt present in the electrolyte. In this case too, the EDLs develop on both sides of the membrane; however, while the EDL in the ES consists of both the counterions and the coions, we encounter the case of *counterion-only* EDL in the CS. Such counterion-only EDL ensures that the EDL potential is negative at the membrane-cytosol interface, but becomes positive deep within the cytosol. Therefore, we witness the most remarkable case of *CI-like electrostatics*. CI has been known to be one of the most fascinating aspects of the EDL electrostatics,

where the EDL electrostatic potential (ψ) within the EDL inverts sign [62–66] [as in Fig. 1(d)] and has been witnessed in presence of multivalent and/or finite sized counterions. Such a changing of the sign of ψ leads to an *inversion of the sign of the net EDL charge* with the EDL consisting of both cations and anions – accordingly, such a phenomenon is known as the *Charge Inversion*. For the present case, of course, this change of sign of ψ occurs for an EDL consisting of only counterions – therefore, there is no inversion of the sign of the net EDL charge and accordingly, we denote this phenomenon as *CI-like electrostatics* and not as *Charge Inversion*. Most importantly, for the present case, this CI-like electrostatics is triggered entirely due to the interplay of the native charge and the specific nature of the semi-permeability of the membrane – the negative charge of the membrane enforces a negative potential at the membrane-cytosol interface, while the selective permeability of the membrane to positive ions (coupled with the symmetry condition at the cytosol centerline) ensures the development of a counterion-only EDL and a positive electrostatic potential far away from the membrane. Very much like the uncharged membrane, here too, the membrane impermeable to positive (negative) ions ensure $\Delta\psi > 0$ ($\Delta\psi < 0$) from the CS to the ES. Most interestingly, such switching of the sign of the EDL electrostatic potential in the CS for a counterion-only EDL (such an EDL develops within a solvent that contains only counterions and is in contact with an oppositely charged semi-permeable membrane that can exchange only counterions) has been very recently reported by Maduar and Vinogradova [67] and can be considered as an important validation of this most non-intuitive membrane-EDL behavior that we report. Of course, as will be detailed later, such an electrostatic potential distribution perfectly satisfies the charge neutrality condition.

The second important finding of this part of the chapter is that an external permeable

salt (i.e., salt whose both cations and anions permeate through the membrane) invariably nullifies the effect of the membrane semi-permeability. This nullification is manifested as a complete elimination of the CI-like electrostatic effect for the case when the membrane is permeable to positive ions only and a substantial lowering of the membrane potential for the case where the membrane is permeable to negative ions only. Finally, we quantify the disjoining pressure associated with the asymmetry of the ionic distribution triggered by the membrane semi-permeability – results demonstrate distinct influences of the CI-like electrostatic effects and external salt effects in the development of the disjoining pressure. *All these extremely non-trivial electrostatics across the membrane results from the asymmetry in the potential distribution between the CS and the ES. The key reason for such asymmetry is the semi-permeable nature of the membrane, which ensures that cytosol side will not have all the ions that are present in the electrolyte side. For example, if the membrane is permeable to cations but impermeable to anions, then the electrolyte side will have both cations and anions, while the cytosol will have only cations. Similalry, if the membrane is permeable to anions but impermeable to cations, then the electrolyte side will have both cations and anions, while the cytosol will have only anions.* While we perform our calculations with parameters similar to that of a phospholipid bilayer plasma membrane, such CI-resembling electrostatics is equally valid for semi-permeable non-plasma membranes as long as the membrane is charged and is permeable (impermeable) to ions of the opposite (similar) sign. We anticipate, therefore, that our presented findings of non-trivial membrane electrostatics based on this very simple PB analysis will open new avenues of membrane applications in a plethora of engineering and scientific disciplines.

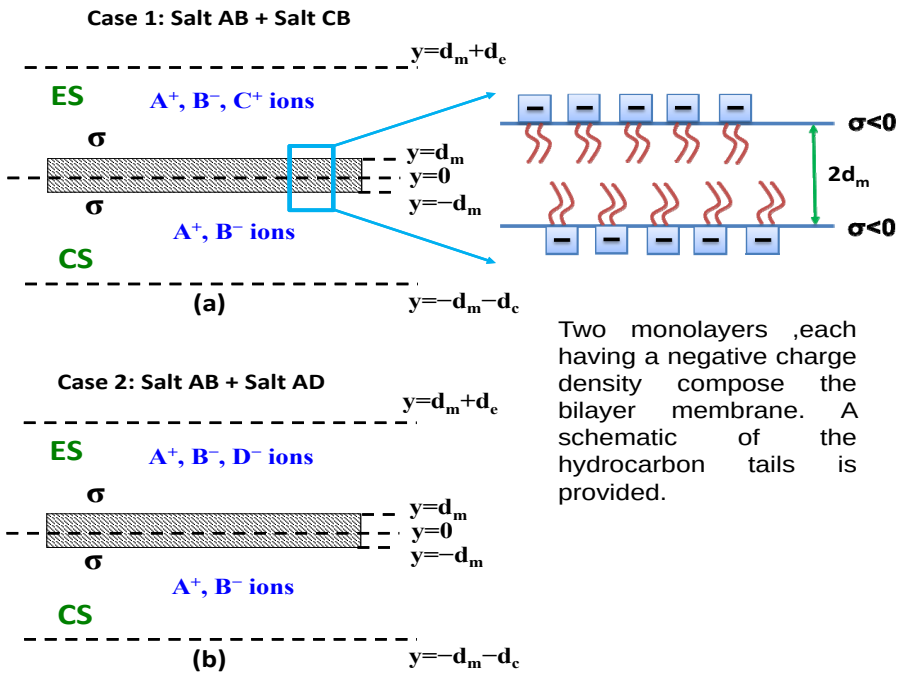

Figure 2.2: Schematic of the geometry for calculation. (a) Case 1: Negatively-charged membrane permeable to negative ions (B^-) and impermeable to positive ions (C^+). (b) Case 2: Negatively-charged membrane permeable to positive ions (A^+) and impermeable to negative ions (D^-). For both cases, we consider an added permeable salt AB, with the membrane being permeable to both cations and anions.

2.1 Theory-Part 1

2.1.1 Electrostatics of semi-permeable negatively-charged plasma membrane

We consider a negatively-charged plasma membrane whose centreline is located at $y = 0$, as shown in Fig. 2. The plasma membrane is assumed to be consisting of a phospholipid bilayer. The hydrophilic end of each bilayer (i.e., the end that is in contact with the electrolyte solution as well as the cytosol) contains negative charges with charge

density σ. We consider the membrane of thickness $2d_m$. Therefore, the membrane-cytosol interface is located at $y = -d_m$, while the membrane-electrolyte interface is located at $y = d_m$. The cell-centreline is located at $y = -d_m - d_c$, while the extracellular centreline is located at $y = d_m + d_e$. We assume the membrane to be semi-permeable. We consider the following two situations:

Case 1: The charged semi-permeable membrane is *permeable to anion* B^- and *impermeable to cation* C^+ of the salt CB [see Figs. 1(c)] with bulk number density $n_{im,\infty}$ in presence of a permeable salt AB with bulk number density n_∞.

Case 2: The charged semi-permeable membrane is *permeable to cation* A^+ and *impermeable to anion* D^- of the salt AD [see Figs. 1(d)] with bulk number density $n_{im,\infty}$ in presence of a permeable salt AB with bulk number density n_∞ (see Fig. 1b).

We consider both the salts as symmetric and monovalent. Henceforth we shall identify these two situations as Case 1 and Case 2.

Under these conditions, the free energy F of the system can be expressed as:

$$F = \int \left[\int_{-d_c-d_m}^{-d_m} f_c dy + \int_{-d_m}^{d_m} f_m dy + \int_{d_m}^{d_e+d_m} f_e dy \right] d^2\mathbf{r} + \int \left[\sigma\psi_{s,m-c} + \sigma\psi_{s,m-e} \right] d^2\mathbf{r}. \tag{2.1}$$

In the above equation, $\psi_{s,m-c}$ and $\psi_{s,m-e}$ are the electrostatic potentials at the membrane-cytosol and membrane-electrolyte interfaces and f_c, f_m, and f_e are the electrostatic energy densities inside the cell, within the membrane, and outside the cell (i.e., within the electrolyte), respectively. Depending on the particular case (Case 1 or Case 2), expressions of these different energy densities will vary. We derive the necessary P-B equations governing the membrane EDL electrostatics by minimizing eq.(2.1) (see Appendix A for the

details). The results are the governing equations for Cases 1 and 2, as summarized below:

Governing Equations for Case 1

$$\begin{aligned}
&\frac{d^2\psi}{dy^2} = -\frac{e}{\epsilon_0\epsilon_c}\left[n_{A^+} - n_{B^-}\right] \quad -(d_m + d_c) \le y \le -d_m,\\
&\frac{d^2\psi}{dy^2} = 0 \qquad\qquad -d_m \le y \le d_m,\\
&\frac{d^2\psi}{dy^2} = -\frac{e}{\epsilon_0\epsilon_e}\left[n_{A^+} - n_{B^-} + n_{C^+}\right] \quad d_m \le y \le d_m + d_e.
\end{aligned} \tag{2.2}$$

$$\begin{aligned}
&n_{A^+} = n_\infty \exp\left(-\frac{e\psi}{k_B T}\right), \quad n_{C^+} = n_{im,\infty} \exp\left(-\frac{e\psi}{k_B T}\right),\\
&n_{B^-} = \left(n_\infty + n_{im,\infty}\right) \exp\left(\frac{e\psi}{k_B T}\right)
\end{aligned} \tag{2.3}$$

Consequently, we may write:

$$\begin{aligned}
&\frac{d^2\psi}{dy^2} = \frac{2n_\infty e}{\epsilon_0\epsilon_c} \sinh\left(\frac{e\psi}{k_B T}\right) + \frac{n_{im,\infty} e}{\epsilon_0\epsilon_c} \exp\left(\frac{e\psi}{k_B T}\right)\\
&\qquad\qquad -(d_m + d_c) \le y \le -d_m,\\
&\frac{d^2\psi}{dy^2} = 0 \qquad\qquad -d_m \le y \le d_m,\\
&\frac{d^2\psi}{dy^2} = \frac{2n_\infty e}{\epsilon_0\epsilon_e} \sinh\left(\frac{e\psi}{k_B T}\right) + \frac{2n_{im,\infty} e}{\epsilon_0\epsilon_e} \sinh\left(\frac{e\psi}{k_B T}\right)\\
&\qquad\qquad\qquad\qquad d_m \le y \le d_m + d_e.
\end{aligned} \tag{2.4}$$

Governing Equations for Case 2

$$\begin{aligned}
&\frac{d^2\psi}{dy^2} = -\frac{e}{\epsilon_0\epsilon_c}\left[n_{A^+} - n_{B^-}\right] \quad -(d_m + d_c) \le y \le -d_m,\\
&\frac{d^2\psi}{dy^2} = 0 \qquad\qquad -d_m \le y \le d_m,\\
&\frac{d^2\psi}{dy^2} = -\frac{e}{\epsilon_0\epsilon_e}\left[n_{A^+} - n_{B^-} - n_{D^-}\right] \quad d_m \le y \le d_m + d_e.
\end{aligned} \tag{2.5}$$

$$
\begin{aligned}
n_{A^+} &= \left(n_\infty + n_{im,\infty}\right) \exp\left(-\frac{e\psi}{k_B T}\right), \\
n_{D^-} &= n_{im,\infty} \exp\left(\frac{e\psi}{k_B T}\right),\ n_{B^-} = n_\infty \exp\left(\frac{e\psi}{k_B T}\right)
\end{aligned} \tag{2.6}
$$

Consequently, we may write:

$$
\begin{aligned}
\frac{d^2\psi}{dy^2} &= \frac{2n_\infty e}{\epsilon_0 \epsilon_c} \sinh\left(\frac{e\psi}{k_B T}\right) + \frac{n_{im,\infty} e}{\epsilon_0 \epsilon_c} \exp\left(-\frac{e\psi}{k_B T}\right) \\
&\qquad -(d_m + d_c) \le y \le -d_m, \\
\frac{d^2\psi}{dy^2} &= 0 \qquad\qquad -d_m \le y \le d_m, \\
\frac{d^2\psi}{dy^2} &= \frac{2n_\infty e}{\epsilon_0 \epsilon_e} \sinh\left(\frac{e\psi}{k_B T}\right) + \frac{2n_{im,\infty} e}{\epsilon_0 \epsilon_e} \sinh\left(\frac{e\psi}{k_B T}\right) \\
&\qquad\qquad d_m \le y \le d_m + d_e.
\end{aligned} \tag{2.7}
$$

In the above equations, $n_{A^+,\infty}$, $n_{B^-,\infty}$, $n_{C^+,\infty}$, and $n_{D^-,\infty}$ are the bulk number densities of the A^+, B^-, C^+, and D^- ions. For case 1, $n_{A^+,\infty} = n_\infty$, $n_{B^-,\infty} = n_\infty + n_{im,\infty}$, and $n_{C^+,\infty} = n_{im,\infty}$. On the other hand for case 2, $n_{A^+,\infty} = n_\infty + n_{im,\infty}$, $n_{B^-,\infty} = n_\infty$, and $n_{D^-,\infty} = n_{im,\infty}$. Further in the above equations, ϵ_0 is the permittivity of free space, $k_B T$ is the thermal energy, e is the electronic charge, and ϵ_e, ϵ_m and ϵ_c are the relative permittivities of the electrolyte, membrane, and the cytosol, respectively.

Electrostatics for cases 1 and 2 will therefore be obtained by solving eqs.(2.4,5.23) in presence of the appropriate boundary conditions on ψ. Eq.(1) can be minimized with respect to $\psi_{s,m-c}$ and $\psi_{s,m-e}$ to yield the electrostatic stress jump condition at the membrane-cytosol and membrane-electrolyte interfaces (valid for both cases 1 and 2), namely (see

Appendix B for detailed derivation):

$$\left(\epsilon_m \frac{d\psi}{dy}\right)_{y=-d_m^+} - \left(\epsilon_c \frac{d\psi}{dy}\right)_{y=-d_m^-} = -\frac{\sigma}{\epsilon_0},$$
$$\left(\epsilon_e \frac{d\psi}{dy}\right)_{y=d_m^+} - \left(\epsilon_m \frac{d\psi}{dy}\right)_{y=d_m^-} = -\frac{\sigma}{\epsilon_0}. \tag{2.8}$$

Eqs. (2.4,5.23) will be solved numerically in presence of the boundary conditions expressed in eq.(5.15) as well as those expressed below:

$$\left(\frac{d\psi}{dy}\right)_{y=-(d_m+d_c)} = 0, \quad (\psi)_{y=-d_m^+} = (\psi)_{y=-d_m^-},$$
$$(\psi)_{y=d_m^+} = (\psi)_{y=d_m^-}, \quad \left(\frac{d\psi}{dy}\right)_{y=(d_m+d_e)} = 0. \tag{2.9}$$

This numerical solution is carried out using the in-house Finite Difference Method code. In this method, we consider uniform grid spacing, a second order central scheme for discretizing both the second order and first order derivatives and a second order bias scheme for discretizing the first order derivative at the boundary and the interface. Of course, the solution of ψ will necessitate knowledge about σ, n_∞, $n_{im,\infty}$, d_m, d_e, d_c, ϵ_c, ϵ_e, and ϵ_m.

Of course, we can show that the above set of equations can be modified to recover the equations governing the membrane electrostatics studied in other papers (e.g., Maduar and Vinogradova [67]), as illustrated in Appendix C.

2.1.2 Charge Neutrality condition

Charge neutrality or the electro-neutrality is established purely through the use of the appropriate governing equations and boundary conditions [eqs.(2.2,2.5,5.15,5.24)], as explained below.

For the charge neutrality condition to hold we should have:

$$\text{Charge density within cytosol} + \text{Charge density within membrane}$$

$$+ \quad \text{Charge density within electrolyte} + 2\sigma = 0. \tag{2.10}$$

Charge Neutrality Condition for Case 1 (Negatively charged membrane permeable to negative ions in presence of a permeable external salt):

For this case, using the first equation of eq.(2.2) and the condition $\left(\frac{d\psi}{dy}\right)_{y=-(d_m+d_c)} = 0$ [please see eq.(5.24)], we can write:

$$\text{Charge density within cytosol} = \int_{-(d_m+d_c)}^{-d_m} e\left(n_{A^+} - n_{B^-}\right) dy$$

$$= -\int_{-(d_m+d_c)}^{-d_m} \epsilon_0\epsilon_c \frac{d^2\psi}{dy^2} dy = \left(\epsilon_0\epsilon_c \frac{d\psi}{dy}\right)_{y=-(d_m+d_c)} - \left(\epsilon_0\epsilon_c \frac{d\psi}{dy}\right)_{y=-d_m} = -\left(\epsilon_0\epsilon_c \frac{d\psi}{dy}\right)_{y=-d_m} \tag{2.11}$$

Similarly, we can write

$$\text{Charge density within membrane} = \int_{-d_m}^{d_m} (\text{Charge contained inside the membrane}) dy = 0 =$$

$$-\int_{-d_m}^{d_m} \epsilon_0\epsilon_m \frac{d^2\psi}{dy^2} dy = \left(\epsilon_0\epsilon_m \frac{d\psi}{dy}\right)_{y=-d_m} - \left(\epsilon_0\epsilon_m \frac{d\psi}{dy}\right)_{y=d_m} \tag{2.12}$$

Eq.(2.12) considers that the net charge contained within the membrane is zero. Please note that σ represents that charge density at the membrane-cytosol and the membrane-electrolyte interfaces and is not the charge contained within the membrane.

Finally, using the third equation of eq.(2.2) and the condition $\left(\frac{d\psi}{dy}\right)_{y=d_m+d_e} = 0$ [please see eq.(5.24)], we can write:

$$\text{Charge density within electrolyte} = \int_{d_m}^{(d_m+d_e)} e\left(n_{A^+} - n_{B^-} + n_{C^+}\right) dy$$

$$= -\int_{d_m}^{(d_m+d_e)} \epsilon_0\epsilon_e \frac{d^2\psi}{dy^2} dy = \left(\epsilon_0\epsilon_e \frac{d\psi}{dy}\right)_{y=d_m} - \left(\epsilon_0\epsilon_e \frac{d\psi}{dy}\right)_{y=(d_m+d_e)} = \left(\epsilon_0\epsilon_e \frac{d\psi}{dy}\right)_{y=d_m} \tag{2.13}$$

Simply adding eqs.(2.11,2.12,2.13) and subsequently using eq.(5.15) we can write:

$$\text{Charge density within cytosol} + \text{Charge density within membrane}$$

$$+ \text{ Charge density within electrolyte} =$$

$$\left[\left(\epsilon_0\epsilon_m\frac{d\psi}{dy}\right)_{y=-d_m} - \left(\epsilon_0\epsilon_c\frac{d\psi}{dy}\right)_{y=-d_m}\right] + \left[\left(\epsilon_0\epsilon_e\frac{d\psi}{dy}\right)_{y=d_m} - \left(\epsilon_0\epsilon_m\frac{d\psi}{dy}\right)_{y=d_m}\right] =$$

$$\left[\left(\epsilon_0\epsilon_m\frac{d\psi}{dy}\right)_{y=-d_m^+} - \left(\epsilon_0\epsilon_c\frac{d\psi}{dy}\right)_{y=-d_m^-}\right] + \left[\left(\epsilon_0\epsilon_e\frac{d\psi}{dy}\right)_{y=d_m^+} - \left(\epsilon_0\epsilon_m\frac{d\psi}{dy}\right)_{y=d_m^-}\right] = -\sigma - \sigma \Rightarrow$$

$$\text{Charge density within cytosol} + \text{Charge density within membrane}$$

$$+ \quad \text{Charge density within electrolyte} + 2\sigma = 0, \tag{2.14}$$

i.e., we recover the charge neutrality condition.

Charge neutrality condition for Case 2 (Negatively charged membrane permeable to positive ions in presence of a permeable external salt):

We can adopt exactly the same procedure and use the different equations of eq.(2.5), the symmetry conditions $\left(\frac{d\psi}{dy}\right)_{y=-(d_m+d_c)} = 0$, $\left(\frac{d\psi}{dy}\right)_{y=d_m+d_e} = 0$ [eq.(5.24)] and the electrostatic stress jump boundary condition [eq.(5.15)] to show that:

$$\text{Charge density within cytosol} + \text{Charge density within membrane}$$

$$+ \quad \text{Charge density within electrolyte} + 2\sigma = 0. \tag{2.15}$$

Of course, using the above analyses it is trivial to show that these set of governing equations and boundary conditions ensure net charge neutrality even for the case of no external salt (which is a special case of the above analysis with $n_\infty = 0$).

2.1.3 Calculation of the disjoining pressure

We define the disjoining pressure across the membrane as [17, 68]:

$$\Pi = (p)_{y=d_m} - (p)_{y=-d_m} + p_{id}, \tag{2.16}$$

where p is the osmotic pressure across the membrane and p_{id} is the pressure corresponding to the ideal solution. Below we calculate Π corresponding to the two different cases studied here.

Disjoining pressure for Case 1 (Negatively charged membrane permeable to negative ions in presence of a permeable external salt):

Pressure gradient across the membrane is always related to the corresponding charge density (ρ_e) as

$$-\frac{dp}{dy} + \rho_e E_y = 0, \tag{2.17}$$

where E_y is the induced electric field across the membrane (due to the ion distribution). We first consider the electrolyte side, where:

$$\rho_e = e\left(n_{C^+} - n_{B^-} + n_{A^+}\right) = -2\left(n_{im,\infty} + n_\infty\right) e \sinh\left(\frac{e\psi}{k_B T}\right). \tag{2.18}$$

Consequently,

$$\frac{dp}{dy} = 2\left(n_{im,\infty} + n_\infty\right) e \sinh\left(\frac{e\psi}{k_B T}\right)\frac{d\psi}{dy}. \tag{2.19}$$

Integrating the above equation in presence of the condition $\psi = 0$ and $p = p_{atm}$ in the bulk electrolyte, we can write:

$$p = p_{atm} + 2\left(n_{im,\infty} + n_{\infty}\right) k_B T \left[\cosh\left(\frac{e\psi}{k_B T}\right) - 1\right]. \tag{2.20}$$

Therefore,

$$(p)_{y=d_m} = p_{atm} + 2\left(n_{im,\infty} + n_{\infty}\right) k_B T \left[\cosh\left(\frac{e\psi}{k_B T}\right)_{y=d_m} - 1\right]. \tag{2.21}$$

We next consider the cytosol side, where:

$$\rho_e = e\left(n_{A^+} - n_{B^-}\right) = -2n_{\infty} e \sinh\left(\frac{e\psi}{k_B T}\right) - n_{im,\infty} \exp\left(\frac{e\psi}{k_B T}\right). \tag{2.22}$$

Consequently,

$$\frac{dp}{dy} = \left[2n_{\infty} e \sinh\left(\frac{e\psi}{k_B T}\right) + n_{im,\infty} \exp\left(\frac{e\psi}{k_B T}\right)\right] \frac{d\psi}{dy}. \tag{2.23}$$

Integrating the above equation in presence of the condition that at the centerline of the cell $p = p_c$ and $\psi = \psi_0$:

$$p = p_c + n_{im,\infty} k_B T \left[\exp\left(\frac{e\psi}{k_B T}\right) - \exp\left(\frac{e\psi_0}{k_B T}\right)\right] + 2n_{\infty} k_B T \left[\cosh\left(\frac{e\psi}{k_B T}\right) - \cosh\left(\frac{e\psi_0}{k_B T}\right)\right]. \tag{2.24}$$

Consequently,

$$(p)_{y=-d_m} = p_c + n_{im,\infty} k_B T \left[\exp\left(\frac{e\psi}{k_B T}\right)_{y=-d_m} - \exp\left(\frac{e\psi_0}{k_B T}\right) \right] + 2n_\infty k_B T \left[\cosh\left(\frac{e\psi}{k_B T}\right)_{y=-d_m} - \cosh\left(\frac{e\psi_0}{k_B T}\right) \right]. \tag{2.25}$$

Therefore the difference of pressure across the membrane in presence of the condition $\psi_{y=d_m} = \psi_{y=-d_m}$ is:

$$(p)_{y=d_m} - (p)_{y=-d_m} = (p_{atm} - p_c) = 2n_\infty k_B T \left[\cosh\left(\frac{e\psi_0}{k_B T}\right) - 1 \right] + n_{im,\infty} k_B T \left[\exp\left(-\frac{e\psi}{k_B T}\right)_{y=d_m} + \exp\left(\frac{e\psi_0}{k_B T}\right) - 2 \right]. \tag{2.26}$$

Consequently, we may express the disjoining pressure as [using $p_{atm} = p_c$, $p_{id} = 2k_B T \left(n_{C^+,bulk} + n_{B^-,bul}$ $2k_B T n_{im,\infty}$ and eq.(2.16)]:

$$\Pi = 2n_\infty k_B T \left[\cosh\left(\frac{e\psi_0}{k_B T}\right) - 1 \right] + n_{im,\infty} k_B T \left[\exp\left(-\frac{e\psi}{k_B T}\right)_{y=d_m} + \exp\left(\frac{e\psi_0}{k_B T}\right) \right]. \tag{2.27}$$

Disjoining pressure for Case 2 (Negatively charged membrane permeable to positive ions in presence of a permeable external salt):

We first consider the electrolyte side, where:

$$\rho_e = e\left(-n_{B^-} - n_{D^-} + n_{A^+}\right) = -2\left(n_{im,\infty} + n_\infty\right) e \sinh\left(\frac{e\psi}{k_B T}\right). \tag{2.28}$$

For the cytosol side:

$$\rho_e = e\left(-n_{B^-} + n_{A^+}\right) = -2n_\infty e \sinh\left(\frac{e\psi}{k_B T}\right) + n_{im,\infty} e \exp\left(-\frac{e\psi}{k_B T}\right). \tag{2.29}$$

Given that the expressions of ρ_e in eq.(28) and eq.(29) are identical to that in eq.(18) and eq.(22) respectively, and the fact that $p_{id} = 2k_B T n_{im,\infty}$ for this case as well, we can infer that the disjoining pressure for this case is also expressed by eq.(27).

2.2 Results and Discussions- Part 1

Here we study the membrane EDL electrostatics for four separate cases. These are:

- Case 1a: Negatively-charged membrane permeable to negative ions and impermeable to positive ions in absence of an external permeable salt.
- Case 1b: Negatively-charged membrane permeable to negative ions and impermeable to positive ions in presence of an external permeable salt.
- Case 2a: Negatively-charged membrane permeable to positive ions and impermeable to negative ions in absence of an external permeable salt.
- Case 2b: Negatively-charged membrane permeable to positive ions and impermeable to negative ions in presence of an external permeable salt.

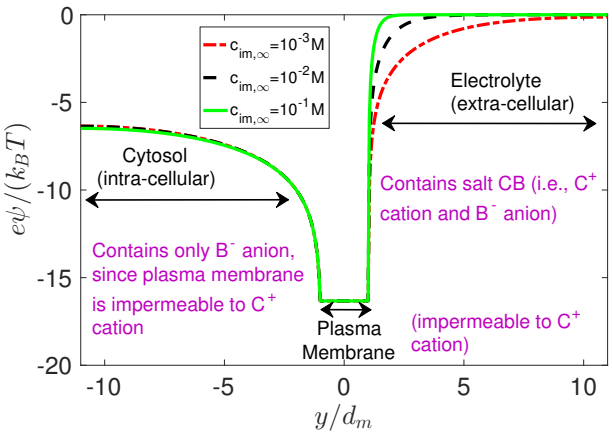

Figure 2.3: Variation of the EDL electrostatics of the semipermeable membrane for different concentrations ($c_{im,\infty}$) of the salt CB. There is no added salt AB. Membrane is impermeable to C^+ ions. The membrane is considered to be of a lipid bilayer membrane with thickness ($d_m = 4\ nm$); hydrophilic end of each layer is assumed to have a charge density of $-1\ e/nm^2$. Other parameters are $d_c = d_e = 1\ \mu m$, $\epsilon_c = 79.8$, $\epsilon_e = 79.8$, and $\epsilon_m = 2$, $k_B = 1.38 \times 10^{-23}\ J/K$, $T = 298\ K$, and $e = 1.6 \times 10^{-19}\ C$.

2.2.1 Case 1a: Negatively-charged membrane permeable to negative ions and impermeable to positive ions in absence of an external salt

Fig. 3 studies the case where a negatively charged membrane is permeable to negative ions of a given salt CB (furnishing C^+ and B^- ions) and there is no external salt. Therefore, while both the cations (C^+) and the anions (B^-) can be present in the ES, only anions (B^-) exist in the CS. We consider a bulk number density of $n_{im,\infty}$ (hence bulk concentration of $c_{im,\infty}$) of this salt. Under these conditions, an EDL consisting of both cations and anions develops on the ES, while an EDL consisting of only coions develops on the CS. As a consequence, we witness a progressive lowering of the screening

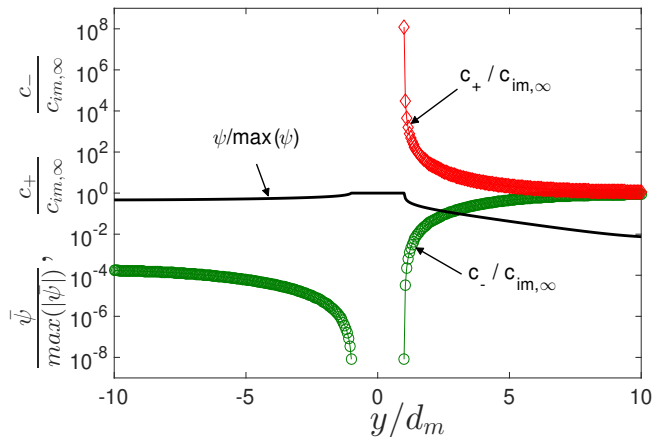

Figure 2.4: Variation of the EDL electrostatic potential and the corresponding ion distribution for $c_{im,\infty} = 0.001\ M$ for this case where a negatively charged membrane is permeable to negative ions with no external salt. All other parameters are identical to that of Fig. 3.

length (or the EDL thickness) in the ES with an increase in the concentration of CB. A much more interesting electrostatics set in on the CS, where there are only coions in the vicinity of the negatively charged membrane [see Fig. 1(c)], forming a coion-only EDL. Obviously, such coions, unlike a standard EDL consisting of both coions and counterions, cannot screen the membrane charge. Therefore, the EDL potential in the vicinity of the charged membrane in the CS will show a $1/y$ decay (where "y" is the distance from the membrane-cytosol interface deep into the membrane) and all the coions will be driven away from the membrane vicinity. However, deep within the cytosol, where the negative magnitude of ψ has substantially lowered (due to the $1/y$-decay), the negative coions will accumulate thereby ensuring a finitely large negative value of the electrostatic potential. Therefore, in the context of the development of the electrostatic potential in the CS, we witness a membrane-charge-dominated behavior in the vicinity of the membrane and a

behavior dictated by the accumulation of permeated ions far away from the membrane. To summarize, the permeating ions ensure a coion-only EDL in the CS and a negative electrostatic potential deep within the cytosol, while the development of the EDL in the electrolyte side ensures a zero electrostatic potential deep within the electrolyte. The membrane potential is this difference between these electrostatic potential values on the two sides of the membrane at locations where the specific effect of the membrane has disappeared – this disappearance happens in the immediate vicinity of the membrane for an uncharged membrane, but occurs far away from the membrane (both in the ES and the CS) for a charged membrane. Of course for both uncharged and charged membranes permeating only negative ions, one will witness a positive membrane potential drop ($\Delta\psi > 0$) across the membrane from the CS to the ES.

The effect of this specific electrostatics on the ion distribution is summarized in Fig. 4. Counterions (C^+ ions) exist only in the ES, while the coions (B^- ions) will exist both in the ES and the CS. However, there will be no ions within the membrane. In the ES, the coions and the counterions obey the standard screening characteristics of an EDL – hence the counterion (coion) concentration decreases (increases) to $c_{im,\infty}$ far away from the membrane from a large (small) value at the membrane-electrolyte interface. On the other hand in the CS, the coions are expelled from the vicinity of the negatively-charged membrane and accumulate deep within the cytosol (i.e., at locations where the negative magnitude of ψ has substantially lowered). This is evident from the significant difference in coion concentration between these two locations. It is very interesting to note that even the accumulated concentration of coions deep within the CS is several orders of magnitude smaller than the bulk concentration $c_{im,\infty}$. This points to the fact that despite being permeable to negative ions, a negatively-charged membrane, on account

of the specific electrostatic behavior will only permeate very small amount of negative ions. This relatively weak accumulation of the permeable coions is a key reason why one witnesses similar bulk potential values (deep within the CS) for different values of $c_{im,\infty}$ (see Fig. 3).

Several very crucial issues pertain to this specific ion concentration and electrostatic potential profiles explicated in Figs. 3 and 4. Firstly, it must be identified that the case studied here showcases a highly non-intuitive situation, where a liquid medium (i.e., the cytosol), despite being in contact with a negatively charged membrane, contains only negative ions. Such a behavior is entirely attributed to the semi-permeable nature of the membrane that enforces a diffusion of negative ions that is strong enough to drive the anions across a negatively-charged membrane overcoming the electrostatic repulsion effects. Of course, very little amount of anions can be transported to the CS by this mechanism as is evident from a very weak (as compared to $c_{im,\infty}$) concentration of anions even deep within the cytosol much away from the negatively-charged membrane. Secondly, this potential and ion concentration profiles very much satisfy the *charge neutrality condition*. These profiles have been obtained by solving eq.(2) in presence of the boundary conditions expressed in eqs.(8,9) – we show in section IIB that the very use of these conditions indeed ensure that the *charge neutrality condition* is satisfied. Of course, it is easy to figure out that the net charge density both in the CS and the ES for this case is positive [see eqs. (11,13)], which balances the negative charge densities at the membrane-electrolyte and membrane-cytosol interfaces. Finally, such an example of a solvent containing only coions in contact with a charged membrane has been recently proposed by Maduar and Vinogradova [67]. In this study, the authors considered a thin layer of solvent separating two semi-permeable membranes capable of exchanging only cations with the solvent.

The authors considered the case of positively-charged membranes and demonstrated finite concentration of cations (or coions) in the solvent (the solvent contained only coions and no counterions) – therefore, just like what we predict here for the CS, Maduar and Vinogradova [67] demonstrated the possibility of a solvent containing only coions in contact with a charged membrane.

2.2.2 Case 1b: Negatively charged membrane permeable to negative ions and impermeable to positive ions in presence of an external salt

Fig. 5 elucidates the case where the findings of the previous subsection is repeated, but in presence of an external permeable salt AB of bulk concentration c_∞ (or bulk number density n_∞). The salt AB being permeable, the membrane can permeate both the A^+ and B^- ions. Consequently, there will be A^+, B^-, and C^+ ions in the ES, while there will be only A^+ and B^- ions in the CS. Accordingly, on both the ES and the CS there will be EDLs that consist of both cations and anions. We consider a concentration of 0.001 M for the salt CB – the plasma membrane is impermeable to the cation of this salt. Hence when the concentration of the added permeable salt AB is much larger ($c_\infty = 0.01, 0.1\ M$), the effect of the semi-permeability of the membrane gets masked. As a consequence, we witness an exactly symmetric electrostatic potential profile in the CS and the ES and for both the EDLs (in the ES and the CS) an identical lowering of the screening length is witnessed with an increase in c_∞. The fact that the electrostatic potential becomes almost symmetric on either sides of the membrane makes the membrane potential negligible. *Most importantly, this result with an external salt conclusively proves that the asymmetry in the electrostatic potential profiles between the CS and the ES is attributed entirely to*

the semi-permeability of the membrane (external salt nullifies this semi-permeability effect and hence nullifies this asymmetry) – the semi-permeability enforces an absence of certain ions in the CS as compared to those present in the ES and this ensures the asymmetry and all other related non-trivial membrane electrostatics that we report here.

On the other hand, for $c_\infty = 0.001\ M$ we find a significant impact of the membrane semi-permeability (since $c_{im,\infty} = 0.001\ M$), demonstrating a significant asymmetry between the potential profiles of the ES and CS. Also, larger c_∞ leads to weaker values of the electrostatic potential within the membrane. This can be justified by smaller EDL thickness (at larger salt concentration) leading to weaker value of the potential for a given membrane charge density. To summarize, we witness that the salt effect reduces the overall impact of the membrane semi-permeability.

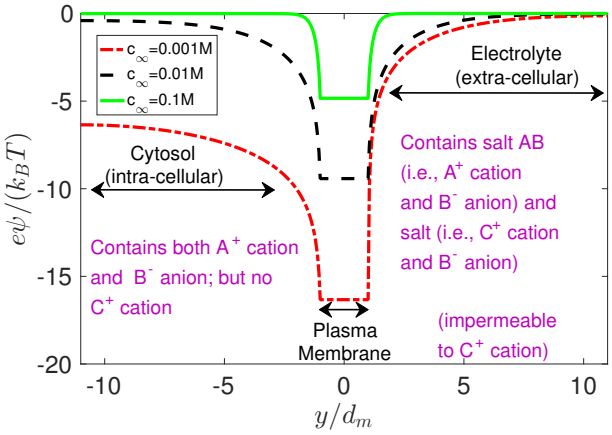

Figure 2.5: Variation of the EDL electrostatics of the semi-permeable membrane for different concentrations (c_∞) of the membrane penetrable salt AB in presence of 0.001 M salt CB with membrane-impermeable cation C^+. Other parameters are identical to that of Fig. 3.

2.2.3 Case 2a: Negatively-charged membrane permeable to positive ions and impermeable to negative ions in absence of an external salt

In Fig. 6, we study the case where a negatively charged membrane is permeable to positive ions (A^+) and impermeable to negative ions (D^-) for the salt AD (with concentration $c_{im,\infty}$) in absence of the external salt AB. Therefore, we shall have both A^+ and D^- ions in the ES, but simply the A^+ ions in the CS. Hence there will be the development of an EDL consisting of coions and counterions in the ES and a counterion-only EDL in the CS. Consequently, in the ES there will be a progressive lowering of the screening length with an increase in $c_{im,\infty}$. However, the most interesting situation is witnessed in the CS that contains only the A^+ cations. *A most remarkable Charge Inversion (CI) like electrostatics is witnessed in the cytosol side.* This CI like electrostatics is characterized by a switching of the sign of the electrostatic potential from large negative values at the membrane-cytosol interface to constant positive values deep within the cytosol. This is the most important finding of this part of this chapter. To the best of our knowledge, such CI and the consequent reversal of the sign of the EDL electrostatic potential (ψ) within the EDL has been typically witnessed for systems developing the EDLs in the presence of multivalent counterions or ions with finite sizes [62–66]. This reversal of the sign of ψ would imply an inversion of the sign of the charge density of the EDL consisting of both coions and counterions, triggering a most unique scenario where locally within the EDL, the coion number density exceeds the counterion number density. This is the reason why this phenomenon is denoted as *Charge Inversion*. In our present case, the EDL being only composed of counterions, there is no possibility of such an inversion in the charge density, since there are no coions. However, the variation of ψ is exactly similar (in terms

of changing the sign within the EDL) to the ψ distribution that characterizes the CI – hence we always denote it as CI-like electrostatics. Of course, for the present case we can attribute such CI-like electrostatic phenomenon to the peculiar behavior that can be associated with the counterion-only EDL – for such an EDL, based on the system parameters, the electrostatic potential has the same sign as that of the membrane charge at the membrane-cytosol interface but reverts sign far away from the membrane where the influence of the membrane charge has got nullified. In Appendix D, we provide a simple analysis based on Debye-Hückel theory that establishes such an occurrence mathematically and pinpoints the conditions corresponding to which counterion-only EDL will lead to CI-like electrostatics. Of course, the resulting membrane potential shows a negative drop from the CS to the ES, given that a positive value of the electrostatic potential deep within the cytosol and a zero potential in the bulk electrolyte. Finally, an increase in the concentration of AD lowers the magnitude of the electrostatic potential in the immediate vicinity of the membrane. In Fig. 7, the corresponding ionic distributions are provided. Distinct EDL-mediated behaviors are witnessed for both cations (A^+) and anions (D^-) in the ES. However, in the CS, where only cations are present, CI-like electrostatic dictates the concentration of the cations. Consequently, cation concentration increases from a value much larger than $c_{im,\infty}$ (at the membrane-cytosol interface) to a value much smaller than $c_{im,\infty}$ deep within the cytosol. It is worthwhile to note here that in a very recent study, Maduar and Vinogradova witnessed a similar CI-like electrostatics for membranes with counterion-only EDLs [67]. While the present study is much different from this work [67] in terms of issues such as consideration of finite membrane thickness with charge densities at both the interfaces of the membrane, consideration of external salt effect, calculation of development of membrane potential, etc. this result by Maduar

and Vinogradova [67] serves as an important validation of our calculation that presents this highly non-intuitive CI-like electrostatics in semi-permeable membranes. Later in section IIIF, we provide a very detailed validation of our work by comparing it with the findings of Ref. 67.

Two important related issues should be discussed here. Firstly, here too the *charge neutrality condition* is perfectly obeyed given that we use eqs.(5,8,9) to obtain the potential profile (under the condition of $n_\infty = 0$, i.e., no external salt) and we have already shown how these equations themselves ensure that the *charge neutrality condition* is satisfied. As an additional check, we numerically compute the charge density values within the cytosol, within the membrane and within the electrolyte for each of the three cases represented in Fig. 6. From eq.(10), we can infer that the charge neutrality condition is ensured when the sum of these charge density values equal -2σ. For the three cases of Fig. 6, we get this sum of the charge density values as -2σ (for the case where $c_{im,\infty} = 0.001\ M$), -1.998σ (for the case where $c_{im,\infty} = 0.01\ M$), and -1.997σ (for the case where $c_{im,\infty} = 0.1\ M$). Therefore, within the numerical error of less than 1%, we ensure the charge neutrality condition. We have made similar checks for all other figures and have ensured that the charge neutrality condition is indeed ensured. We do not provide these numbers corresponding to the other figures for the sake of brevity. The second key issue is that the boundary condition at the cytosol centerline is that of symmetry in ψ, given that the cytosol is bounded between two membranes. This symmetry condition ($d\psi/dy = 0$) at a distance from the charged surface that is much larger than the EDL thickness translates into a condition of $\psi = 0$ for the case where the EDL consists of both the coions and the counterions. On the contrary, this symmetry condition (at a distance from the charged surface that is much larger than the EDL thickness) for a counterion-only EDL leads to

a non-zero ψ – exactly the same thing has been obtained in the paper of Maduar and Vinogradova [67].

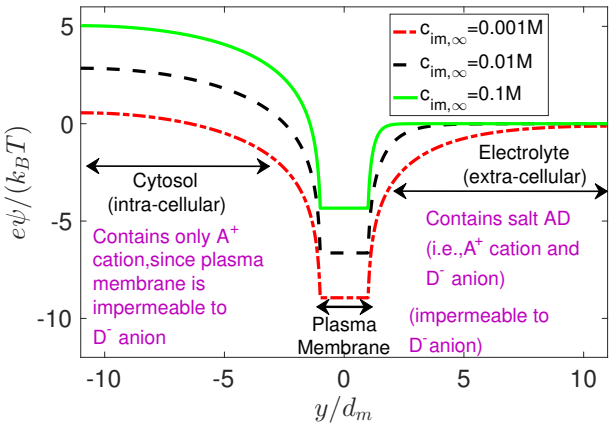

Figure 2.6: Variation of the EDL electrostatics of the semi-permeable membrane for different concentrations ($c_{im,\infty}$) of the salt AD. There is no added salt AB. Membrane is impermeable to D^- ions. Other parameters are identical to that of Fig. 3.

2.2.4 Case 2b: Negatively-charged membrane permeable to positive ions and impermeable to negative ions in presence of an external salt

In Fig. 8, we repeat the case studied in Fig. 6, but in presence of an external salt AB of concentration c_∞. Therefore, now in the ES, we have A^+, B^- and D^- ions, while in the CS there will be A^+ and B^- ions. Therefore, here too, there will be EDLs consisting of coions and counterions in both the ES and the CS. Just like the case where the negatively-charged is membrane permeable to negative ions (see Fig. 5), here too, we find that the external salt masks the impact of the semi-permeable membrane. As a consequence, the EDL-mediated electrostatics on the ES gets dictated by the value of c_∞, while the CI-like electrostatic effect gets significantly nullified in the CS (see the cases corresponding to

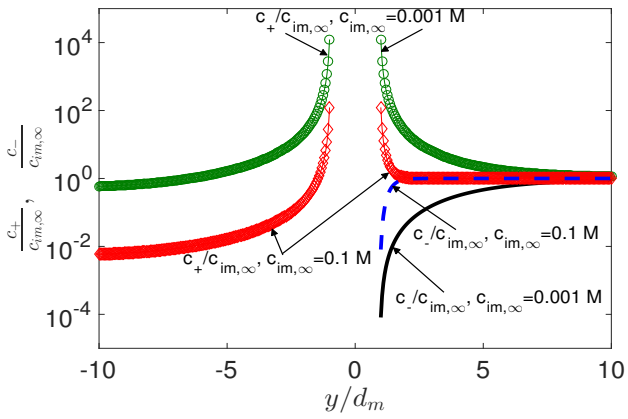

Figure 2.7: Variation of the EDL electrostatic potential and the corresponding ion distribution for $c_{im,\infty} = 0.01, 0.001\ M$ for this case where a negatively charged membrane is permeable to positive ions of the salt CB in absence of any external salt. All other parameters are identical to that of Fig. 3.

$c_\infty = 0.1\ M$). In fact, for $c_\infty = 0.1\ M$ and $c_{im,\infty} = 0.001\ M$, we obtain the case where the electrostatic potential profiles are identical in both the ES and the CS, resulting in very weak membrane potential. This conclusively proves once again that any asymmetry in the electrostatic potential and ion concentration profiles witnessed between the CS and the ES is entirely due to the semi-permeability effects of the membrane – the external salt, by nullifying the membrane permeability effect, also nullifies this asymmetry. Of course, for the case where $c_{im,\infty} \gg c_\infty$ (e.g., the case where $c_{im,\infty} = 0.1\ M$ and $c_\infty = 0.001\ M$), we recover a behavior that is characteristic of a semi-permeable negatively charged membrane permeating only positive ions (as depicted in Fig. 6).

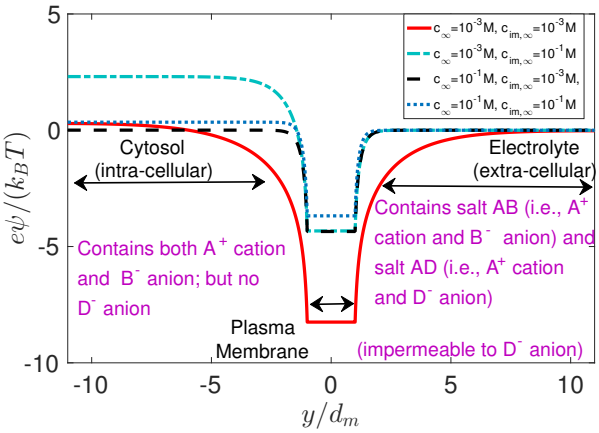

Figure 2.8: Variation of the EDL electrostatics of the semi-permeable membrane for different concentrations (c_∞) of the membrane penetrable salt AB in presence of different concentration of salt AD with membrane-impermeable anion D^-. Other parameters are same as that in Fig. 3.

2.2.5 Variation of the disjoining pressure

Fig. 9 provides the variation of the disjoining pressure Π [see eq.(21)] with concentration $c_{im,\infty}$ for Case 1 (negatively-charged membrane permeable to negative ions). Firstly, for the case where there is no external salt (i.e., case 1a, please see Figs. 3,4), we witness a large magnitude of the disjoining pressure that increases almost linearly with the concentration $c_{im,\infty}$. This large magnitude of Π can be justified from extremely large value $\bar{\psi}$ at membrane-electrolyte interface (see Fig. 3). On the other hand, the linear increase in Π with $c_{im,\infty}$ can be justified from the fact that change in concentration has little effect in changing the electrostatic potential at the membrane-electrolyte interface (see Fig. 3), while the expression for Π shows a linear increase with $n_{im,\infty}$ (or $c_{im,\infty}$) [please see eq.(21)]. Presence of an external salt invariably reduces the electrostatic potential at the membrane-electrolyte interface (see Fig. 5); as a consequence, there is a progressive

lowering in Π with an increase in c_∞ (concentration of the external salt) for a given value of $c_{im,\infty}$. Of course, such external-salt-mediated lowering of the disjoining pressure can be extremely significant ensuring the integrity of the membrane in the face of the extremely large disjoining pressure.

Fig. 10 shows the variation of the disjoining pressure Π [see eq.(21)] with concentration $c_{im,\infty}$ for Case 2 (negatively-charged membrane permeable to positive ions). We first consider the case without any external salt (i.e., Case 2a, please see Figs. 6,7). Unlike Case 1a, here Π remains virtually constant with $c_{im,\infty}$ and increases with $c_{im,\infty}$ only for relatively large values of $c_{im,\infty}$. Increase in salt concentration decreases the magnitude of the negative electrostatic potential at the membrane-cytosol interface (see Fig. 6), but at the same time increases the positive value of the electrostatic potential (ψ_0) deep within the cytosol. Such unique variation of the electrostatic potential within the cytosol, attributable to the *Charge Inversion* behavior, ensures that while the contribution of the potential at the membrane-cytosol interface to Π goes down, the contribution of the potential deep within the cytosol goes up. This justifies, in particular for low to medium ranges of $c_{im,\infty}$, why over a wide range of $c_{im,\infty}$ we witness a very little change in Π. However, when $c_{im,\infty}$ becomes large the increase in electrostatic potential deep within the cytosol gets so much augmented that it eventually overcomes the effect of lowering of the potential at the membrane-cytosol interface, thereby leading to an increase in Π. Therefore, we establish that this unique CI effect will lead to a most interesting situation – we shall witness a virtually constant Π despite an increase in concentration of impermeable ions for a semi-permeable membrane. Also it is worthwhile to note that Π for this case is invariably smaller than that for Case 1a, attributable to a lesser electrostatic potential both at the membrane-cytosol interface as well as deep within the cytosol. Fi-

nally, for this case too, we witness a progressive lowering of Π with the concentration (c_∞) of the added external permeable salt. When $c_\infty \gg c_{im,\infty}$ (e.g., when $c_\infty = 0.1\ M$ and $c_{im,\infty} = 0.001\ M$), the electrostatic potential at the membrane-cytosol interface is reduced, while $\psi_0 \approx 0$. As a consequence, Π shows a substantial reduction. On the other hand, when $c_\infty \ll c_{im,\infty}$, we recover Π values close to the no-external-salt case.

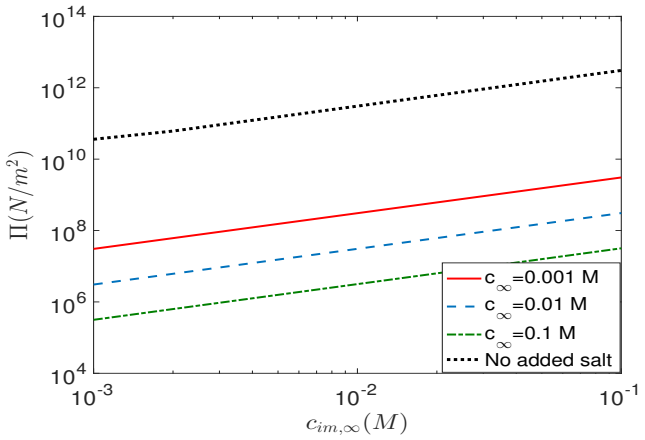

Figure 2.9: Variation of the disjoining pressure Π with $c_{im,\infty}$ (concentration of CB, where the membrane is permeable to B^- ions, but impermeable to C^+ ions) for different values of c_∞ of the permeable salt AB. Other parameters are identical to that of Fig. 3.

2.2.6 Comparison with previous study

Charge inversion like electrostatic potential in context of the electrostatics of the semi-permeable membrane has been recently reported by Maduar and Vinogradova [67]. In this subsection, we shall validate our theory by demonstrating that our theory reproduces the results of Maduar and Vinogradova. But to make this comparison, we shall first like to compare the two systems. As shown in Fig. 11(a), unlike the present case, the membrane considered by Maduar and Vinogradova is infinitely thick and also contains

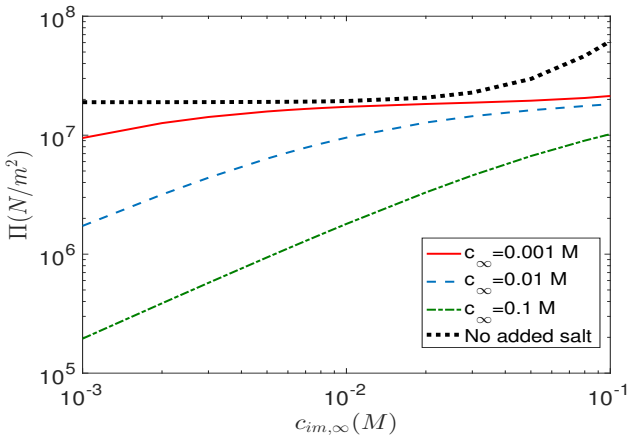

Figure 2.10: Variation of the disjoining pressure Π with $c_{im,\infty}$ (concentration of AD, where the membrane is permeable to A^+ ions, but impermeable to D^- ions) for different values of c_∞ of the permeable salt AB. Other parameters are identical to that of Fig. 3.

both positive and negative ions. On the other hand, the electrolyte solution in contact with this membrane can only contain positive ions. Therefore, the semi-permeability of the membrane is in allowing only one kind of ion (i.e., positive ions) to permeate into the electrolyte solution. Our system is different. It consists of a finite thickness membrane that does not contain any ions but exhibits its semi-permeability by ensuring that it partitions the electrolyte and cytosol sides with the electrolyte side having both positive and negative ions while the cytosol side having either only positive or only negative ions. Let us now see how we can modify our system so that it exactly represents, in terms of the ionic environment, the situation of Maduar and Vinogradova. This modification has been illustrated by comparing Figs. 11(a) and Fig. 11(b). In terms of the ion content, the electrolyte side of our configuration is equivalent to the membrane of Ref. 67 (since both of them can contain both positive and negative ions), while the cytosol side of our configuration is equivalent to the electrolyte side of Ref. 67 (since both of them can contain

only a given type of ion, which is positive ion). Therefore, if we keep on narrowing the thickness of our membrane, we shall effectively get the same configuration (in terms of ion content) as the Maduar and Vinogradova. In Figs. 11(c-f), we illustrate how our theory exactly reproduces the result of Maduar and Vinogradova by a progressive lowering of the membrane thickness.

2.3 Conclusions- Part 1

This part of the chapter unravels two highly interesting effects in the context of semi-permeable membrane EDL electrostatics: firstly, we discover a unique *Charge Inversion* like electrostatic behavior induced by the interplay of the membrane charge and its permeability, and secondly, we elucidate the role of an external permeable salt in nullifying the effects induced by the semi-permeable membrane. These findings, to the best of our knowledge, provide a hitherto unknown picture for the EDL-induced electrostatics of a semi-permeable membrane. While the calculations are based on the parameters specific to the biological plasma membrane, the findings are equally relevant to general charged, semi-permeable membranes. For example, in case the membrane is positively-charged, this CI like electrostatic behavior will be witnessed in case the membrane is permeable to negative ions and impermeable to positive ions. Of course, the model is based on the simple PB approach. Given the relatively large values of $e\psi/(k_BT)$ at the membrane-cytosol or membrane-electrolyte interfaces, a relevant future study will be to develop this semi-permeable membrane EDL electrostatics accounting for the effects of the non-PB elements like finite ion size effect, solvent polarization, and ion-ion correlations. An equally interesting future work can be to see how the consideration of the divalent and the trivalent counterions (either permeable or impermeable) may affect the overall EDL calculations

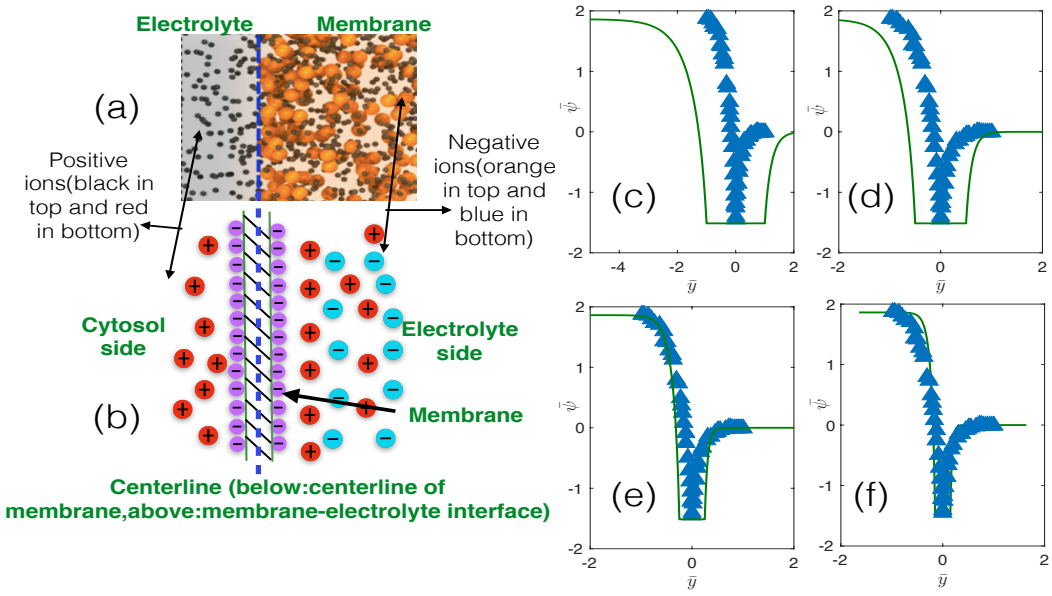

Figure 2.11: (a) Schematic of the semi-permeable-membrane-electrolyte system studied by Maduar and Vinogradova [67]. The figure has been reproduced from S. R. Maduar and O. I. Vinogradova, "Electrostatic interactions and electro-osmotic properties of semipermeable surfaces", *J. Chem. Phys.*, Vol. 145, 164703 (2016), with the permission of AIP Publishing. (b) Schematic of the membrane-cytosol-electrolyte system used in our study. The case shown here considers a negatively charged semi-permeable membrane, permeable only to positive ions. In the text (see section IIIF), we discuss how we ensure equivalence of the two systems in terms of the ion content. (c-f) Demonstration of the manner in which our theoretical result (shown as continuous line) perfectly reproduces the results of Ref. 67 (shown with filled triangle markers) when the thickness of the membrane (in our case) is progressively lowered. The comparison is carried out for the following parameter values used in Ref. 67: $\sigma_{ND} = -5$ [$\sigma_{ND} = \sigma/(\sqrt{\epsilon_0 \epsilon_r k_B T n_\infty})$ is the dimensionless charge density at the membrane-electrolyte interface] and $\lambda/h = 1/10\sqrt{2}$ [where h is the gap between the two membranes and $\lambda = \sqrt{\epsilon_0 \epsilon_r k_B T/(2 n_\infty e^2)}$ is the EDL thickness].

– we anticipate that for this case, the membrane electrostatics might well be dictated by a relative interplay of the CI-like-electrostatic inducing effects of the membrane (i.e., the effect studied in this chapter) with the actual CI effects induced by the multivalent counterions.

2.4 Derivation of the governing P-B equations for the membrane EDL electrostatics

We start with the free energy F of the system expressed as:

$$\begin{aligned} F = \quad & \int \left[\int_{-d_c-d_m}^{-d_m} f_c dy + \int_{-d_m}^{d_m} f_m dy + \int_{d_m}^{d_e+d_m} f_e dy \right] d^2\mathbf{r} \\ & + \int \left[\sigma\psi_{s,m-c} + \sigma\psi_{s,m-e} \right] d^2\mathbf{r}. \end{aligned} \tag{2.30}$$

In the above equation, $\psi_{s,m-c}$ and $\psi_{s,m-e}$ are the electrostatic potentials at the membrane-cytosol and membrane-electrolyte interfaces and f_c, f_m, and f_e are the electrostatic energy densities inside the cell, within the membrane, and outside the cell (i.e., within the electrolyte), respectively. Depending on the particular case (Case 1 or Case 2), expressions of these different energy densities will vary, as shown below:

$$\begin{aligned} (f_c)_{Case1} &= -\frac{\epsilon_0\epsilon_c}{2}|\frac{d\psi}{dy}|^2 + e\psi\left(n_{A^+} - n_{B^-}\right) \\ &+ k_BT\left[n_{A^+}\left(\ln\left(\frac{n_{A^+}}{n_{A^+,\infty}} \right) - 1 \right) + n_{B^-}\left(\ln\left(\frac{n_{B^-}}{n_{B^-,\infty}} \right) - 1 \right) \right], \end{aligned} \tag{2.31}$$

$$(f_m)_{Case1} = -\frac{\epsilon_0\epsilon_m}{2}|\frac{d\psi}{dy}|^2, \tag{2.32}$$

$$(f_e)_{Case1} = -\frac{\epsilon_0\epsilon_e}{2}|\frac{d\psi}{dy}|^2 + e\psi\left(n_{A^+} - n_{B^-} + n_{C^+}\right) +$$
$$k_BT\left[n_{A^+}\left(\ln\left(\frac{n_{A^+}}{n_{A^+,\infty}}\right) - 1\right) + n_{B^-}\left(\ln\left(\frac{n_{B^-}}{n_{B^-,\infty}}\right) - 1\right) + n_{C^+}\left(\ln\left(\frac{n_{C^+}}{n_{C^+,\infty}}\right) - 1\right)\right] \quad (2.33)$$

On the other hand, for case 2 we can write:

$$\begin{aligned}(f_c)_{Case2} &= -\frac{\epsilon_0\epsilon_c}{2}|\frac{d\psi}{dy}|^2 + e\psi\left(n_{A^+} - n_{B^-}\right) \\ &+ k_BT\left[n_{A^+}\left(\ln\left(\frac{n_{A^+}}{n_{A^+,\infty}}\right) - 1\right) + n_{B^-}\left(\ln\left(\frac{n_{B^-}}{n_{B^-,\infty}}\right) - 1\right)\right], \quad (2.34)\end{aligned}$$

$$(f_m)_{Case2} = -\frac{\epsilon_0\epsilon_m}{2}|\frac{d\psi}{dy}|^2, \quad (2.35)$$

$$(f_e)_{Case2} = -\frac{\epsilon_0\epsilon_e}{2}|\frac{d\psi}{dy}|^2 + e\psi\left(n_{A^+} - n_{B^-} - n_{D^-}\right) +$$
$$k_BT\left[n_{A^+}\left(\ln\left(\frac{n_{A^+}}{n_{A^+,\infty}}\right) - 1\right) + n_{B^-}\left(\ln\left(\frac{n_{B^-}}{n_{B^-,\infty}}\right) - 1\right) + n_{D^-}\left(\ln\left(\frac{n_{D^-}}{n_{D^-,\infty}}\right) - 1\right)\right] \quad (2.36)$$

In the above equations, $n_{A^+,\infty}$, $n_{B^-,\infty}$, $n_{C^+,\infty}$, and $n_{D^-,\infty}$ are the bulk number densities of the A^+, B^-, C^+, and D^- ions. For case 1 [(represented by eqs.(2.31-2.33)], $n_{A^+,\infty} = n_\infty$, $n_{B^-,\infty} = n_\infty + n_{im,\infty}$, and $n_{C^+,\infty} = n_{im,\infty}$. On the other hand, for case 2 [represented by eqs. (2.34-2.36)], $n_{A^+,\infty} = n_\infty + n_{im,\infty}$, $n_{B^-,\infty} = n_\infty$, and $n_{D^-,\infty} = n_{im,\infty}$. Further in the above equations, ϵ_0 is the permittivity of free space, k_BT is the thermal energy, e is the electronic charge, and ϵ_e, ϵ_m and ϵ_c are the relative permittivities of the electrolyte, membrane, and the cytosol, respectively.

Eq. (2.30) can be minimized with respect to ψ, n_{A^+}, n_{B^-}, and n_{C^+} for Case 1 and with respect to ψ, n_{A^+}, n_{B^-}, and n_{D^-} for case 2 yielding the equilibrium conditions (or the governing equations) as summarized in the main text.

2.5 Derivation of eq.(5.15)- The membrane electrolyte and cytosol interface BC

Considering ψ_s to be either $\psi_{s,m-c}$ or $\psi_{c,m-e}$ and ϵ_r to be a general relative permittivity, we may write:

$$\begin{aligned}&\frac{\delta F}{\delta \psi_s} = 0,\\ &\Rightarrow \frac{\delta}{\delta \psi_s}\left[\int -\frac{\epsilon_0\epsilon_r}{2}|\frac{d\psi}{dy}|^2 d^3\mathbf{r}\right] + \frac{\delta}{\delta \psi_s}\left[\int \sigma\psi_s d^2\mathbf{r}\right] = 0.\end{aligned} \tag{2.37}$$

Let us define

$$\frac{d\phi}{dy} = \left(\frac{d\psi}{dy}\right)^2, \tag{2.38}$$

and similarly

$$\frac{d\phi_s}{dy} = \left(\frac{d\psi_s}{dy}\right)^2. \tag{2.39}$$

Consequently, employing divergence theorem, we may write:

$$\begin{aligned}-\int \frac{\epsilon_0\epsilon_r}{2}|\frac{d\psi}{dy}|^2 d^3\mathbf{r} \quad &= -\frac{\epsilon_0\epsilon_r}{2}\int \left(\frac{d\phi}{dy}\right) d^3\mathbf{r}\\ &= -\frac{\epsilon_0\epsilon_r}{2}\int \phi_s d^2\mathbf{r}\end{aligned} \tag{2.40}$$

Using eq.(2.40) in eq.(2.37), we can write:

$$\frac{\delta F}{\delta \psi_s} = 0 \Rightarrow \frac{\delta}{\delta \psi_s}\int \left[-\frac{\epsilon_0\epsilon_r}{2}\phi_s + \sigma\psi_s\right] d^2\mathbf{r} = 0. \tag{2.41}$$

Eq.(2.41) implies

$$\begin{aligned}
&\frac{\delta}{\delta\psi_s}\left[-\frac{\epsilon_0\epsilon_r}{2}\phi_s+\sigma\psi_s\right]=0\\
&\Rightarrow -\frac{\epsilon_0\epsilon_r}{2}\frac{\partial\phi_s}{\partial\psi_s}+\frac{\epsilon_0\epsilon_r}{2}\frac{d}{dy}\left(\frac{\partial\phi_s}{\partial\psi_s'}\right)+\sigma=0\\
&\Rightarrow \frac{\epsilon_0\epsilon_r}{2}\frac{\partial}{\partial\psi_s'}\left(\frac{d\phi_s}{dy}\right)+\sigma=0\\
&\Rightarrow \frac{\epsilon_0\epsilon_r}{2}\frac{\partial}{\partial\psi_s'}\left(\psi_s'^2\right)+\sigma=0\Rightarrow\epsilon_r\psi_s'=-\frac{\sigma}{\epsilon_0}.
\end{aligned}\tag{2.42}$$

Consequently. we should get:

$$\begin{aligned}
&\left(\epsilon_m\frac{d\psi}{dy}\right)_{y=-d_m^-}-\left(\epsilon_c\frac{d\psi_1}{dy}\right)_{y=-d_m^+}=-\frac{\sigma}{\epsilon_0},\\
&\left(\epsilon_e\frac{d\psi}{dy}\right)_{y=d_m^-}-\left(\epsilon_m\frac{d\psi_2}{dy}\right)_{y=d_m^+}=-\frac{\sigma}{\epsilon_0}.
\end{aligned}\tag{2.43}$$

2.6 Derivation of the governing equations for the case studied in Maduar and Vinogradova [67] using the equations for the present problem

Maduar and Vinogradova [67] considered an infinite membrane (extending from $h/2 \leq x < \infty$) containing small cations (with a valence z, with $z > 0$) and large anions (with a valence Z, with $Z < 0$). The membrane is in contact with a finite thickness (extending from $0 \leq x \leq h/2$) of an electrolyte solution. The membrane semi-permeability is reflected in terms of only the cations being able to leave the membrane and go into the electrolyte solution, while the anions remain confined within the semi-infinite membrane. Also the membrane-electrolyte interface is charged. We now try to see if eqs.(2.5,5.15,5.24) of our model can be modified to yield the governing equations of Maduar and Vinogradova [67]. Here the membrane is permeable to negative ions [hence we consider eq.(2.5)]. Also there is no cytosol and the membrane (containing both cations and anions without any external

permeable salt) have semi-infinite extension. Consequently, the first important issue is that the first equation of eq.(2.5), representing the equation within the cytosol, is non-existent. Secondly, both cations and anions are present within the membrane and the membrane extends between $h/2 \leq x < \infty$ (considering only the right half of the system). Thirdly, the electrolyte is confined between $0 \leq x \leq h/2$ and contains only positive ions, since the membrane does not allow the passage of the large-sized negative ions from the membrane interior to the electrolyte solution. Fourthly, the relative permittivities (ϵ) both inside and outside the membrane are identical. Fifthly, there is only one interface (membrane-electrolyte interface), where a charge density is specified. Finally, the coordinates are described in terms of "x" and not "y".

Under these conditions, we can express eq.(2.5) as:

$$\begin{aligned} \frac{d^2\psi}{dx^2} &= -\frac{e\left(zn_+ + Zn_-\right)}{\epsilon\epsilon_0} \quad h/2 \leq x < \infty, \\ \frac{d^2\psi}{dx^2} &= -\frac{e\left(zn_+\right)}{\epsilon\epsilon_0} \quad 0 \leq x \leq h/2, \end{aligned} \tag{2.44}$$

where $n_\pm$ are the number densities of the cations and anions. Of course, we can use the Boltzmann distribution [similar to eq.(2.6)] to express $n_\pm$ as:

$$n_+ = n_\infty \exp\left(-\frac{ez\psi}{k_B T}\right), \quad n- = N_\infty \exp\left(-\frac{eZ\psi}{k_B T}\right), \tag{2.45}$$

where n_∞ and N_∞ are the bulk concentrations of the cations and the anions respectively. Of course, n_∞ and N_∞ are related to each other as (due to the electroneutrality condition):

$$ZN_\infty + zn_\infty = 0 \tag{2.46}$$

Of course the above equation reduces to $N_\infty = n_\infty$ for our studied case where $z = 1$ and $Z = -1$. Using eqs.(2.45,2.46) we can rewrite eq.(2.44) as:

$$\frac{d^2\psi_o}{dx^2} = -\frac{ezn_\infty}{\epsilon\epsilon_0}\left[\exp\left(-\frac{ez\psi_0}{k_BT}\right) - \exp\left(-\frac{eZ\psi_0}{k_BT}\right)\right] \quad h/2 \leq x < \infty,$$
$$\frac{d^2\psi_i}{dx^2} = -\frac{ezn_\infty}{\epsilon\epsilon_0}\exp\left(-\frac{ez\psi_i}{k_BT}\right) \quad 0 \leq x \leq h/2, \tag{2.47}$$

where ψ_o and ψ_i are the electrostatic potential outside the electrolyte (i.e., inside the membrane) and inside the electrolyte (i.e., outside the membrane). Considering a dimensionless potential $\phi_{i,o} = ez\psi_{i,o}/(k_BT)$, $\tilde{Z} = Z/z$, and an inverse EDL thickness κ_i [where $\kappa_i^2 = z^2e^2n_\infty/(\epsilon\epsilon_0 k_BT)$], we can re-write eq.(2.47) as:

$$\frac{d^2\phi_o}{dx^2} = -\kappa_i^2\left[\exp\left(-\phi_o\right) - \exp\left(-\tilde{Z}\phi_o\right)\right] \quad h/2 \leq x < \infty$$
$$\frac{d^2\phi_i}{dx^2} = -\kappa_i^2\exp\left(-\phi_i\right) \quad 0 \leq x \leq h/2. \tag{2.48}$$

Eq.(2.48) is exactly identical to eqs.(1,2) in Maduar and Vinogradova [67].

The stress jump boundary condition at the membrane electrolyte interface [the one equivalent to eq.(5.15)] reduces to (with $\epsilon_e = \epsilon_m = \epsilon$ and $\tilde{\sigma}$ replacing σ, since $\tilde{\sigma}$ represents the dimensional charge density in Ref. [67]):

$$\left(\frac{d\psi}{dx}\right)_{(x=h/2)^+} - \left(\frac{d\psi}{dx}\right)_{(x=h/2)^-} = -\frac{\tilde{\sigma}}{\epsilon\epsilon_0} \tag{2.49}$$

Consequently, we get:

$$\left(\frac{d\phi_i}{dx}\right)_{x=h/2} - \left(\frac{d\phi_o}{dx}\right)_{x=h/2} = \kappa_i\sigma, \tag{2.50}$$

where $\sigma = \frac{4\pi\ell_B\tilde{\sigma}/e}{\kappa_i}$ [with $\ell_B = z^2e^2/(4\pi\epsilon\epsilon_0 k_BT)$ being the Bjerrum length] is the dimensionless charge density in Maduar and Vinogradova [67]. Please note that in our theory,

we use σ as the dimensional charge density, while in Ref. 67 σ is considered a dimensionless charge density. Eq.(2.50) is the boundary condition expressed in eq.(3) in Ref. [67]. Other boundary conditions in Maduar and Vinogradova are the symmetry at the electrolyte centreline (i.e., $d\phi_i/dx = 0$ at $x = 0$) and equality of the electrostatic potential at the electrolyte-membrane interface. These same boundary conditions are also present for the case we study – please see the 3rd and the 4th boundary conditions in eq.(5.24), where the condition $(\psi)_{y=d_m^+} = (\psi)_{y=d_m^-}$ is equivalent to $(\phi_o)_{x=h/2} = (\phi_i)_{x=h/2}$ and the condition $\left(\frac{d\psi}{dy}\right)_{y=(d_m+d_e)} = 0$ is equivalent to $\left(\frac{d\phi_i}{dx}\right)_{x=0}$. Finally, the boundary condition deep within the membrane in Ref. [67] is that of zero potential, i.e., $(\phi_o)_{x\to\infty} = 0$. On the other hand, we have considered an equivalent finite cytosol, so that this last boundary condition is a symmetry condition at the cytosol centerline.

Through this appendix section we establish, therefore, that we can recover the governing equations and boundary conditions dictating the membrane electrostatics of an existing study [67] from our set of equations and boundary conditions. Of course, we have solved these same set of equations as that expressed Maduar and Vinogradova [67] and have recovered their results – we do not repeat those simulations here for the sake of brevity.

2.7 Counterion-only EDL electrostatics in the cytosol side in absence of an external salt: Debye-Hückel analysis

For this case, the counterion-only EDL developed in the cytosol side consists of only A^- ions. Consequently, the EDL electrostatics can be described as:

$$\frac{d^2\psi}{dy^2} = -\frac{en_{A^-}}{\epsilon_0\epsilon_c} = -\frac{en_{im,\infty}\exp\left(-\frac{e\psi}{k_BT}\right)}{\epsilon_0\epsilon_c} \approx -\frac{en_{im,\infty}\left(1-\frac{e\psi}{k_BT}\right)}{\epsilon_0\epsilon_c} \Rightarrow \frac{d^2\bar{\psi}}{d\bar{y}^2} = \frac{\bar{\psi}}{2\bar{\lambda}^2} - \frac{1}{2\bar{\lambda}^2}, \tag{2.51}$$

where $\bar{\psi} = e\psi/(k_BT)$, $\bar{y} = y/d_m$, $\bar{\lambda} = \lambda/d_m$ ($\lambda = \sqrt{\epsilon_0\epsilon_c k_BT/(2n_{im,\infty}e^2)}$).

Eq.(2.51) can be solved analytically in presence of the following dimensionless boundary conditions:

$$\left(\frac{d\bar{\psi}}{d\bar{y}}\right)_{\bar{y}=-1} = K, \quad \left(\frac{d\bar{\psi}}{d\bar{y}}\right)_{\bar{y}=-1-d_c/d_m} = 0, \tag{2.52}$$

where $K = \bar{\sigma}/\bar{\lambda}^2$ and $\bar{\sigma} = \sigma/(2n_{im,\infty}ed_m)$. This analytical solution yields the expression for $\bar{\psi}$ (valid between $-1 - d_c/d_m \leq y \leq -1$) as:

$$\bar{\psi} = \frac{\sqrt{2}K\bar{\lambda}}{\exp\left(\frac{2\frac{d_c}{d_m}+1}{\sqrt{2}\bar{\lambda}}\right) - \exp\left(\frac{1}{\sqrt{2}\bar{\lambda}}\right)}\left[\exp\left(\frac{2(\frac{d_c}{d_m}+1)}{\sqrt{2}\bar{\lambda}}\right)\exp\left(\frac{\bar{y}}{\sqrt{2}\bar{\lambda}}\right) + \exp\left(\frac{-\bar{y}}{\sqrt{2}\bar{\lambda}}\right)\right] + 1. \tag{2.53}$$

From eq.(2.53), we can obtain:

$$\left(\bar{\psi}\right)_{\bar{y}=-1} = \sqrt{2}\frac{\bar{\sigma}}{\bar{\lambda}}\coth\left(\frac{\bar{d}_c}{\sqrt{2}\bar{\lambda}}\right) + 1, \tag{2.54}$$

and

$$\left(\bar{\psi}\right)_{\bar{y}=-1-d_c/d_m} = \sqrt{2}\frac{\bar{\sigma}}{\bar{\lambda}}\frac{1}{\sinh\left(\frac{\bar{d}_c}{\sqrt{2}\bar{\lambda}}\right)} + 1. \tag{2.55}$$

Given that $d_c \gg \lambda$, we can easily identify why $\left(\bar{\psi}\right)_{\bar{y}=-1-d_c/d_m} \approx 1$, while $\left(\bar{\psi}\right)_{\bar{y}=-1} \approx \sqrt{2}\frac{\bar{\sigma}}{\bar{\lambda}}+1$. Therefore, while $\bar{\psi}$ is invariably positive deep within the cytosol, whether or not $\bar{\psi}$ will be negative at the membrane-cytosol interface is dictated by the value of $\bar{\sigma}/\bar{\lambda}$. For example, for the present case of $\sigma = -1\ e/nm^2$, we witness $\left(\bar{\psi}\right)_{\bar{y}=-1} < 0$ (for all values of $c_{im,\infty}$ studied here), which will ensure a *Charge Inversion* like electrostatic phenomenon. On the other hand, for a much smaller magnitude of σ (e.g., $\sigma = -10^{-3}\ e/nm^2$), we shall witness $\left(\bar{\psi}\right)_{\bar{y}=-1} > 0$ (for all values of $c_{im,\infty}$ studied here), i.e., there will be no *Charge Inversion* like electrostatic phenomenon.

2.8 Positive zeta potential of a negatively-charged semi-permeable plasma membrane- Part 2

The negative charge of the plasma membrane (PM) severely affects the nature of the moieties that may enter or leave the cells as well as controls a large number of ion-interactions-mediated intracellular and extracellular events. In this letter, we report our discovery of a most fascinating scenario, where one interface (e.g., membrane-cytosol interface) of the negatively charged PM shows a positive surface (or ζ) potential, while the other interface (e.g., membrane-electrolyte interface) still shows a negative ζ potential. Therefore, we encounter a completely unexpected situation where an interface (e.g., membrane-cytosol interface) that has a negative surface charge density demonstrates a positive ζ potential. We establish that the attainment of such a property by the membrane can be ascribed to an interplay of the nature of the membrane semi-permeability and the electrostatics of the electric double layer (or EDL) established on either side of the charged membrane. We anticipate that such a membrane property can lead to such

capabilities of the cell (in terms of accepting or releasing certain kinds of moieties as well regulating cellular signaling) that was hitherto inconceivable.

Semi-permeable plasma membranes (PMs) surrounding biological cells play a vital role in dictating the traffic in and out of the cell and governing cellular signaling [28,69–76]. While the phospholipid bilayer architecture of the membrane makes it impermeable to ions, the opening up of the ion channels [11, 12] present in the membrane architecture makes it permeable to small ions. This ensures that the PM becomes semi-permeable and the ion exchange controlling the signal transduction vital for the survival and functioning of the cells becomes possible [13, 14]. Additionally, the negative charge density of the PM (or analogously the charge density of the membrane-electrolyte and membrane-cytosol interfaces), along with this semi-permeable nature of the membrane (the effect of the semi-permeability depends on the nature of the ions present inside and outside the cell), dictates the equilibrium ion distribution across the membrane in the form of the two electric double layers (EDLs) that develop at the membrane-cytosol interface (MCI) and membrane-electrolyte interface (MEI) [1, 17, 34, 36, 47, 49, 67, 77].

This ion distribution, bearing the signature of the negative charge density of the PM, is responsible for a large number of biophysical and physiological events such as the ATP synthesis by mitochondria [18], control of the intracellular Ca^{2+} ions [19, 20] (that in turn regulate intracellular functions like signal transduction [78], activity of the calmodulin-regulated enzymes [79], functioning of mitochondria [80], etc.), death of cancer cells [21], cell-antibody interactions [81], light-induced cellular excitation [82], binding of proteins to membranes using the cationic head group of the proteins [85, 86], use of the cationic cell-penetrating peptides for delivering cargo to the cells [87, 88], localization of components that control the cellular signaling in plants like *Arabidopsis* [89], regulation

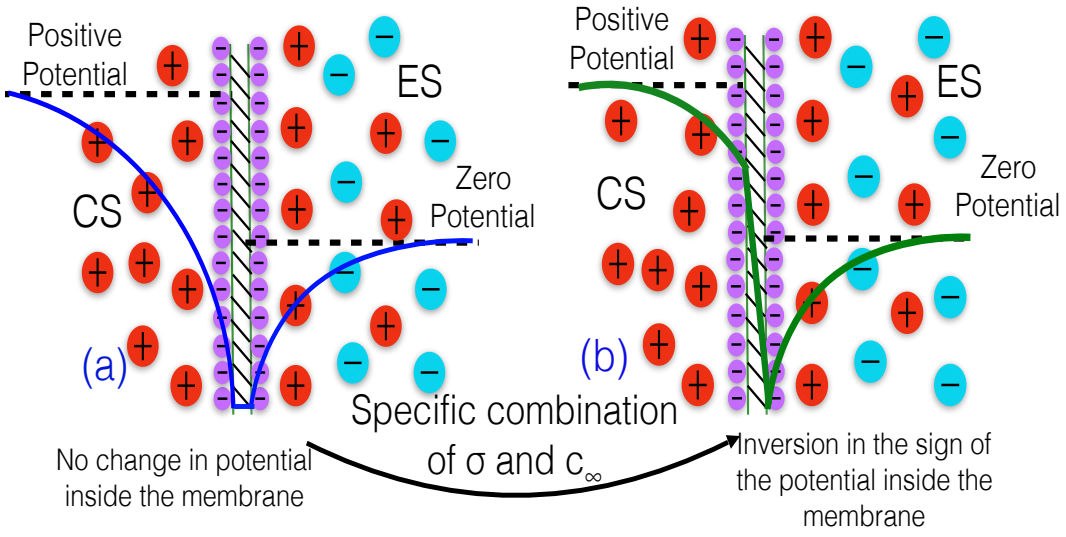

Figure 2.12: Schematic of the negatively-charged semi-permeable plasma membrane, permeable to positive ions of the salt AD. Therefore, both A^+ and D^- ions exist in the electrolyte side (ES), while only A^+ ions exist in the cytosol side (CS). (a) Schematic of the potential distribution across the membrane. We consider that $\sigma - c_\infty$ combination that ensures that ζ potential at both the membrane-cytosol and membrane-electrolyte interfaces are negative. We find a CI-like electrostatic behavior at the cytosol centerline, as witnessed in our previous study [77]. (b) Schematic of the potential distribution across the membrane. We consider that specific $\sigma - c_\infty$ combination for which the membrane attains a positive ζ potential at the MCI, but a negative ζ potential at the MEI.

of nanoparticle-membrane interactions for successful drug delivery [156], and many more. In this part of this chapter, we report our discovery where such negatively-charged PM demonstrates a most extraordinary and hitherto unknown situation where one side of the PM remains negative (demonstrating a negative ζ potential), but the other side becomes positive (demonstrating a positive ζ potential) [see Fig. 1(b)]. Therefore for this "other" side, we get a highly non-intuitive situation where there exists a ζ potential and a surface charge density of opposite signs at a given interface – such a scenario has been known

for materials like glass exhibiting chemical equilibrium boundary condition [91], but has not been unravelled for a bilayer membrane. The critical question here is: *Which is this "other side" that demonstrates a positive ζ potential?* This is the side where the ion distribution gets affected by the semi-permeable nature of the membrane. For example, if the extracellular or the electrolyte side (ES) contains both positive and negative ions and the negatively charged membrane is permeable only to positive ions, then the intracellular or the cytosol side (CS) will develop a counterion-only (or cation-only) EDL – consequently, it will be the MCI that will show a positive ζ potential. On the other hand, if the ES is affected (in terms of the ion distribution) due to this membrane semi-permeability, the MEI will demonstrate a positive ζ potential. Of course, the inception of this positive ζ potential becomes only possible for certain specific conditions, namely a combination of (a) a relatively weak magnitude of σ, (b) a large (biologically-relevant) concentration (c_∞) of the salt, and (c) a negatively-charged membrane permeating only positive ions (see Fig. 1). In this letter, we demonstrate the attainment of this property by the membrane (where $\zeta_{MCI} > 0$) considering that the CS gets affected due to the membrane semi-permeability. We provide a detailed phase-space of the parameters ($\sigma - c_\infty$ combination) where this situation of $\zeta_{MCI} > 0$ is witnessed. Finally, we end with specific examples where this particular membrane property may significantly impact biological and physiological events as well as non-biological applications in a manner that has remained elusive till date.

2.9 Theory

We consider a semi-permeable lipid bilayer PM, as shown in Fig. 1(a). We consider the membrane to be negatively charged – both the MCI and MEI have a charge density of σ (where $\sigma < 0$). For the present case, we consider that the ES contains a symmetric

monovalent salt AD, furnishing a monovalent cation A^+ and a monovalent anion D^-. The semi-permeable membrane is considered to be impermeable to negative ions but permeable to positive ions. We have developed the EDL electrostatic theory for such a case in a previous paper [77]. Here we briefly discuss this theory – the central findings of this present paper stems from studying the electrostatic properties of the PM for conditions that were missed in our previous paper [77]. The membrane will develop two separate EDLs – an EDL each at the MEI and the MCI. The equation governing the EDL electrostatic potential ψ in the entire system can be expressed as:

$$\begin{aligned}
&\frac{d^2\psi}{dy^2} = -\frac{n_{A^+}}{\epsilon_0\epsilon_c} \quad for \;\; -(d_m + d_c) \leq y \leq -d_m, \\
&\frac{d^2\psi}{dy^2} = 0 \qquad\quad for \;\; -d_m \leq y \leq d_m, \\
&\frac{d^2\psi}{dy^2} = -\frac{n_{A^+} - n_{D^-}}{\epsilon_0\epsilon_e} \quad for \;\; d_m \leq y \leq (d_m + d_e).
\end{aligned} \tag{2.56}$$

In the above equation, n_{A^+} and n_{D^-} are the number densities of the A^+ and D^- ions, ϵ_0 is the permittivity of free space, ϵ_c, ϵ_m, and ϵ_e are the relative permittivities of the cytosol, membrane, and electrolyte, $2d_m$ is the membrane thickness (hence the MEI and the MCI are located at $y = +d_m$ and $y = -d_m$, respectively), and $d_e + d_m$ and $-d_c - d_m$ denote the electrolyte and the cytosol centrelines. Eq.(1) clearly shows the influence of the membrane semi-permeability – while the ψ distribution on the ES depends on the number densities of both A^+ and D^- ions, ψ on the CS depends on the number density of only A^+ ions. Finally, the membrane itself cannot contain any ion – hence ψ within the membrane has no dependence on the number density of the ions. n_{A^+} and n_{D^-} appearing in eq.(1) can be expressed using the Boltzmann distribution as:

$$n_{A^+} = n_\infty \exp\left(-\frac{e\psi}{k_B T}\right), \quad n_{D^-} = n_\infty \exp\left(\frac{e\psi}{k_B T}\right), \tag{2.57}$$

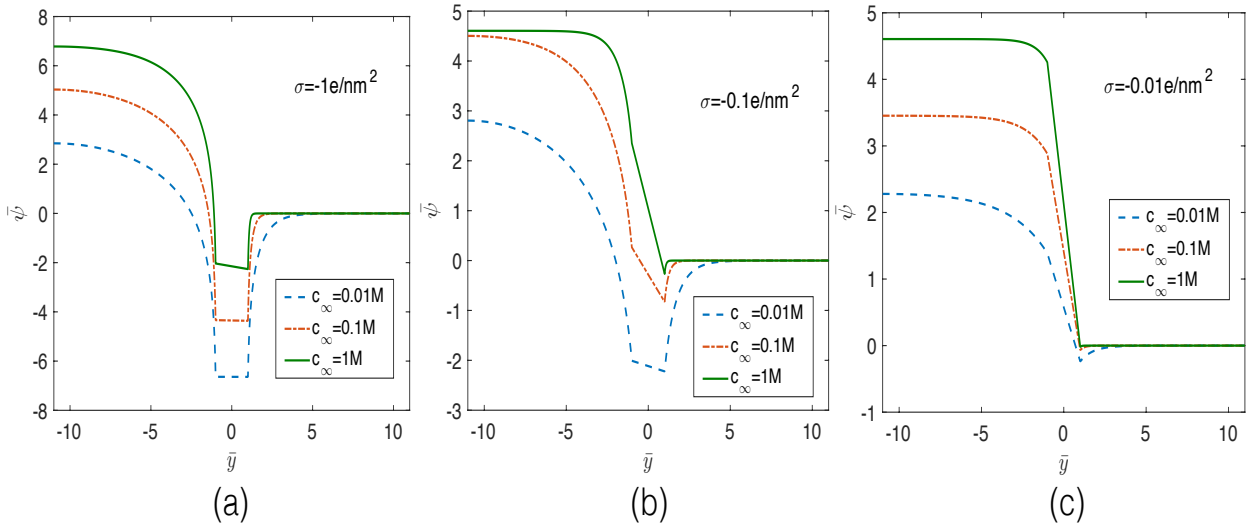

Figure 2.13: Variation of the dimensionless EDL electrostatic potential $\bar{\psi} = e\psi/(k_B T)$ with $\bar{y} = y/d_m$ for the different values of concentration of the salt AD for (a) $\sigma = -1\ e/nm^2$, (b) $\sigma = -0.1\ e/nm^2$, and (c) $\sigma = -0.01\ e/nm^2$.

where $k_B T$ is the thermal energy and $n_\infty = 10^3 N_A c_\infty$ is the bulk number density of the salt AD (c_∞ is the bulk concentration of the salt AD in M and N_A is the Avogadro number). The equation that results by using eq.(2) in eq.(1) is finally solved numerically (see [77] for discussion on the detailed numerical procedure) in presence of the following boundary conditions:

$$\begin{aligned}
&\left(\epsilon_m \frac{d\psi}{dy}\right)_{y=-d_m^+} - \left(\epsilon_c \frac{d\psi}{dy}\right)_{y=-d_m^-} = -\frac{\sigma}{\epsilon_0}, \\
&\left(\epsilon_e \frac{d\psi}{dy}\right)_{y=d_m^+} - \left(\epsilon_m \frac{d\psi}{dy}\right)_{y=d_m^-} = -\frac{\sigma}{\epsilon_0}, \\
&\left(\frac{d\psi}{dy}\right)_{y=-(d_m+d_c)} = 0, \quad (\psi)_{y=-d_m^+} = (\psi)_{y=-d_m^-}, \\
&(\psi)_{y=d_m^+} = (\psi)_{y=d_m^-}, \quad \left(\frac{d\psi}{dy}\right)_{y=(d_m+d_e)} = 0.
\end{aligned} \tag{2.58}$$

2.10 Results

Fig. 2.13 shows the variation of the electrostatic potential ψ across the membrane (located in $-1 \leq \bar{y} \leq 1$, where $\bar{y} = y/d_m$) for different values of membrane charge density σ and the concentration of the salt c_∞. We witness (explained in details later), the most remarkable situation where for a negatively charged semi-permeable bilayer membrane, the MCI attains a positive surface (or ζ) potential while the MEI retains a negative surface (or ζ) potential in presence of relatively weaker values of σ and larger (or biologically-relevant) values of c_∞. This is the central result of the paper.

We first consider the case of a large magnitude of σ, i.e., $\sigma = -1\ e/nm^2$ [see Fig. 2.13(a)]. Firstly, we can note that at the MCI, the sign of $d\psi/dy$ both at the membrane and cytosol sides is negative. This directly follows from the corresponding electrostatic stress jump condition at the MCI (i.e., at $y = -d_m$) [see eq. (3)]. Things are different, however, at the MEI. A large negative σ leads to a large negative ζ potential at the MEI, given that the EDL in the ES consists of both cations and anions. More importantly, this large σ leads to a large jump in the electrostatic stress at the membrane-electrolyte interface – consequently, despite a large positive $d\psi/dy$ on the electrolyte side of the MEI, we witness not only a very weak $|d\psi/dy|$ at the membrane side of the MEI but also a changed sign of the $d\psi/dy$ on the membrane side of the MEI [dictated by the electrostatic stress jump condition at the MEI, see eq.(3)]. Such a scenario becomes very much evident, particularly for large c_∞, from the values of the dimensionless electrostatic potential gradient on the membrane and the electrolyte sides of the MEI, as illustrated in Table S1 in the Supplementary Material (SM). The small negative magnitude of $d\psi/dy$ on the membrane side of the MEI ensures virtually horizontal $\psi - vs - y$ variation within the membrane

(since $d\psi/dy$ remains constant within the membrane); consequently, the ζ potential at the MCI is very similar to that of the MEI and hence negative. The increase in the salt concentration decreases the EDL thickness (λ) and consequently decreases the magnitude of the ζ potential at both the MEI and the MCI. This decrease in ζ potential can be ascribed to the fact that $|\zeta| \propto \lambda|\sigma|$. Of course, the respective behaviors of the ψ profiles in the ES and the CS are dictated by the nature of the ions constituting the EDL. For the ES, the EDL being constituted by both the coions and counterions, one witnesses a standard EDL behavior where the electrostatic potential decays away from the charged MEI and larger salt concentration leads to a steeper decay (or smaller λ). On the other hand, in the CS the semi-permeability of the membrane ensures a pure counterion-only EDL [77], which in conjunction with the symmetry boundary condition at the cytosol centerline [see eq.(3)], leads to the most remarkable charge-inversion-like (CI-Like) electrostatics. This CI-like behavior is quantified by ψ changing sign from negative (at the MCI) to positive at the cytosol centerline. In our recent paper, we have identified this CI-like electrostatic behavior, which is a characteristic of the counterion-only EDL system witnessed for the case of a semi-permeable membrane [77].

We next consider the case of $\sigma = -0.1\ e/nm^2$ [see Fig. 2.13(b)]. Here a weak value of σ leads to a weak value of ζ potential at the MEI. σ being small, the jump in the electrostatic stress is also small. However, the corresponding reduction in the positive value of the electrostatic potential gradient on the electrolyte side of the MEI outweighs the reduction in the negative magnitude of σ (see Table S1 in the SM). Combination of these factors ensures that $d\psi/dy$ not only changes sign on the membrane side of the MEI, but it also has a much larger negative value (see Table S1 in the SM)). Since the membrane does not contain any charge, $d\psi/dy$ remains constant (at this large negative value) within

the membrane, leading to a finite decrease in the negative magnitude of ψ from the MEI to the MCI (see the result corresponding to $c_\infty = 0.01\ M$). The most intriguing situation, where the MCI develops a positive ζ potential, sets in for larger (biologically relevant) values of salt concentration ($c_\infty = 0.1, 1\ M$). For these values of c_∞, the ζ potential of the MEI interface is small and consequently $d\psi/dy$ on electrolyte side of the MEI is also very small. As a consequence, even this weak electrostatic stress jump condition (caused by the small negative σ) ensures an even larger (as compared to the case of $c_\infty = 0.01\ M$) negative gradient of the electrostatic potential (i.e., $d\psi/dy < 0$) on the membrane side of the MEI (see Table S1 in the SM). As a result, the electrostatic potential inverts sign across the membrane ensuring a positive ζ potential at the MCI. Thus we now have $\zeta_{MCI} > 0$ but $\zeta_{MEI} < 0$. Furthermore, such a situation implies that the MCI, despite having a negative surface charge density, exhibits a positive ζ potential. Opposite signs of the ζ potential and the charge density at a given interface have been witnessed for systems like glass surfaces [91], but has not been witnessed for any membrane or biologically relevant surfaces. Of course, an increase in c_∞ from 0.1 M to 1 M causes a further decrease in $d\psi/dy$ on the electrolyte side of the MEI, ensuring that the electrostatic stress jump condition makes the negative value of $d\psi/dy$ on the membrane side of the MEI even larger (see Table S1 in the SM). As a consequence, one witnesses an even larger positive value of ζ at the MCI. We finally study this ψ variation for even smaller σ i.e., $\sigma = -0.01\ e/nm^2$ [see Fig. 2(c)]. For this σ value too, the decrease in the positive magnitude of $d\psi/dy$ on the electrolyte side of the MEI overwhelms the decrease in the corresponding contribution of a negative σ (see Table S1 in the SM), eventually leading to a large constant negative value of $d\psi/dy$ within the membrane and hence a large positive ζ potential at the MCI. In fact, for $\sigma = -0.01\ e/nm^2$, this particular membrane property ($\zeta_{MEI} < 0,\ \zeta_{MCI} > 0$)

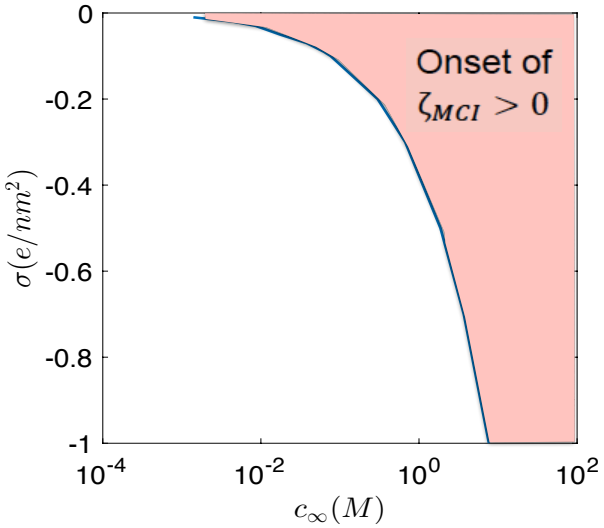

Figure 2.14: $\sigma - c_\infty$ phase-space dictating the attainment of the particular property of the membrane where $\zeta_{MCI} > 0$.

is witnessed even for relatively weak salt concentration. Finally, in Fig. 2.14, we plot the $\sigma - c_\infty$ phase-space that governs the attainment of this particular property of the membrane where $\zeta_{MCI} > 0$. As is evident from Figs. 2(b,c), a reduction in the magnitude of σ allows the attainment of this membrane property even for relatively small values of c_∞.

2.11 Discussions

Ref. [67] showed the possibility where a negatively charged semi-permeable membrane permeating only positive ions may lead to a positive electrostatic potential away from the membrane. In our recent study [77], we showed that our model (the one used here as well) is identical to that of [67] and can indeed recover such a situation (where a negatively charged membrane develops a positive potential away from the membrane). In fact, in [77] we show how reducing the membrane thickness actually allows one to exactly recover the plot of Ref. 19. Such a situation, where a negatively charged membrane develops a

positive potential away from the membrane, is also witnessed in Fig. 2(a) in this paper for the cases with a large σ. However, unlike [67]or [77], in the present paper we are able to pinpoint a $\sigma - c_\infty$ combination that allows a large enough constant negative $d\psi/dy$ within the membrane that enforces the electrostatic potential to change from a negative (at the MEI) to a positive (at the MCI) value across the membrane. Hence such a membrane property (where ζ_{MCI} and ζ_{MEI} are of opposite signs), attributed to a combination of a finite membrane thickness and a specified $\sigma - c_\infty$ combination, is only witnessed here and not in Refs. [67] and [77].

In this part of the chapter, we provide results corresponding to the case where the ion distribution in the CS has been affected due to the membrane permeability to only positive ions and consequently the MCI develops a positive ζ potential for appropriate $\sigma - c_\infty$ combination. As discussed earlier, this same positive ζ potential can be ensured for the MEI in case the membrane semi-permeability affects the ion distribution in the ES. Lipid bilayers demonstrating a surface charge density of $\sigma = -0.1\ e/nm^2$ or smaller is very common [92, 93] as is the large c_∞ values $(0.1, 1\ M)$ [94, 95] – these are the parameter ranges where we demonstrate the membrane to have ζ_{MCI} and ζ_{MEI} of opposite signs. As an actual example where our theory can be applicable, we consider a semi-permeable negatively charged DPPC bilayer membrane permeating only cations. The DPPC membrane has a typical surface charge density of $\sim -5 \times 10^{-3}\ C/m^2$ and in a presence of a salt concentration of $0.1\ M$ [102, 103] one can witness ζ_{MCI} and ζ_{MEI} to be of opposite signs, i.e., $\bar{\zeta}_{MEI} = -0.2525$ (or $\zeta_{MEI} = -5.8\ mV$) and $\bar{\zeta}_{MCI} = 2.3101$ (or $\zeta_{MCI} = +53.3\ mV$). Of course, we shall get a $\zeta_{MCI} < 0$ and $\zeta_{MEI} > 0$ in case the ES (instead of the CS) is affected by the membrane semi-permeability (see Fig. S1 and more discussions in the SM).

The proposed theory established a unique situation where we can make the ζ potential positive at either the MEI or the MCI interface. A positively-charged MEI will imply that the PM can repel and hence reject a large number of highly toxic heavy metal ions (e.g., Cu^{2+}, Pb^{2+}, As^{3+}, As^{5+}, etc.) [83, 84] thereby ensuring the survival of several plants and animals in toxic soil and water. Similarly, a MEI with a positive ζ potential can prevent the membrane binding of the Colicin El Channel, thereby nullifying its large cytotoxic activities [85]. Furthermore, such a MEI with a positive ζ potential can alter (and hence make more effective) events such as the use of anionic cell-penetrating peptides for cargo-delivery inside cells [96–98], membrane binding of Bacillus thuringiensis phosphatidylinositol-specific phospholipase C (BtPI-PLC), which is a secreted virulence factor [99, 100], etc. Similarly, an MCI with a positive ζ potential can hinder the secretion of proteins by gram-negative bacteria thereby hindering the formation of biofilms and reducing the pathogenicity [101], alter the pathways of cell signaling in plants cells [89], etc.

While the present theory focuses on biological plasma membranes, the finding is absolutely true for any charged semi-permeable bilayer membrane that operates under similar σ and c_∞ conditions and is permeable only to ions of opposite charges. Therefore, the present theory will be immensely useful for providing key ideas for developing biofouling-resistant semi-permeable water desalination membranes [104], developing important varieties of lipid-bilayer-encapsulated nanoparticles (or protocells) for more efficient drug delivery [105, 106] and gene delivery [107] and curvature-based protein sensing [108, 109], etc. To summarize, in this letter we demonstrate a most remarkable situation where a semi-permeable and charged bilayer membrane can attain on one of its sides, in the contact with a solution, a positive ζ potential despite having a negative surface charge

density. Such a property has never been reported in context of bilayer membranes and holds immense potential to radically transform a large number of biophysical and applied physics applications ranging from more effective drug and cargo delivery to cells and reducing the cytotoxic influence of metal ions to conceiving techniques of fabricating more efficient biofouling-resistant water-purifying membranes.

Chapter 3: Effect of plasma membrane semi-permeability in making the membrane electric double layer capacitances significant- GC theory

In this chapter we study the effects of the EDL on the capacitance measurement of the lipid bilayer. The EDL capacitances on both the cytosol side and electrolyte side influences the capacitance and causes a decrease in the overall capacitance.[1]

Quantifying the intrinsic capacitance of the plasma membrane of a biological cell can provide deep insights and enable monitoring of a large number of biophysical events such as egg fertilization [110–112], synaptic vesicle fusion [113,114], membrane retrieval or endocytosis [114,115], activities of the receptor cells [116], activities of secretory cells [117, 118], gating of the membrane-bound ionic channels [119,120], etc. This capacitance, often measured under a voltage clamp condition [113], is considered as the intrinsic capacitance of the membrane $C_m \approx 1\ \mu F/cm^2$ [120]. On the other hand, the very charged nature of the plasma membrane separating the intracellular and the extracellular liquids, will enforce a development of separate electric double layers (or EDLs) at the interface of the membrane with both the liquids [17, 28–46, 67, 77, 121]. While this membrane EDL has been vital for controlling a number of physiological activities ranging from controlling cell

[1]Contents of this chapter has been published as: *S. Sinha, H. S. Sachar, and S. Das, Langmuir, 34, 1760-1766 (2018)*

death [21] and cellular signal transduction [78] to membrane-antibody interactions [81] and ATP synthesis by mitochondria [18], the importance of the membrane EDL in affecting the overall effective membrane-EDL capacitance (C_{eff}) has been invariably neglected. Such an approach has stemmed from the fact that the EDL capacitances ($C_{EDL,CS}$ or the capacitance associated with the EDL formed on the cytosol side and $C_{EDL,ES}$ or the capacitance associated with the EDL formed on the electrolyte side) are often identified to be much larger than C_m for biologically realistic ion concentrations and C_m, $C_{EDL,CS}$, and $C_{EDL,ES}$ are all in series [see Fig. 1(d)] so that $C_{eff} = [\frac{1}{C_m} + \frac{1}{C_{EDL,CS}} + \frac{1}{C_{EDL,ES}}]^{-1} \approx C_m$. This notion of a relative unimportance of the EDLs in deciding C_{eff} has been extensively proposed in the existing literature [50, 122, 123].

In the present chapter, we re-visit this notion that the plasma membrane EDL will inevitably be unimportant in deciding this C_{eff}. Rather, through a simple Poisson-Boltzmann (PB) model, we establish that in the presence of certain values of the system parameters such as the salt concentration (c_∞) and the membrane surface charge density (σ), C_{EDL} for both the permeable and semi-permeable membranes can become significantly small to affect C_{eff}. We consider a particular type of a semi-permeable membrane – a negatively-charged semi-permeable membrane permeating only positive ions from the electrolyte side to the cytosol side. We demonstrate that the extent of lowering of C_{EDL} (and consequently, C_{eff}) can be significantly more enhanced for the semi-permeable membrane as compared to the fully membrane membrane. Moreover, the range of the system parameters over which this lowering of C_{eff} is encountered is significantly larger for the semi-permeable membrane. These are the central results of this paper. Our analysis first probes the electric double layer electrostatic potential (ψ) for both the permeable and semi-permeable membranes [see Figs. 3.1(a-c) for the schemat-

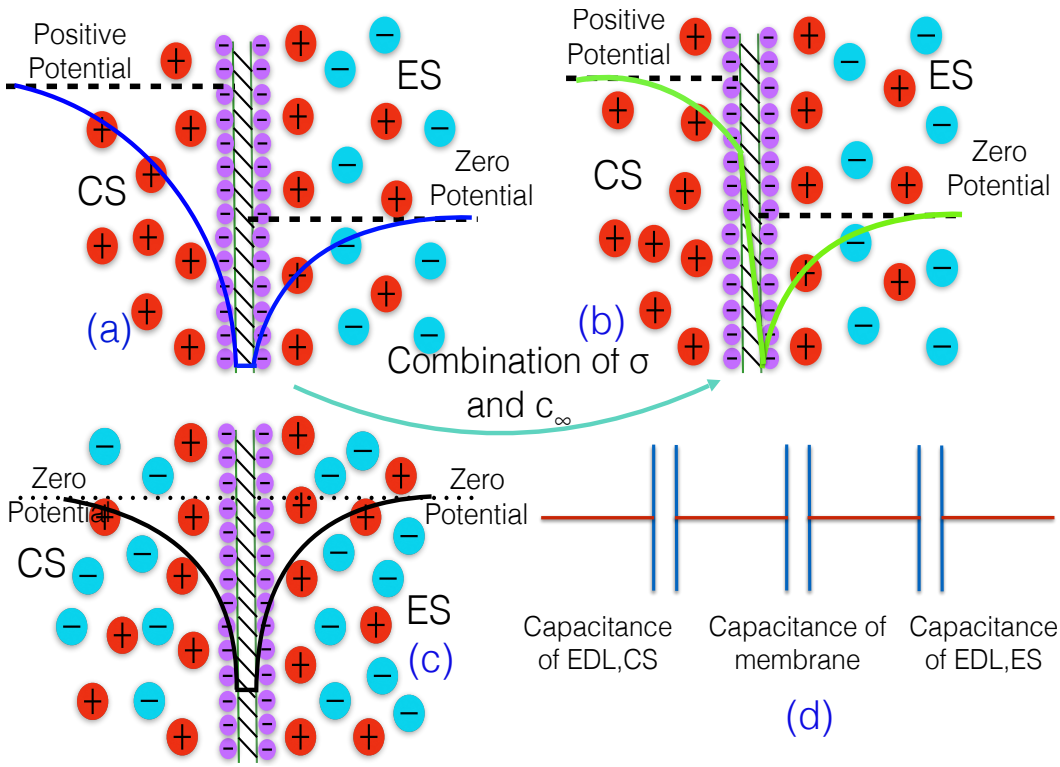

Figure 3.1: (a) Schematic representation of electrostatic potential profile for a negatively-charged semi-permeable membrane permeable only to positive ions and demonstrating a charge-inversion (CI) like behavior in the cytosol side (CS) [77], characterized by the attainment of a positive electrostatic potential deep within the cytosol. (b) Schematic representation of the electrostatic potential profile for a negatively-charged semi-permeable membrane permeable to only positive ions and demonstrating a positive ζ potential at the MCI. Certain conditions of σ and c_∞ enforce the attainment of the condition shown in (b) from the condition shown in (a). (c) Schematic representation of the electrostatic potential profile for a fully permeable membrane. (d) Schematic of the capacitances of the EDLs of the cytosol and the electrolyte sides and the intrinsic capacitance of the membrane, with all the capacitances being in series. Parts (a) and (b) of this figure have been reprinted from Sinha et al. [121] with the permission of AIP Publishing.

ics]. In two recent papers [77, 121], we have computed this ψ for both fully permeable and semi-permeable plasma membranes – a negatively-charged semi-permeable plasma membrane permeating only positive ions demonstrate extremely weird charge inversion (CI) like electrostatics [67, 77] and develops a positive ζ potential at the membrane-cytosol-interface (MCI). We use this ψ information to compute $C_{EDL,CS}$ and $C_{EDL,ES}$ and demonstrate that the presence of CI-like electrostatics in the cytosol side or the attainment of a positive ζ potential at the MCI makes $C_{EDL,CS}$ small enough so as to ensure that C_{eff} gets massively affected by the EDL capacitance. Complete ignorance of such highly non-trivial semi-permeable membrane EDL electrostatics, revealed only very recently theoretically [67, 77, 121], has forbidden identification of such situations where C_{EDL} can decisively influence C_{eff}. It is worthwhile to note that under any measurement technique, one can measure C_{eff} and not C_m. This is due to the fact that it is not possible to decouple the effect of the nanometer-thick EDLs bound to the membrane on its either side. For cases where C_{EDL} affects C_{eff}, $C_m < C_{eff}$ – hence equating C_{eff} (measured) to C_m would imply an underprediction of C_m. This measured C_m (or C_{eff}) value is used to predict a variety of membrane parameters (e.g., membrane surface area) and physiological events associated with the membrane (see above). All these parameters and events would therefore be erroneously predicted on account of the underprediction of C_m. Therefore, we anticipate that our present paper, which will also be useful in providing the foundation for understanding the EDL electrostatics for membranes with curvatures (e.g., nanoparticle-supported lipid bilayer [124–126]), would motivate the biophysicists and biologists to more carefully infer about the different biophysical phenomena on the basis of the measurement of membrane capacitance under those conditions of membrane semi-permeability, membrane surface charge density and salt concentration for which C_{EDL}

affects C_{eff}.

3.1 Theory

3.1.1 General EDL theory for the capacitance of the plasma-membrane-EDL system

In this subsection, we shall propose a general theory for the electrostatics and the capacitances of the plasma-membrane-EDL system employing the standard Gouy-Chapman Poisson-Boltzmann model. The equations for the EDL electrostatic potential (ψ) and the relevant boundary conditions have already been discussed in our previous papers [77,121]. We repeat them here for the sake of continuity. We consider a plasma membrane, as shown in Fig. 1(a-c). The membrane consists of a lipid bilayer with the bilayers having no volume charge. However, the hydrophilic heads of the bilayers are charged with a charge density of σ (in C/m^2). We consider $\sigma < 0$. Therefore, both the MCI and the membrane-electrolyte interface (MEI) have a surface charge density of σ. Both the cytosol and the electrolyte contain ions and form individual EDLs at their interfaces with the membrane [see Fig. 1(a-c)] – the nature of this EDL is governed by the membrane permeability. In this subsection, we shall provide a general theory that is valid for both permeable and semi-permeable membranes, or in other words valid regardless of the cytosol and the electrolyte EDL compositions.

We consider that the EDL electrostatic potential ψ is governed by the Poisson equation

as described below:

$$\begin{aligned}
&\frac{d^2\psi}{dy^2} = -\frac{\rho_{e,c}}{\epsilon_0\epsilon_c} \qquad for \;\; -(d_m + d_c) \leq y \leq -d_m, \\
&\frac{d^2\psi}{dy^2} = 0 \qquad\qquad for \;\; -d_m < y < d_m, \\
&\frac{d^2\psi}{dy^2} = -\frac{\rho_{e,e}}{\epsilon_0\epsilon_e} \qquad for \;\; d_m \leq y \leq (d_m + d_e).
\end{aligned} \tag{3.1}$$

In the above equations, $\rho_{e,c}$ and $\rho_{e,e}$ are the charge densities of the cytosol and the electrolyte EDLs respectively, ϵ_c and ϵ_e are the relative permittivites of the cytosol and the electrolyte, ϵ_0 is the permittivity of free space, $2d_m$ is the membrane thickness, and $2d_e$ and $2d_c$ are the thicknesses of the electrolyte and the cytosol.

Eq.(3.1) needs to be solved in presence of the following boundary conditions:

$$\begin{aligned}
&\left(\epsilon_m \frac{d\psi}{dy}\right)_{y=-d_m^+} - \left(\epsilon_c \frac{d\psi}{dy}\right)_{y=-d_m^-} = -\frac{\sigma}{\epsilon_0}, \\
&\left(\epsilon_e \frac{d\psi}{dy}\right)_{y=d_m^+} - \left(\epsilon_m \frac{d\psi}{dy}\right)_{y=d_m^-} = -\frac{\sigma}{\epsilon_0}, \\
&\left(\frac{d\psi}{dy}\right)_{y=-(d_m+d_c)} = 0, \quad (\psi)_{y=-d_m^+} = (\psi)_{y=-d_m^-}, \\
&(\psi)_{y=d_m^+} = (\psi)_{y=d_m^-}, \quad \left(\frac{d\psi}{dy}\right)_{y=(d_m+d_e)} = 0.
\end{aligned} \tag{3.2}$$

In the above equation, ϵ_m is the relative permittivity of the membrane.

Under these conditions, the charge density within the cytosol EDL can be expressed as [using eqs.(3.1,6.2)]:

$$\begin{aligned}
&\sigma_{EDL,CS} = \int_{-(d_m+d_c)}^{-d_m} \rho_{e,c} dy = \\
&-\epsilon_0\epsilon_c \int_{-(d_m+d_c)}^{-d_m} \left(\frac{d^2\psi}{dy^2}\right) dy = \\
&-\epsilon_0\epsilon_c \left[\left(\frac{d\psi}{dy}\right)_{y=-d_m} - \left(\frac{d\psi}{dy}\right)_{y=-(d_m+d_c)}\right] = \\
&-\epsilon_0\epsilon_c \left(\frac{d\psi}{dy}\right)_{y=-d_m} = -\sigma - \epsilon_0\epsilon_m \left(\frac{d\psi}{dy}\right)_{y=-d_m}.
\end{aligned} \tag{3.3}$$

Similarly, the net charge density within the electrolyte EDL can be expresses as [using eqs.(3.1,6.2)]:

$$\sigma_{EDL,ES} = \int_{d_m}^{d_m+d_e} \rho_{e,e} dy = -\epsilon_0\epsilon_e \int_{d_m}^{d_m+d_e} \left(\frac{d^2\psi}{dy^2}\right) dy = -\epsilon_0\epsilon_e \left[\left(\frac{d\psi}{dy}\right)_{y=d_m+d_e} - \left(\frac{d\psi}{dy}\right)_{y=d_m}\right] = -\epsilon_0\epsilon_e \left(\frac{d\psi}{dy}\right)_{y=d_m} = -\sigma + \epsilon_0\epsilon_m \left(\frac{d\psi}{dy}\right)_{y=d_m}. \tag{3.4}$$

Finally, the cytosol EDL capacitance can be expressed as [using eq.(3.3)]

$$C_{EDL,CS} = |\frac{\sigma_{EDL,CS}}{\psi_{y=-d_m} - \psi_{y=-(d_m+d_c)}}| = |\frac{\sigma}{\psi_{y=-d_m} - \psi_{y=-(d_m+d_c)}}|, \tag{3.5}$$

while the electrolyte EDL capacitance can be expressed as [using eq.(3.4)]

$$C_{EDL,ES} = |\frac{\sigma_{EDL,ES}}{\psi_{y=d_m} - \psi_{y=d_m+d_e}}| = |\frac{\sigma}{\psi_{y=d_m} - \psi_{y=d_m+d_e}}|. \tag{3.6}$$

From eqs.(3.3-3.6) it is apparent that we would need the ψ profile to compute $C_{EDL,CS}$ and $C_{EDL,ES}$. ψ profiles for both the cases of fully permeable and semi-permeable membranes are discussed later. Given that the three capacitances, namely the cytosol EDL capacitance ($C_{EDL,CS}$), intrinsic capacitance of the membrane (C_m) and the electrolyte EDL capacitance ($C_{EDL,ES}$) are all in series, we may obtain the effective capacitance C_{eff} as:

$$C_{eff} = \frac{1}{\frac{1}{C_{EDL,CS}} + \frac{1}{C_m} + \frac{1}{C_{EDL,ES}}}. \tag{3.7}$$

3.1.2 Case 1: Case of fully-permeable membrane

For this case, we consider a salt AB of bulk concentration c_∞ (or bulk number density of $n_\infty = 10^3 N_A c_\infty$, where N_A is the Avogadro number) where the membrane is permeable to both monovalent cation A^+ and monovalent anion B^-. We consider the membrane to be negatively charged (i.e., $\sigma < 0$), and consequently the EDLs formed both in the cytosol and the electrolyte side consists of A^+ ions as counterions and B^- ions as coions. As a result, one can write, employing Boltzmann distribution for the cations and the anions:

$$\rho_{e,c} = \rho_{e,e} = e\left(n_{A^+} - n_{B^-}\right) = -2n_\infty e \sinh\left(\frac{e\psi}{k_B T}\right). \tag{3.8}$$

We obtain the EDL electrostatic potential profile ψ by using eq.(3.8) in eq.(3.1) and then solving ψ numerically in presence of the boundary conditions expressed in eq.(6.2). Once ψ is obtained, we use eqs.(3.5,3.6,3.7) to obtain the final value of the effective capacitance of the plasma-membrane-EDL system for a fully permeable plasma membrane.

3.1.3 Case 2: Case of a semi-permeable membrane

Here we consider the case of a negatively charged plasma membrane permeable to only positive ions. We consider the salt AD to be present in the electrolyte side. The membrane is semi-permeable to the salt AD, i.e., it permeates the cation A^+, but does not permeate the anion D^-. Therefore, there is no D^- ions in the cytosol side. The bulk concentration of AD is c_∞ (or equivalently a bulk number density of $n_\infty = 10^3 N_A c_\infty$). Under these conditions, one may write (using Boltzmann distribution):

$$\rho_{e,e} = e\left(n_{A^+} - n_{D^-}\right) = -2en_\infty \sinh\left(\frac{e\psi}{k_B T}\right), \tag{3.9}$$

$$\rho_{e,c} = en_{A^+} = en_\infty \exp\left(-\frac{e\psi}{k_B T}\right). \tag{3.10}$$

For this case, ψ can be obtained by using eqs.(3.9,3.10) in eq.(3.1) and then solving the resulting equation numerically in presence of the boundary conditions expressed in eq.(6.2). Once ψ has been obtained, C_{eff} can be computed using eqs.(3.5,3.6,3.7).

3.2 Results and Discussions

3.2.1 Capacitance for fully permeable plasma membrane (Case 1)

Fig. 2 shows the electrostatic potential profile ψ and the corresponding capacitances $C_{EDL,CS}$, $C_{EDL,ES}$ (please note that for a fully semi-permeable membrane, $C_{EDL,CS} = C_{EDL,ES}$) and C_{eff} for a fully permeable membrane as a function of c_∞ and σ. This potential profile, shown in Figs. 2(a-c) has already been partly discussed in our previous paper [77]; we repeat the discussion here for the sake of continuity. The membrane being fully permeable it supports a standard EDL (composed of both coions and counterions) on both the MCI and the MEI. Accordingly, we get a perfectly symmetric ψ distribution. Moreover, a decrease in the salt concentration increases the EDL thickness (λ) on both the electrolyte and the cytosol sides and also leads to a larger magnitude of (identical) ψ at the MEI and the MCI. Furthermore, the EDLs at both the MCI and the MEI being standard EDLs formed of both coions and counterions and the fact that $d_c \gg \lambda$ and $d_e \gg \lambda$, the condition of $(d\psi/dy)_{-d_m-d_c} = (d\psi/dy)_{d_m+d_e} = 0$ would ensure $(\psi)_{-d_m-d_c} = (\psi)_{d_m+d_e} \to 0$. This implies that the electrostatic potential is almost zero both deep within the electrolyte as well as deep within the cytosol. Consequently, a larger magnitude of ψ at the MEI (or MCI) due to weaker c_∞ (or a larger λ) for a given σ would imply a larger value of$\Delta\psi$ (or the magnitude of the total potential drop) within the electrolyte (or the cytosol) for a smaller c_∞. Accordingly, a smaller c_∞ would lead to a smaller value of $C_{EDL,CS}$ or

$C_{EDL,ES}$ [see Fig. 2(d)] and hence a smaller value (< 1) of C_{eff}/C_m [see Fig. 2(e)]. On the other hand, a larger σ would lead to a larger ψ at the MEI and the MCI [see Fig. 2(a-c)] and therefore would lead to a larger potential drop across the electrolyte and the cytosol. However, the increase in σ counters this effect of the increase in the potential drop in dictating the overall EDL capacitance value. For a very large σ, the effect of the enhancement in σ overwhelms the effect of the increase in the potential drop. On the other hand, for a smaller σ, these two effects are pretty similar. Therefore, one witnesses a much larger increase in C_{EDL} as σ increases from 0.1 C/m^2 to 1 C/m^2 as compared to what happens when σ increases from 0.01 C/m^2 to 0.01 C/m^2. This variation in C_{EDL} eventually ensures a significantly weak decrease of C_{eff} for large σ, but substantially noticeable decrease in C_{eff} for weaker σ. However, even for weaker σ, the EDL-mediated lowering of C_{eff} for a fully permeable membrane is witnessed only at a significantly weak value of ($\leq 10^{-2}$ M) of the salt concentration.

3.2.2 Capacitance for a semi-permeable plasma membrane (Case 2)

Fig. 3 shows the electrostatic potential profile (ψ) and the capacitances $C_{EDL,CS}$, $C_{EDL,ES}$, and C_{eff} for the negatively charged semi-permeable plasma membrane permeating only positive ions (from the electrolyte to the cytosol side) for different combinations of σ and c_∞. Like the case of the permeable membrane, for this case as well, the ψ profile [shown in Fig. 3(a-c)] has already been discussed in our previous papers [77, 121] and we repeat it here for the sake of continuity and better explanation of the variation of the capacitance. In comparison to the case of a fully permeable membrane, here we witness distinctly larger EDL-mediated decrease of C_{eff}/C_m. *This decrease can be as large as 25% (or even more) for small (but experimentally supported [92, 93, 102, 103]) values of* σ *and*

c_∞. *Secondly, unlike the fully permeable membrane, for the semi-permeable membrane a finite decrease in* C_{eff} *is witnessed even for a significantly large range of electrolyte salt concentration. These are the central results of the paper and to the best of our knowledge show for the first time such a significant influence of the EDL capacitance in the overall EDL-plasma-membrane effective capacitance.* The semi-permeable nature of the membrane, allowing only positive ions to permeate from the ES to the CS, leads to the formation of a *counterion-only EDL* at the MCI [77, 121] and is responsible for several highly non-intuitive phenomena such as CI-like electrostatics [67, 77] and attainment of a positive ζ potential at the MCI [121]. This CI-like electrostatics refers to a situation where the EDL electrostatic potential deep within the cytosol (i.e., at a location where the net charge content is zero, i.e., $d\psi/dy = 0$) becomes positive despite the MCI being negative charged and having a negative ζ potential [see Fig. 3(a)]. An even more non-intuitive occurrence is the development of *a positive zeta potential at the MCI itself*, which we attribute to the development of a steep constant electrostatic potential gradient within the membrane [see Fig 3(b,c)]. Occurrence of such a positive ζ potential is witnessed typically for weak σ and large salt concentration. The electrolyte side, on the other hand, bears a standard EDL (consisting of both coions and counterions) and does not demonstrate such non-intuitive effects. Therefore, $C_{EDL,ES}$ remains significantly high (as for the case of the fully permeable membrane) [see Fig. 3(e)], while $C_{EDL,CS}$, on account of the effect like CI-like electrostatics and positive ζ potential at the MCI, encounters a distinct lowering [see Fig. 3(e)] that eventually ensures a lowering of C_{eff}/C_m [see Fig. 3(f)].

For relatively small σ and small c_∞, C_{eff} for the semi-permeable membrane is distinctly smaller than C_{eff} for the fully permeable membrane. For such a combination of σ and c_∞, the cytosol side demonstrates a distinct CI-Like electrostatics [see Fig. 3(a)],

characterized by a negative ζ potential at the MCI and a large positive electrostatic potential deep within the cytosol. Consequently, one encounters a large $|\Delta\psi|$ across the EDL supported at the MCI. This large $|\Delta\psi|$, coupled with a weak σ, eventually leads to a small $C_{EDL,CS}$ [see Fig. 3(d)] ensuring a significant lowering of C_{eff} [see Fig. 3(f)]. Increase in salt concentration for such weak values of σ eventually leads to an attainment of a positive ζ potential at the MCI [see Fig. 3(b,c)] [121]. The potential deep within the cytosol is also positive. Hence the corresponding $|\Delta\psi|$ is much smaller. Accordingly, $C_{EDL,CS}$ is larger [see Fig. 3(d)] effecting a much smaller decrease in C_{eff}. This explains the increase in C_{eff} with an increase in c_∞. However, despite such a decrease, the extent of the reduction of C_{eff} for the semi-permeable membrane remains significantly larger at larger salt concentration as compared to the case of a fully permeable membrane. Decrease in σ decreases the jump in $|\Delta\psi|$ in both the CS and ES; however, given that $|\Delta\psi|$ for the CS is dictated by the attainment of either CI-Like electrostatics (for lesser c_∞) or the attainment of a positive ζ potential at the MCI (for a larger c_∞), this decrease for the CS is not as strong as the case of a fully permeable membrane. Consequently, the effect of the reduction of σ dictates $C_{EDL,CS}$ [see Fig. 3(d)], ensuring a reduction in C_{eff} with a reduction in σ [see Fig. 3(f)].

3.2.3 $\sigma - c_\infty$ phase space governing the reduced C_{eff}

Finally in Fig. 4, we provide the σ-c_∞ phase-space that shows the region where $C_{eff}/C_m < 0.8$, i.e., there is at least 20% reduction in the effective capacitance on account of the finite contribution of the membrane EDL capacitances. We consider the cases of both the fully permeable and semi-permeable membranes. This phase-space gives us a clear idea about the operating range of concentration and charge density of the membrane

where the effective capacitance will get influenced by the properties of the membrane and the EDL formed around the membrane. Examples of membranes operating at these regimes of concentration can be found in literature [102,103] and from Fig. 4 it is intuitive the manner in which the EDL effects are significantly more important in affecting C_{eff} for the semi-permeable membrane.

3.3 Conclusions

To summarize, our newly discovered semi-permeable plasma membrane EDL electrostatic phenomena of CI-like electrostatics and attainment of a positive ζ potential at the MCI [77,121] ensure a significant lowering of the EDL capacitance eventually leading to a noticeable decrease of the overall capacitance (C_{eff}) of the plasma-membrane-EDL system. The EDL-mediated decrease in C_{eff} is also witnessed for a fully permeable membrane, albeit this decrease, in comparison to that for the semi-permeable membrane, is significantly weaker and persists across a much smaller range of parameter. These phenomena of CI-like electrostatics and $(\zeta)_{MCI} > 0$, attributable to the semi-permeability-driven development of counterion-only EDL at the CS, has not been identified previously. This has forbidden the identification of this situation where the EDL capacitance may become significantly small giving rise to a most noteworthy situation where the membrane EDL capacitance may significantly influence the overall plasma-membrane-EDL-capacitance.

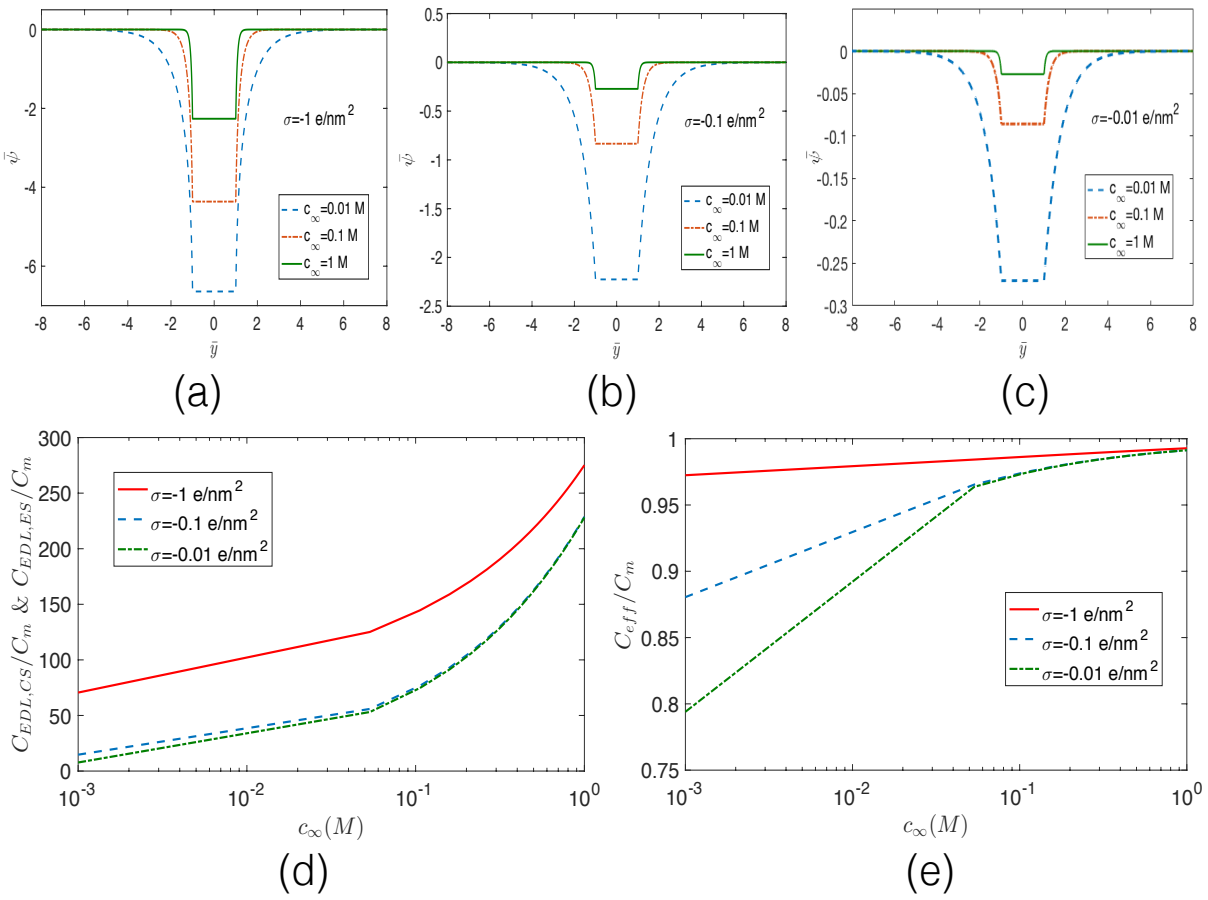

Figure 3.2: Electrostatic potential profiles and capacitances of a negatively charged fully permeable plasma membrane.Electrostatic potential profiles as a function of the salt concentration (c_∞) are provided for (a) $\sigma = -1e/nm^2$, (b) $\sigma = -0.1e/nm^2$, and (c) $\sigma = -0.01e/nm^2$. (d) Variation of the capacitances (made dimensionless with the intrinsic membrane capacitance C_m) associated with the EDLs in the CS ($C_{EDL,CS}$) and the ES ($C_{EDL,ES}$) with c_∞ for different values of σ. The membrane being fully permeable, the EDL on the ES is identical to the EDL on the CS, making $C_{EDL,ES} = C_{EDL,CS}$. (e) Variation of the membrane-EDL effective capacitance C_{eff}, made dimensionless with C_m, with c_∞ for different values of σ. For these plots, we consider $\bar{\psi} = e\psi/(k_BT)$, $\bar{y} = y/d_m$, $C_m = 1\ \mu F/cm^2$, $d_m = 4\ nm$, $d_c = d_e = 1\ \mu m$, $\epsilon_0 = 8.8 \times 10^{-12}\ F/m$, $\epsilon_e = \epsilon_c = 79.8$, $\epsilon_m = 3.9$, $e = 1.6 \times 10^{-19}\ C$, $k_BT = 4.11 \times 10^{-21}\ J$.

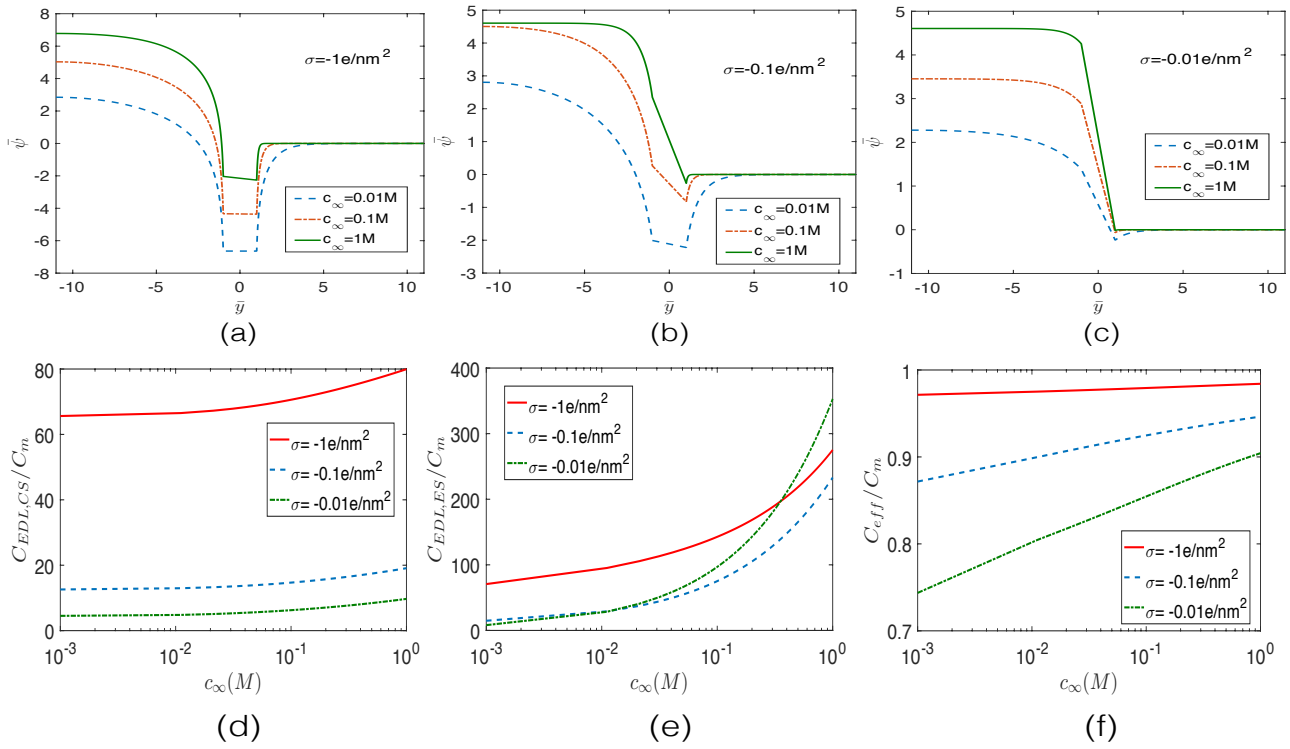

Figure 3.3: Electrostatic potential profiles and capacitances of a negatively charged semi-permeable plasma membrane permeating only positive ions from the electrolyte side (ES) to the cytosol side (CS). Electrostatic potential profiles as a function of the salt concentration (c_∞) are provided for (a) $\sigma = -1e/nm^2$, (b) $\sigma = -0.1e/nm^2$, and (c) $\sigma = -0.01e/nm^2$. (d) The capacitance of the EDL on the CS is represented with respect to the concentration of the electrolyte in comparison to the capacitance of the membrane (taken as $1\mu F/cm^2$). (d) Variation of the capacitance associated with the EDL on the cytosol side $C_{EDL,CS}$, made dimensionless with C_m with the salt concentration (c_∞) for different σ. (e) Variation of the capacitance associated with with the EDL on the electrolyte side $C_{EDL,ES}$, made dimensionless with C_m, with the salt concentration (c_∞) for different σ. (f) Variation of the membrane-EDL effective capacitance C_{eff}, made dimensionless with C_m, with the salt concentration (c_∞) for different σ. For these plots, we consider $\bar{\psi} = e\psi/(k_B T)$ and $\bar{y} = y/d_m$. All other parameters are identical to that used in Fig. 2.

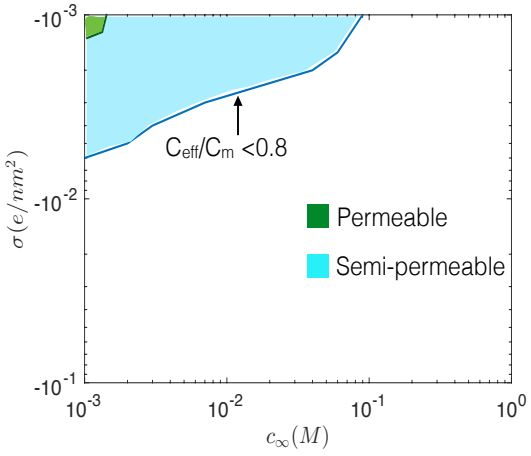

Figure 3.4: σ - c_∞ phase space showing the zone where $C_{eff}/C_m < 0.8$ for a fully permeable membrane (shown in green) and a semi-permeable membrane (shown in blue). The semi-permeable membrane is negatively-charged, permeating only positive ions and the phase space corresponding to the semi-permeable membrane completely encloses the phase space corresponding to the fully permeable membrane. All other parameters are identical to that used in Fig. 2.

Chapter 4: Role of plasma membrane surface charges in dictating the feasibility of membrane-nanoparticle interactions

In this chapter we study the problem of attraction of a NP towards the lipid bilayer. The EDL distribution plays a significant role in this process. It causes a repulsion between the NP and the bilayer whereas van der Waal's causes attraction. The interplay of these two along with the thermal fluctuations causes the system to have a length scale defined here as a critical length for adhesion to happen. This chapter thus deals with the feasibility of the adhesion process.[1]

Functionalized, target-specific nanoscale vehicles such as nanoparticles have offered capabilities of interacting with biological cells and get internalized by the cells and in the process offer opportunities of delivering drugs to the infected cells [127–131], medical imaging [132–135], hyperthermia therapy [136–138], replicating and understanding the processes by which viruses can be recognized [139], and many more. The most significant mechanism triggering such NP-cell interaction is the interaction between the ligands engineered on the NPs and the receptors of the plasma membrane of the cells. This problem is very well studied theoretically [140, 142–144, 146–155, 188, 190] with several of the stud-

[1] Contents of this chapter have been published as: *S. Sinha, H. Jing, H.S. Sachar, and S. Das, Applied Physics Letters, 111, 263702 (2017)*

ies pointing out the manner in which the chemical energy gained due to the strong (and often irreversible) receptor-ligand (R-L) binding provides the energy for deforming (bending and stretching) the membrane that is essential for adhesion-mediated internalization of the NPs. Issues such as the effect of NP size and shape, density of ligand grafting, variability in the stiffness of the membrane, entropy of mixing of receptors, kinetics of receptor-ligand interactions, etc in dictating the R-L binding have been probed in these papers. However, most surprisingly very little theoretical research has been carried out on elucidating the role of the membrane surface charges and the surrounding ionic environment on the membrane-NP interactions. This is specially surprising given the massive exploration of the EDL theory [1, 17, 34, 36, 47, 49, 67, 77, 121] and its resulting connotations (e.g., development of a membrane potential [1], regulation of cellular signalling [78], ATP synthesis by mitochondria [18], death of cancer cells [21], etc.) for a charged bilayer plasma membrane as well as significant experimental endeavour in elucidating the role of membrane and NP charges on membrane-NP interactions [156–158].

In this letter, we carry out a theoretical analysis on how factors such as the membrane surface charge density (σ), concentration of the electrolyte salt (c_∞), nature of the membrane (semi)-permeability, and the electrical nature and the size of the approaching NP affects the membrane-NP interactions. We shall simply focus on the role of these factors in dictating whether or not the membrane-NP interactions (or the corresponding R-L interactions) will be initiated. We shall consider a simplistic 1-D NP (see Fig. 1) and for such a particle the onset of the R-L interactions require $d_g < d_{RL}$ (where d_g is the membrane-NP separation distance and d_{RL} is R-L bond length). The interplay of factors like σ, c_∞ and nature of membrane permeability triggers an electrostatic potential (of same sign as that at the membrane surface) at the NP surface, which in turn repels the

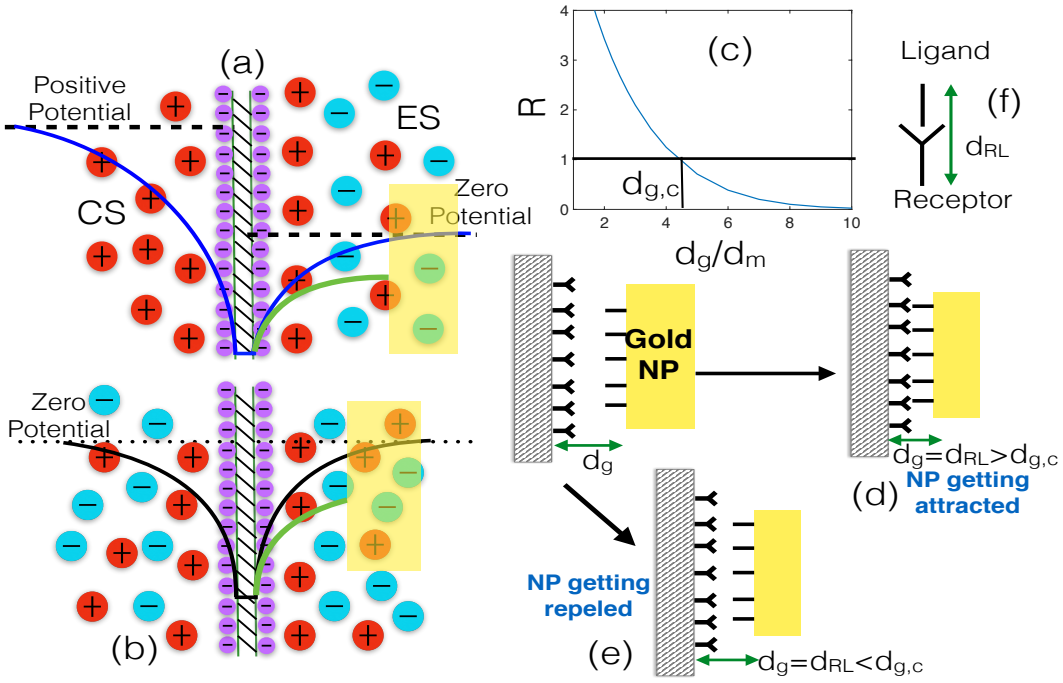

Figure 4.1: Schematic of the EDL electrostatics for (a) a semi-permeable membrane and (b) fully permeable membrane. For both the cases an approaching gold NP (from the electrolyte side) attains a negative potential on its surface, which repels it from the membrane. (c) Variation of the dimensionless repulsion energy R (made dimensionless with k_BT) as a function of the separation distance d_g between the membrane and the NP. Thermal energy (k_BT) can overcome repulsion energy only when $d_g > d_{g,c}$. Hence a R-L interaction becomes possible (such interaction is necessary for the NP-membrane binding) for $d_{RL} > d_{g,c}$ [see (d)], while the NP is driven away from the membrane for $d_{RL} < d_{g,c}$ [see (e)]. (f) Schematic of the R-L bond and quantification of the R-L length d_{RL}.

NP away from the membrane. Smaller d_g implies a larger repulsion. On the other hand, thermal fluctuations overcome this repulsion bringing the NP closer to the membrane. $d_{g,c}$ denotes the critical separation distance where these two effects (electrostatic repulsion and thermal fluctuations) balance each other. For $d_g < d_{g,c}$, electrostatic repulsion nvariably overcomes the thermal fluctuations. We infer that only when $d_{g,c} < d_{RL}$, there is a possibility of a R-L interaction and the subsequent membrane-NP subsequent binding. Fig. 1 schematically captures this hypothesis. The purpose of this paper is to calculate this $d_{g,c}$ as a function of σ, c_∞ and other system parameters and therefore quantify how the membrane surface charge, salt concentration and other related factors would ensure whether at all the NP will interact with the membrane. Our results establish that for both permeable and semi-permeable membranes, decrease in c_∞ and increase in σ increase the value of this electrostatic repulsion for a given separation distance, which in turn would imply an increase in $d_{g,c}$. Consequently, smaller c_∞ and larger σ would necessitate the use of such R-L combination that would lead to a larger length of the R-L complex. Finally, we end by discussing the manner in which our theory (a) may help in designing NPs for drug delivery to cancer cells, (b) explain recent experimental findings, and (c) help to better understand the release of certain moieties (e.g. exosomes) by the cells.

4.1 Theory

We first consider the electric double distribution between an approaching metallic 1-D NP and the charged bilayer PM. The PM separates the electrolyte side (ES) and the cytosol side (CS), with the NP being located at the ES. We have recently developed a detailed EDL theory for both permeable and semi-permeable plasma membranes [77,121]. Here the theory will be modified due to the presence of the intervening 1-D gold NP, which

will change the EDL distribution in case $d_g \leq \lambda$ (where λ is the EDL thickness). Under these conditions, the EDL potential distribution ψ is governed by the following equations:

$$\begin{aligned} \frac{d^2\psi}{dy^2} &= -\frac{\rho_{e,c}}{\epsilon_0\epsilon_c} \quad for \quad -(d_m + d_c) \leq y \leq -d_m, \\ \frac{d^2\psi}{dy^2} &= 0 \quad for \quad -d_m \leq y \leq d_m, \\ \frac{d^2\psi}{dy^2} &= -\frac{\rho_{e,e}}{\epsilon_0\epsilon_e} \quad for \quad d_m \leq y \leq (d_m + d_g). \end{aligned} \tag{4.1}$$

Here $\rho_{e,c}$ and $\rho_{e,e}$ are the EDL charge densities in the ES and CS, ϵ_c, ϵ_m, and ϵ_e are the relative permittivities of the cytosol, membrane, and the electrolyte, ϵ_0 is the permittivity of free space, $2d_m$ is the membrane thickness, $y = -(d_m + d_c)$ is the location of the cytosol centerline and $y = d_m + d_g$ is the location of the NP surface. Here we neglect the EDL distribution for $y > (d_m + d_g + d_t)$ (d_t is the thickness of the NP) as we assume that d_t is large enough to make $(d_m + d_g + d_t) \gg \lambda$. For a membrane that is fully permeable to a salt AB, $\rho_{e,c} = \rho_{e,e} = e\,(n_{A^+} - n_{B^-}) = 2n_\infty \sinh\,(\frac{e\psi}{k_BT})$. On the other hand, for a membrane that is semi-permeable to a salt AD allowing the passage of only cations (A^+) from the ES to the CS, $\rho_{e,c} = en_{A^+} = en_\infty \exp\,(-\frac{e\psi}{k_BT})$ and $\rho_{e,e} = e(n_{A^+} - n_{D^-}) = 2n_\infty \sinh\,(\frac{e\psi}{k_BT})$. Here in order to express the ion number density n_i, we always employ the Boltzmann distribution, so that $n_i = n_\infty \exp\,(-\frac{ez_i\psi}{k_BT})$. Here e is the electronic charge, k_BT is the thermal energy, n_∞ is the bulk ion number density, and z_i is the ion valence (here we always consider $|z_i| = 1$). Once $\rho_{e,c}$ and $\rho_{e,e}$ are known, ψ is obtained by solving eq.(1) in the presence of the following boundary conditions (considering zero charge at the metal

NP surface):

$$\left(\epsilon_m \frac{d\psi}{dy}\right)_{y=-d_m^+} - \left(\epsilon_c \frac{d\psi}{dy}\right)_{y=-d_m^-} = -\frac{\sigma}{\epsilon_0},$$
$$\left(\epsilon_e \frac{d\psi}{dy}\right)_{y=d_m^+} - \left(\epsilon_m \frac{d\psi}{dy}\right)_{y=d_m^-} = -\frac{\sigma}{\epsilon_0},$$
$$\left(\frac{d\psi}{dy}\right)_{y=-(d_m+d_c)} = 0, \quad (\psi)_{y=-d_m^+} = (\psi)_{y=-d_m^-},$$
$$(\psi)_{y=d_m^+} = (\psi)_{y=d_m^-}, \quad \left(\frac{d\psi}{dy}\right)_{y=(d_m+d_g)} = 0, \tag{4.2}$$

where σ is the surface charge density at the membrane surfaces, i.e., at the membrane-cytosol interface (MCI) and the membrane-electrolyte interface (MEI). Once ψ has been obtained, the disjoining pressure in the entire ES [i.e., $d_m \leq y \leq (d_m + d_g)$] can be expressed as (see Supplementary material and [**?**, **?**]):

$$\Pi = -\frac{1}{2}\epsilon_0 \epsilon_e \left(\frac{d\psi}{dy}\right)^2 + 2n_\infty k_B T \left[\cosh\left(\frac{e\psi}{k_B T}\right) - 1\right]. \tag{4.3}$$

Expression in eq.(3) is position invariant (see Supplementary material) and hence it is valid at any y in the ES. Consequently, the ratio R of the electrostatics repulsion energy (E_{elec}) to the thermal energy ($k_B T$) associated with the metal NP can be expressed as (see the Supplementary Material):

$$R = 2A_{NP} d_g n_\infty \left[\cosh\left(\frac{e\psi_{NP}}{k_B T}\right) - 1\right], \tag{4.4}$$

where ψ_{NP} is the electrostatic potential at the NP surface and A_{NP} is the characteristic NP surface cross section area. We define a critical separation distance $d_{g,c}$ such that $R_{d_g=d_{g,c}} = 1$ and $R_{d_g>d_{g,c}} < 1$, $R_{d_g<d_{g,c}} > 1$ [see Figs. 2(b) and 3(b)].

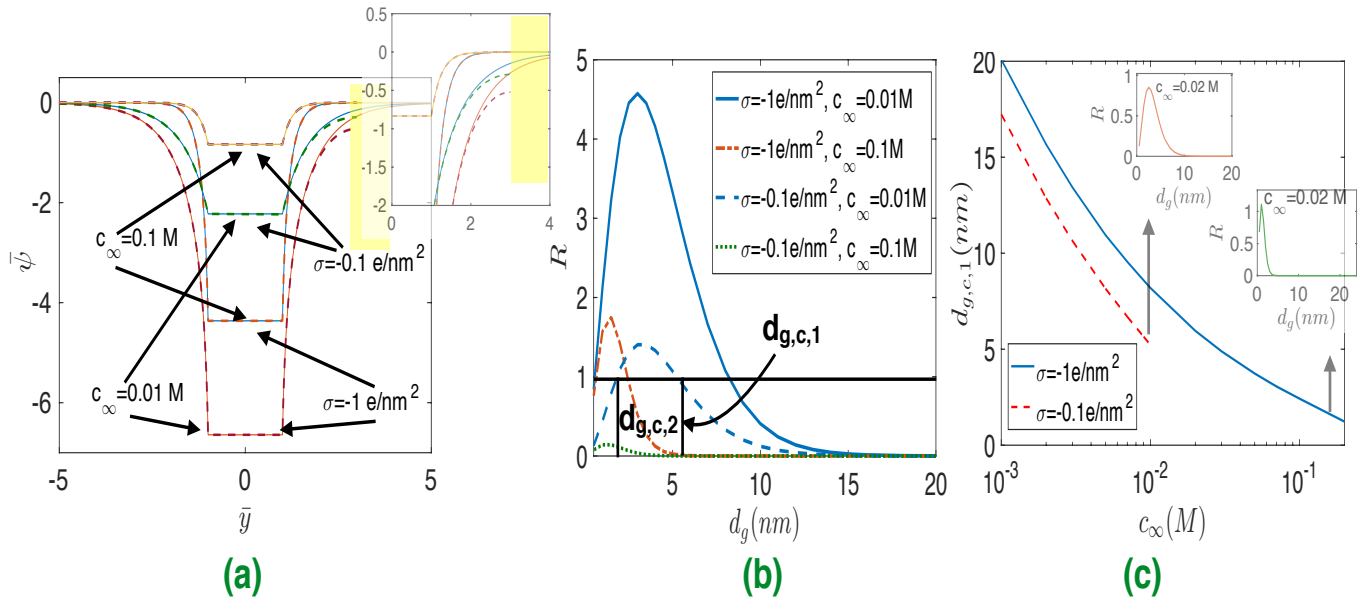

Figure 4.2: (a) Variation of the dimensionless EDL electrostatic potential $\bar{\psi} = e\psi/(k_B T)$ with $\bar{y} = y/d_m$ with and without the gold NP (the gold NP being positioned at a distance of $\bar{y} = 3$ from the MEI in the electrolyte side) for different values of c_∞ and σ. (b) Variation of the ratio R [see eq.(4)] and the corresponding identification of $d_{g,c}$ for different combinations of c_∞ and σ. (c) Variation of $d_{g,c}$ with c_∞ for different σ. Results are shown for fully permeable membrane. Different parameters considered here are $\epsilon_0 = 8.8 \times 10^{-12}\ C/(Vm)$, $\epsilon_e = \epsilon_c = 79.8$, $\epsilon_m = 2$, $d_m = 4\ nm$, $d_c = 1\ \mu m$, $k_B = 1.38 \times 10^{-23}\ J/K$, $e = 1.6 \times 10^{-19}\ C$, and $A_{NP} = 100\ nm^2$.

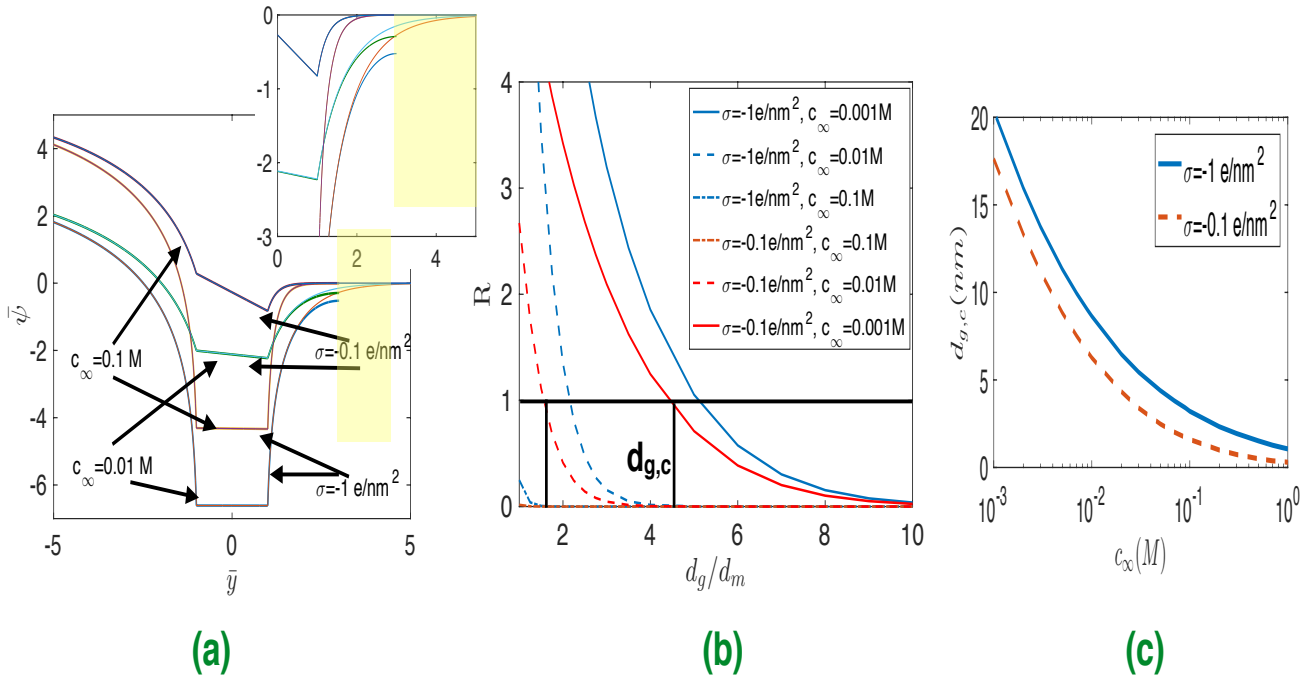

Figure 4.3: (a) Variation of the dimensionless EDL electrostatic potential $\bar{\psi} = e\psi/(k_B T)$ with $\bar{y} = y/d_m$ with and without the gold NP (the gold NP being positioned at a distance of $\bar{y} = 3$ from the MEI in the electrolyte side) for different values of c_∞ and σ. (b) Variation of the ratio R [see eq.(4)] and the corresponding identification of $d_{g,c}$ for different combinations of c_∞ and σ. (c) Variation of $d_{g,c}$ with c_∞ for different σ. Results are shown for semi-permeable negatively-charged membrane permeating only positive ions from the ES to CS. Different parameters considered here are same as that of Fig. 2.

4.2 Results

R-L interaction is possible for $d_g < d_{RL}$. On the other hand, there can be either of the two situations for a given combination of the parameter values: (a) $d_{g,c} > d_{RL}$ or (b) $d_{g,c} < d_{RL}$. For the case of $d_{g,c} > d_{RL}$, if $d_g = d_{g,c}$, the separation distance is too high for the R-L interaction to set in. Therefore, d_g must be reduced and made smaller than $d_{g,c}$. However, for $d_g < d_{g,c}$, $R > 1$ and hence the electrostatic repulsion outweighs the thermal fluctuations ensuring that there is no R-L interaction. On the other hand for $d_{g,c} < d_{RL}$, when $d_g = d_{RL}$ (i.e., the condition that will trigger the possible onset of the $R - L$ interaction), $d_g > d_{g,c}$. Consequently, $R < 1$ and hence the thermal fluctuations may overcome the electrostatic repulsions ensuring a stable R-L bond and hence trigger the onset of the NP-membrane adhesion. *Therefore, the present study provides a hitherto unexplored design parameter for the NP-membrane interaction, namely how one can select the optimal sizes of the ligand-receptor complexes in response to the salt concentration in the vicinity of the cells and charge density of the membrane.*

4.2.1 Case of Fully permeable plasma membrane

Fig. 2 provides $\bar{\psi} = e\psi/(k_B T)$, R, and $d_{g,c}$ variation for a fully permeable membrane, which is characterized by the presence of the membrane-embedded protein channels that allow exchange of all the existing ions across the membrane. Fig. 2(a) shows the effect of the presence of the metal NP on $\bar{\psi}$. Results clearly show the attainment of a negative electrostatic potential at the metal NP surface. Smaller salt concentration implies larger EDL thickness λ, which in turn ensures a larger $\bar{\psi}$ at the membrane-electrolyte interface

(MEI) [77, 121]. Furthermore, larger λ implies weaker decay of $\bar{\psi}$ from the MEI. These two effects ensure a much larger $\bar{\psi}$ at the metal NP surface for a given separation distance d_g. On the other hand, for a given c_∞, larger σ would obviously imply a much larger $\bar{\psi}$ at both the MEI and the NP surface. Accordingly, R (signifying the dimensionless electrostatic repulsion) is significantly larger corresponding to a given separation distance d_g for both weak c_∞ and larger σ [see Fig. 2(b)]. Given that R always increases with a decrease in d_g, we should therefore witness $d_{g,c}$, which is the value of the critical d_g when $R = 1$, increasing as c_∞ is reduced and σ is increased [see Fig. 2(c)].

4.2.2 Case of semi-permeable plasma membrane

Here we consider a semi-permeable plasma membrane, which is characterized by the presence of membrane-embedded protein channels that allow only the passage of the cations (A^+) of the salt AD from the ES to the CS across the negatively charged membrane. As revealed by our previous papers [77, 121], the most interesting electrostatic behavior (e.g., development of charge-inversion-like electrostatics or attainment of zeta potential and surface charge densities of opposite signs at the membrane-cytosol interface) is witnessed for this particular case of membrane semi-permeability. Fig. 3(a) provides the $\bar{\psi}$ distribution for this case with and without the presence of the gold NP in the ES. Here too we find that a decrease in c_∞ and an increase in σ increases the (negative) values of $\bar{\psi}$ at the MEI and and the metal NP surface, ensuring a much larger value of R (for a given d_g) [see Fig. 3(b)] and $d_{g,c}$ [see Fig. 3(c)].

4.2.3 Discussions

The length of the R-L complex (d_{RL}) can vary significantly, ranging from 10 nm to 40 nm [159–163]. Larger d_{RL} would imply greater chances of the R-L interactions in presence of a larger $d_{g,c}$ (or a larger electrostatic repulsion). Such a design information can help designing ligands for the NPs for targeted delivery of drugs to cancer cells. For example, breast cancer cells are known to exist in an environment containing $NaCl$ concentration of 0.1-0.2 M [164]. Moreover, for nearly neutral pH these cells demonstrate a surface charge density of $\sim -0.1\ e/nm^2$ (or $\sim -0.02\ C/m^2$) [165]. This would lead to $d_{g,c} = 1.6 d_m \approx 7\ nm$ (for a fully permeable membrane); consequently, following our theory, we can design the corresponding ligands for the NPs such that $d_{RL} > 5\ nm$. It is also interesting to note that recent experiments have demonstrated that the repulsive interaction between the cells and NPs decay significantly on increasing the salt concentration [166], thereby promoting the chances of membrane-NP interactions. This is exactly what is indicated by our theory – increase in salt concentration decreases $d_{g,c}$ for a fixed σ and hence would increase the potential of membrane-NP interaction for a given d_{RL}.

This paper provides a framework for deciphering the role of electrostatics in dictating whether or not a NP would interact with a cell membrane from the ES. Given that we obtain a complete description of the electrostatics in both the intracellular and extracellular sides of the membrane, the same mathematical framework can be used to probe the feasibility of interaction of an intracellular moiety (e.g., exosomes) with the MCI of the membrane [167]. Of course, based on the nature of the moiety, the EDL electrostatic description would change – e.g., for an exosome, which is itself a membrane bound vesicle, one would need to account for the presence of the lipid bilayer of the exosome. However,

once the EDL electrostatics has been calculated, we can use it to compute the net electrostatic repulsion, which in turn would help us to quantify the strength of the driving factors (e.g., chemical potential) that will overcome such repulsion and ensure that the moiety (exosome) physically interact with MCI in order to trigger the subsequent release of the exosome. In fact, we believe that this paper will serve as an important basis that will determine the role of electrostatics in dictating the onset of any interaction involving the plasma membrane and other extracellular or intracellular moiety [168–171].

The model proposed here considers several simplifications. For example, we do not consider van der Waals (vdW) interactions between the NP and the membrane. Typically the vdW attractions will become important for a separation distance d_g of one to few nanometers and may counter the electrostatic repulsions in cases the repulsion act over such length scales (i.e., when the salt concentration is large and $d_{g,c}$ is only a few nanometers). On the other hand, the typical length of R-L complexes (10-40 nm) would imply that the NP would rarely be at such a proximity of the NP where the vdW effect may be important. Hence we neglect consequence of the vdW forces. The model also considers a simplified 1-D NP and not a more standard spherical NP. While the consideration of a spherical NP would have necessitated consideration of a 2-D EDL distribution, the central idea would have remained the same. For the case of a spherical NP, d_g (and hence $d_{g,c}$) would be determined from the distance of closest approach. Here when $d_g < d_{RL}$, there will be formation of only one or a few RL bonds. However, owing to the large chemical energy gained, even such small number of bonds may be sufficient to trigger the curving of the membrane and hence start the NP internalization process [166].

To summarize, we propose a theory that helps us to design the NP size and the ligand sizes for ensuring the onset of this membrane-NP interaction in the presence of a given

electrostatic environment dictated by the membrane charge density and the surrounding ion concentration. Of course, in actual experiments, the lack of such design information has meant adsorbing positive functional groups on the metal NPs [157] in order to overcome the membrane-NP electrostatic repulsion. The use of such functional groups invariably reduces the flexibility in the types NPs that can be used for a given kind of biological cell. Therefore, we anticipate that the present study will provide an interesting and hitherto unknown design option that will ensure greater flexibility in engineering NPs for applications based on membrane-NP interactions. Furthermore, the general mathematical framework proposed here will be useful in understanding the feasibility of interaction between a plasma membrane and different intracellular and extracellular species.

Chapter 5: Surface charges promote nonspecific nanoparticle adhesion to stiffer membranes

In this chapter we study the problem of NSA and try to understand how the EDL effects the whole process of NSA. EDL actually enhances adhesion and hence can be useful in favoring adhesion on stiffer membranes. Membrane stiffening can happen due to various reasons like cholestoric effects and other physiological conditions.[1]

5.1 Introduction

Nonspecific adhesion (NSA) of nanoparticles (NPs) to plasma membranes (PMs) refer to the physical attachment of the NPs to the PMs without involving specific receptor-ligand (R-L) interactions [172, 173]. Probing such NSA is important for understanding the NP-induced cytotoxicity [175–177, 202] (which, in turn, helps to engineer non-toxic and bio-compatible NPs [178, 179], anti-microbial NPs for biomedical and environmental applications [180, 181], and NPs for killing cancer cells [175, 176, 182]), NP-mediated regulation of cell proliferation [175, 176, 183] and protein expression [175, 184], fabrication of biomimetic NPs by non-specific interactions between bio-membrane and NPs [185–187], and many more. Unlike the extensive studies exploring the different theoretical facets of

[1] Contents of this chapter have been published as: *S. Sinha, H. Jing, H. S. Sachar, and S. Das, Applied Physics Letters, 112, 163702 (2018)*

the R-L-interaction mediated specific NP-membrane adhesion (see the theoretical papers cited in the review article by Zhang et al. [188]), relatively less theoretical effort has been devoted to understand the theory concerning the NSA of NPs [189].

The most obvious starting point for modelling the NSA of NPs would be the thermodynamic framework that specifies the effects that provide the necessary energy for bending the membrane on account of the NSA [see Fig. 1(a)]. For the specific adhesion, the large gain in the chemical energy on account of the formation of the R-L bond as well as the entropic energy change associated with the mixing of the receptors in the deformed part of the membrane has been identified to provide the energy for bending the membrane overcoming the bending stiffness [190]. Therefore, NP adhesion to a membrane is possible only when there is some mechanism to cause a finite membrane deformation overcoming the membrane stiffness. For the NP NSA, as we propose here, this drive for overcoming the membrane stiffness is provided by the change in wetting energy associated with the physical attachment of the NP to the membrane surface [see Fig. 1(b)]. Of course, this picture is valid for the case when one disregards the effect of the membrane surface charge and the electric double layer (or EDL) that is induced (on both sides of the membrane) by this surface charge. A NP approaching the membrane from the extracellular side and attaching non-specifically to the membrane would destroy both the EDL as well as the membrane surface charge at the location where the NP attaches. As a consequence, *there will be a decrease in the net electrostatic energy of the system, which in turn would provide the energy for the NSA of the NP to a much stiffer membrane [see Fig. 1(c,d)]. This is the central finding of this chapter.* Our analysis identifies a critical dimensionless bending modulus $\tilde{\kappa}$ of the membrane. $\tilde{\kappa}$ characterizes the maximum value of the stiffness of a membrane to which NP NSA adhesion becomes possible. This maximum value is

larger than the maximum value of the stiffness of a membrane to which NP NSA adhesion might occur without the surface charge effects – hence surface charges promote adhesion to $stiffer$ membranes. Of course, in presence of surface charges adhesion will also occur to any membrane with dimensionless bending modulus $\tilde{\kappa}'$ ($\tilde{\kappa}' < \tilde{\kappa}$), but for that case the membrane deformation will be more. We anticipate that our finding will be pivotal in regulating delivery of drugs and other chemical entities to cells that have stiffer membranes owing to certain pathological or physiological conditions [191], fabricating biomimetic NPs with NPs encapsulated in cholesterol-rich lipid bilayers [192], using NPs as sensors for quantifying the rigidity of stiff membranes, etc.

5.2 Free energy formulation

Here we consider the free energy change associated with the triggering of the NSA, regardless of the manner (spontaneous or field-driven) in which the NP approaches and attaches to the membrane. The free energy change may be expressed as:

$$\Delta U = \Delta U_{surf} + \Delta U_{bend} + \Delta U_{ent} + \Delta U_{elec}, \tag{5.1}$$

where ΔU_{surf} is the change in surface energy associated with the physical attachment of the NP with the membrane, ΔU_{bend} is the increase in the bending energy associated with the deformation of the membrane caused by the physical attachment of the NP to the membrane, ΔU_{ent} is the free energy change associated with the entropy of mixing of the membrane-bound receptors on the membrane surface i.e., outside the zone of adhesion but within the wrapping zone, and ΔU_{elec} is the change in the electrostatic energy caused by the destruction of the EDL at the adhesion zone caused by the physical attachment of the NP to the membrane surface.

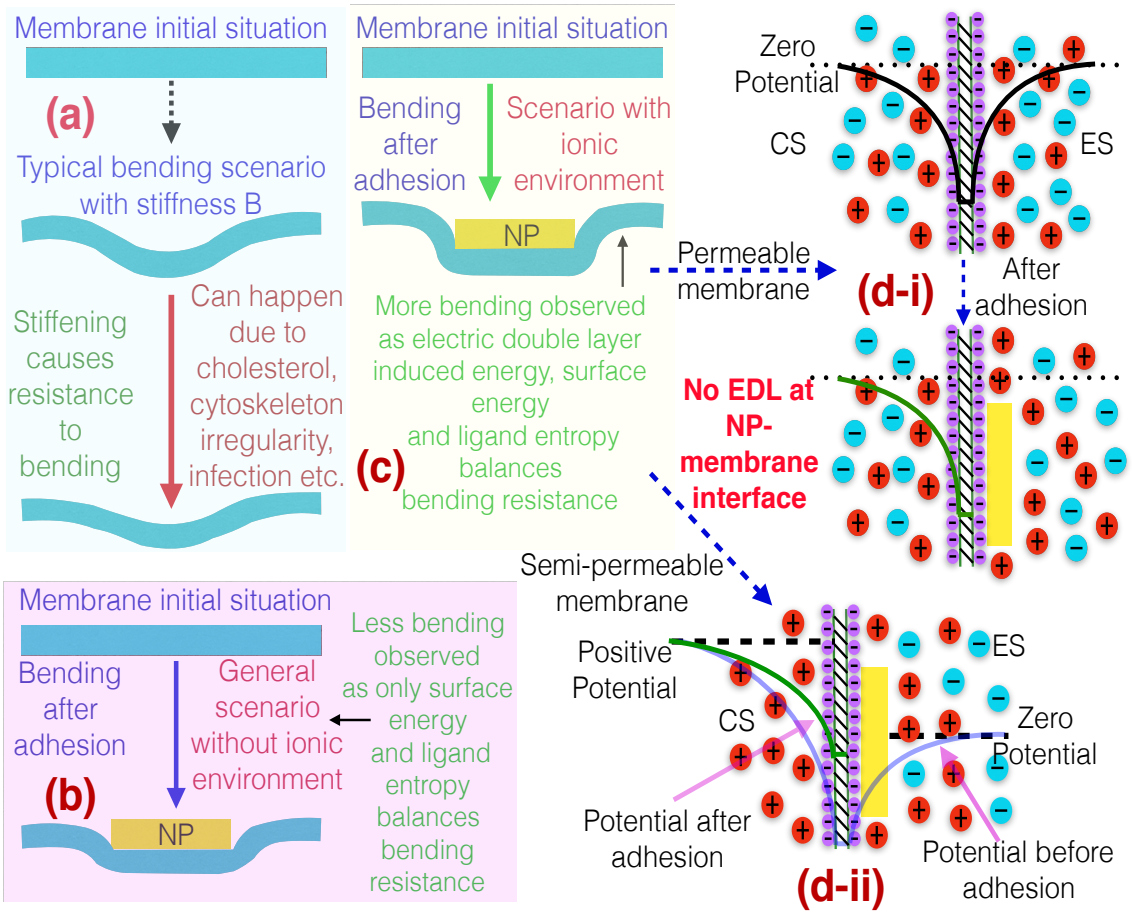

Figure 5.1: Schematic depicting the surface charge mediated NSA of NPs to stiffer membranes. (a) Description of the bending and the role of the bending modulus B. (b) NP NSA without electrostatic effects – absence of any ionic condition will lead to the NP NSA and hence bending of a less PM. (c)) NP NSA in presence of the electrostatic effects (i.e., membrane surface charges and the resulting EDL) – presence of the ionic condition will lead to the NP NSA and hence bending of a much stiffer PM. (d-i) NSA of the NP to the fully-permeable plasma membrane – ion and ψ distribution before (see top of d-i) and after (see bottom of d-i) the NP adhesion. (d-ii) NSA of the NP to the semi-permeable plasma membrane and the ion and ψ distribution before and after the adhesion.

5.2.1 Calculation of ΔU_{surf}

The change in the surface energy due to the physical attachment of the NP to the membrane is the total surface energy after adhesion ($U_{surf,final}$) minus the total surface energy before adhesion ($U_{surf,init}$). Obviously,

$$U_{surf,init} = A\gamma_{ml} + A_{np}\gamma_{nl}, \tag{5.2}$$

and

$$U_{surf,final} = (A - A_b)\,\gamma_{ml} + \left(A_{np} - A_b\right)\gamma_{nl} + A_b\gamma_{mn}, \tag{5.3}$$

yielding

$$\Delta U_{surf} = U_{surf,final} - U_{surf,init} = A_b\left(\gamma_{mn} - \gamma_{ml} - \gamma_{nl}\right). \tag{5.4}$$

In the above equations, $A = A_b + A_+$ is the total membrane area that is affected, A_b is the area for the zone of adhesion, A_{np} is the NP surface area and γ_{ij} is the surface tension between components i and j (here $m : membrane$, $n : NP$, $l : liquid$)

5.2.2 Calculation of ΔU_{bend}

ΔU_{bend} denotes the increase in the bending energy associated with the bending of the membrane caused by the attachment of the NP to the membrane. Following Yuan and Zhang [190], we can write:

$$\Delta U_{bend} = \frac{2B}{R^2}A_b = \left(\frac{2BA_0}{k_BTR^2}\right)\left(\frac{A_b}{A_0}\right) = \tilde{\kappa}\left(\frac{A_b}{A_0}\right)(k_BT), \tag{5.5}$$

where k_BT is the thermal energy, A_0 is the cross sectional area of the receptor ($\sqrt{A_0}$ serves as the characteristic length scale of the problem), B is the bending modulus of the membrane, and R is the characteristic length scale of the NP.

5.2.3 Calculation of ΔU_{ent}

The change in the entropic energy during the NSA process is due to the mixing of the membrane-bound receptors in the zone outside the zone of adhesion but in the wrapping zone. Area of this zone is $A_+ = A - A_b$ and the number of receptors in this zone is $n - n_b$ (where n is the total number of membrane-bound receptors in area A and n_b is the total number receptors in the NSA zone). Under this condition:

$$\frac{\Delta U_{ent}}{k_B T} = (n - n_b)\left[\ln\left(\frac{A_0\,(n - n_b)}{A - A_b}\right)\right] + \frac{A - A_b - A_0(n - n_b)}{A_0}\left[\ln\left(\frac{A - A_b - A_0(n - n_b)}{A - A_b}\right)\right] \tag{5.6}$$

5.2.4 Calculation of ΔU_{EDL}

We can write:

$$\begin{aligned} \Delta U_{elec} &= U_{elec,fin} - U_{elec,init} = \left[A_b W_{elec,2} + (A - A_b)\, W_{elec,1}\right] - A W_{elec,1} \\ &= A_b \left(W_{elec,2} - W_{elec,1}\right) = A_b \Delta W_{elec}, \end{aligned} \tag{5.7}$$

where $W_{elec,1}$ is the electrostatic wetting tension associated with the EDL formed at the membrane (i.e., EDLs formed on either sides of the membrane) without the NP and $W_{elec,2}$ is the electrostatic wetting tension associated with the EDL formed at the membrane wrapped with the NP (i.e., the EDL is formed only in the cytosol side).

Calculation of $W_{elec,1}$:

In order to calculate $W_{elec,1}$ we first need to obtain the EDL profile at the NP-free mem-

brane. This is obtained by minimizing the following free energy functional:

$$F_1 = \int \left[\int_{-d_c-d_m}^{-d_m} f_{c1} dy + \int_{-d_m}^{d_m} f_{m1} dy + \int_{d_m}^{d_e+d_m} f_{e1} dy \right] d^2\mathbf{r} + \int \left[\sigma_{m-c} \psi_{s1,m-c} + \sigma_{m-e} \psi_{s1,m-e} \right] d^2\mathbf{r}. \quad (5.8)$$

In the above equation, f_{c1}, f_{m1}, and f_{e1} are the electrostatic energy densities inside the cell, inside the membrane, and inside the electrolyte outside the membrane, and they can be expressed as:

$$\begin{aligned} f_{c1} &= -\frac{\epsilon_0 \epsilon_c}{2} \left| \frac{d\psi}{dy} \right|^2 + e\psi \left(n_{A^+} - n_{B^-} \right) \\ &+ k_B T \left[n_{A^+} \left(\ln \left(\frac{n_{A^+}}{n_{A^+,\infty}} \right) - 1 \right) + n_{B^-} \left(\ln \left(\frac{n_{B^-}}{n_{B^-,\infty}} \right) - 1 \right) \right] \end{aligned} \quad (5.9)$$

$$f_{m1} = -\frac{\epsilon_0 \epsilon_m}{2} \left| \frac{d\psi}{dy} \right|^2, \quad (5.10)$$

$$\begin{aligned} f_{e1} &= -\frac{\epsilon_0 \epsilon_e}{2} \left| \frac{d\psi}{dy} \right|^2 + e\psi \left(n_{A^+} - n_{B^-} \right) \\ &+ k_B T \left[n_{A^+} \left(\ln \left(\frac{n_{A^+}}{n_{A^+,\infty}} \right) - 1 \right) + n_{B^-} \left(\ln \left(\frac{n_{B^-}}{n_{B^-,\infty}} \right) - 1 \right) \right]. \end{aligned} \quad (5.11)$$

Finally, $\sigma_{m-c} = \sigma$ is the charge density at the membrane-cytosol interface (caused by the charge on the lipid-head of the lipid layer), $\sigma_{m-e} = \sigma$ is the charge density at the membrane-electrolyte interface (caused by the charge on the lipid-head of the other lipid layer), and $\psi_{s1,m-c}$ and $\psi_{s1,m-e}$ are the electrostatic potentials at the membrane-cytosol and membrane-electrolyte interfaces, respectively.

Eq. (5.8) is based on the assumption that the membrane is permeable (in the cytosol side) only to negative ions, while there is salt on the electrolyte side of the membrane. Eq. (5.8) can be minimized with respect to ψ, n_{A^+}, and n_{B^-} yielding the equilibrium conditions as (in presence of the conditions: $n_{A^+,\infty} = n_\infty$, $n_{B^-,\infty} = n_\infty$)

$$\begin{aligned}
\frac{d^2\psi}{dy^2} &= \frac{e}{\epsilon_0\epsilon_c}\left[n_{A^+} - n_{B^-}\right] \quad -(d_m + d_c) \le y \le -d_m, \\
\frac{d^2\psi}{dy^2} &= 0 \qquad\qquad -d_m \le y \le d_m, \\
\frac{d^2\psi}{dy^2} &= -\frac{e}{\epsilon_0\epsilon_e}\left[n_{A^+} - n_{B^-}\right] \quad d_m \le y \le d_m + d_e.
\end{aligned} \tag{5.12}$$

$$n_{A^+} = n_\infty \exp\left(-\frac{e\psi}{k_B T}\right), \quad n_{B^-} = n_\infty \exp\left(\frac{e\psi}{k_B T}\right) \tag{5.13}$$

Consequently, we may write:

$$\begin{aligned}
\frac{d^2\psi}{dy^2} &= \frac{2n_\infty e}{\epsilon_0\epsilon_c}\sinh\left(\frac{e\psi}{k_B T}\right) \quad -(d_m + d_c) \le y \le -d_m, \\
\frac{d^2\psi}{dy^2} &= 0 \qquad\qquad -d_m \le y \le d_m, \\
\frac{d^2\psi}{dy^2} &= \frac{2n_\infty e}{\epsilon_0\epsilon_e}\sinh\left(\frac{e\psi}{k_B T}\right) \quad d_m \le y \le d_m + d_e.
\end{aligned} \tag{5.14}$$

Further eq.(5.8) can be minimized with respect to $\psi_{s1,m-c}$ and $\psi_{s1,m-e}$ to yield the electrostatic stress jump condition at the membrane-cytosol and membrane-electrolyte interfaces, namely

$$\begin{aligned}
\left(\epsilon_m \frac{d\psi}{dy}\right)_{y=-d_m^+} - \left(\epsilon_c \frac{d\psi_1}{dy}\right)_{y=-d_m^-} &= -\frac{\sigma}{\epsilon_0}, \\
\left(\epsilon_e \frac{d\psi}{dy}\right)_{y=d_m^+} - \left(\epsilon_m \frac{d\psi_2}{dy}\right)_{y=d_m^-} &= -\frac{\sigma}{\epsilon_0},
\end{aligned} \tag{5.15}$$

Eq. (5.14) will be solved in presence of the boundary conditions expressed in eq.(5.15) as

well as those expressed below:

$$\left(\frac{d\psi}{dy}\right)_{y=-(d_m+d_c)} = 0, \quad (\psi)_{y=-d_m^+} = (\psi)_{y=-d_m^-},$$
$$(\psi)_{y=d_m^+} = (\psi)_{y=d_m^+}, \quad \left(\frac{d\psi}{dy}\right)_{y=(d_m+d_e)} = 0. \tag{5.16}$$

In above equations, ϵ_c, ϵ_e, and ϵ_m are the relative permittivities of the liquid within the cell (cytosol), extracellular liquid, and the lipid membrane.

Once the equilibrium EDL potential and ion distribution profiles are obtained, we can compute $W_{EDL,1}$ as:

$$\begin{aligned} W_{elec,1} &= \int_{-d_c-d_m}^{-d_m} f_{c1,eq}dy + \int_{-d_m}^{d_m} f_{m1,eq}dy + \int_{d_m}^{d_e+d_m} f_{e1,eq}dy \\ &+ \sigma_{m-c}\psi_{s1,m-c,eq} + \sigma_{m-e}\psi_{s1,m-e,eq}. \end{aligned} \tag{5.17}$$

Calculation of $W_{elec,2}$:

In order to calculate $W_{elec,2}$ we first need to obtain the EDL profile at the NP-free membrane. This is obtained by minimizing the following free energy functional:

$$F_2 = \int \left[\int_{-d_c-d_m}^{-d_m} f_{c2}dy + \int_{-d_m}^{d_m} f_{m2}dy + \sigma_{m-c}\psi_{s2,m-c} \right] d^2\mathbf{r}. \tag{5.18}$$

In the above equation, f_{c2} and f_{m2} are the electrostatic energy densities inside the cell and inside the membrane; there is no EDL at the NP(metal)-membrane interface. We can express:

$$f_{c2} = -\frac{\epsilon_0\epsilon_c}{2}|\frac{d\psi}{dy}|^2 + e\psi\left(n_{A^+} - n_{B^-}\right) + k_BT\left[n_{A^+}\left(\ln\left(\frac{n_{A^+}}{n_{A^+,\infty}}\right) - 1\right) + n_{B^-}\left(\ln\left(\frac{n_{B^-}}{n_{B^-,\infty}}\right) - 1\right)\right]. \quad (5.19)$$

$$f_{m2} = -\frac{\epsilon_0\epsilon_m}{2}|\frac{d\psi}{dy}|^2, \quad (5.20)$$

Eq. (5.18) can be minimized with respect to ψ and n_{B^-} yielding the equilibrium conditions as (in presence of the conditions: n_∞, $n_{B^-,\infty} = n_\infty$)

$$\begin{aligned} \frac{d^2\psi}{dy^2} &= \frac{e}{\epsilon_0\epsilon_c}\left[n_{A^+} - n_{B^-}\right] \quad -(d_m + d_c) \le y \le -d_m, \\ \frac{d^2\psi}{dy^2} &= 0 \qquad\qquad -d_m \le y \le d_m, \end{aligned} \quad (5.21)$$

$$n_{B^-} = n_\infty \exp\left(\frac{e\psi}{k_BT}\right). \quad (5.22)$$

Consequently, we may write:

$$\begin{aligned} \frac{d^2\psi}{dy^2} &= \frac{2n_\infty e}{\epsilon_0\epsilon_c}\sinh\left(\frac{e\psi}{k_BT}\right) \quad -(d_m + d_c) \le y \le -d_m, \\ \frac{d^2\psi}{dy^2} &= 0 \qquad\qquad -d_m \le y \le d_m. \end{aligned} \quad (5.23)$$

Further eq.(5.18) can be minimized with respect to $\psi_{s2,m-c}$ to yield the electrostatic stress jump condition at the membrane-cytosol interface, namely

$$\left(\epsilon_m\frac{d\psi}{dy}\right)_{y=-d_m^+} - \left(\epsilon_c\frac{d\psi_1}{dy}\right)_{y=-d_m^-} = -\frac{\sigma}{\epsilon_0}. \quad (5.24)$$

Eq. (5.23) will be solved in presence of the boundary conditions expressed in eq.(5.24) as well as those expressed below:

$$\left(\frac{d\psi}{dy}\right)_{y=-(d_m+d_c)} = 0, \quad (\psi)_{y=-d_m^+} = (\psi)_{y=-d_m^-}, \quad \left(\frac{d\psi}{dy}\right)_{y=d_m} = 0. \quad (5.25)$$

Once the equilibrium EDL potential and ion distribution profiles are obtained, we can compute $W_{EDL,2}$ as:

$$W_{elec,2} = \int_{-d_c-d_m}^{-d_m} f_{c2,eq} dy + \int_{-d_m}^{d_m} f_{m2,eq} dy + \sigma_{m-c} \psi_{s2,m-c,eq}. \tag{5.26}$$

Therefore, we can can finally obtain ΔU_{elec} by using eqs.(S16,5.26) in eq.(5.7).

5.2.5 Derivation of the condition for ligand-receptor system in the vicinity of adhesion zone

Considering the expression of ΔU appearing in eq.(3) of the main paper, we can write:

$$\frac{1}{k_B T} \frac{\partial \Delta U}{\partial n_b} = 0 \Rightarrow -\ln\left(\frac{(n-n_b)\,A_0}{A-A_b}\right) + 1 + \ln\left(1 - \frac{(n-n_b)\,A_0}{A-A_b}\right) - 1 = 0$$
$$\Rightarrow \ln\left(\frac{\xi_+}{1-\xi_+}\right) = 0 \Rightarrow \xi_+ = \frac{1}{2}, \tag{5.27}$$

where $\xi_+ = \frac{(n-n_b)A_0}{A-A_b}$ is the dimensionless area associated with the receptors in the area A_+. The condition expressed in eq.(5.27) refers to an equilibrium condition as evident from the second derivative of ΔU with respect to n_b, as elucidated below:

$$\frac{1}{k_B T} \frac{\partial^2 \Delta U}{\partial n_b^2} = \frac{1}{k_B T} \frac{\partial}{\partial \xi_+} \left[-\ln\left(\frac{\xi_+}{1-\xi_+}\right)\right] \frac{\partial \xi_+}{\partial n_b} = -\frac{1}{k_B T} \left[\frac{1}{\xi_+} + \frac{1}{1-\xi_+}\right] \frac{\partial}{\partial n_b} \left[\frac{(n-n_b)A_0}{A-A_b}\right] =$$
$$\frac{1}{k_B T} \left[\frac{1}{\xi_+} + \frac{1}{1-\xi_+}\right] \left(\frac{A_0}{A-A_b}\right) > 0. \tag{5.28}$$

Hence we indeed perform a *minimization*, i.e., establish the condition at equilibrium.

5.2.6 Derivation of the expression for non-dimensional bending stiffness

Considering the expression of ΔU appearing in eq.(3) of the main paper, we can write [using eq.(5.27)]:

$$\begin{aligned}
&\frac{1}{k_BT}\frac{\partial \Delta U}{\partial A_b} = 0 \Rightarrow \frac{n-n_b}{A-A_b} - \frac{1}{A_0}\ln\left[1-\frac{(n-n_b)A_0}{A-A_b}\right] - \frac{1}{A_0} + \frac{1}{A_0}\left[1-\frac{(n-n_b)A_0}{A-A_b}\right] \\
+ &\left[\tilde{\kappa} + \frac{(S+\Delta W_{elec})A_0}{k_BT}\right]\frac{1}{A_0} = 0 \Rightarrow -\frac{1}{A_0}\ln\left[1-\frac{(n-n_b)A_0}{A-A_b}\right] + \left[\tilde{\kappa} + \frac{(S+\Delta W_{elec})A_0}{k_BT}\right]\frac{1}{A_0} = 0 \\
&\Rightarrow -\ln\left(1-\xi_+\right) + \left[\tilde{\kappa} + \frac{(S+\Delta W_{elec})A_0}{k_BT}\right] = 0 \\
&\Rightarrow \tilde{\kappa} = \ln\left(\frac{1}{2}\right) - \frac{A_0\left(S+\Delta W_{elec}\right)}{k_BT}.
\end{aligned} \tag{5.29}$$

The condition expressed in eq.(5.29) refers to an equilibrium condition as evident from the second derivative of ΔU with respect to A_b, as elucidated below [of course, we use the condition of $\tilde{\kappa} + \frac{A_0(S+\Delta W_{elec})}{k_BT} = \ln\left(\frac{1}{2}\right)$]:

$$\begin{aligned}
\frac{1}{k_BT}\frac{\partial^2 \Delta U}{\partial A_b^2} &= \left[-\left(\frac{1}{A_0}\right)\left(\frac{1}{1-\frac{n-n_b}{A-A_b}A_0}\right)\right]\frac{\partial}{\partial A_b}\left[1-\frac{n-n_b}{A-A_b}A_0\right] \\
&= \left(\frac{1}{1-\frac{n-n_b}{A-A_b}A_0}\right)\frac{n-n_b}{\left(A-A_b\right)^2} > 0.
\end{aligned} \tag{5.30}$$

Therefore, here too, we perform a *minimization*, i.e., establish the condition at equilibrium. Using these expression, we can eventually write:

$$\begin{aligned}
\frac{\Delta U}{k_BT} &= \left[\frac{A_0\left(S+\Delta W_{elec}\right)}{k_BT} + \tilde{\kappa}\right]\frac{A_b}{A_0} + (n-n_b)\left[\ln\left(\frac{A_0\left(n-n_b\right)}{A-A_b}\right)\right] \\
&+ \frac{A-A_b-A_0(n-n_b)}{A_0}\left[\ln\left(\frac{A-A_b-A_0(n-n_b)}{A-A_b}\right)\right],
\end{aligned} \tag{5.31}$$

where $S = \gamma_{mn} - \gamma_{ml} - \gamma_{nl}$ is the spreading parameter (with γ_{ij} being the surface tension between components i and j; here $m : membrane$, $n : NP$, $l : liquid$), A_b is the

area of the zone of adhesion, $A = A_b + A_+$ (where A_+ is the area of the zone outside the zone of adhesion but in the wrapping zone), k_BT is the thermal energy, A_0 is the cross sectional area of the receptor ($\sqrt{A_0}$ serves as the characteristic length scale of the problem), $\tilde{\kappa} = \frac{2BA_0}{k_BTR^2}$ (B is the bending modulus of the membrane and R is the characteristic length scale of the NP), $\Delta W_{elec} = \Delta U_{elec}/A_b$ is the per unit area change in the electrostatic energy, n is the total number of membrane-bound receptors in area A and n_b is the total number receptors in the NSA zone. The above equation will be minimized with respect to n_b and A_b. Minimization with respect to n_b yields (see the Supplementary Material for detailed derivation):

$$\xi_+ = \frac{1}{2}, \tag{5.32}$$

where $\xi_+ = \frac{(n-n_b)A_0}{A-A_b}$ is the dimensionless area associated with the receptors in the area A_+. Similarly, the minimization of eq.(5.31) with respect to A_b yields using eq.(5.32) (see the Supplementary Material for detailed derivation):

$$\tilde{\kappa} = \ln\left(\frac{1}{2}\right) - \frac{A_0\left(S + \Delta W_{elec}\right)}{k_BT}. \tag{5.33}$$

Eq.(5.33) is the central equation of this paper relating the dimensionless bending energy of the membrane with the per unit area wetting (S) and electrostatic (ΔW_{elec}) energies. As will be shown below $\Delta W_{elec} < 0$, i.e., there is a decrease in the net per unit area electrostatic free energy on account of the membrane-NP NSA that destroys the EDL formed at the membrane-electrolyte interface. As a consequence, for a given change in the surface energy (i.e., a given S), we witness a larger value of $\tilde{\kappa}$. In other words, from eq.(5.33) we can infer that in presence of the membrane surface charges it is possible to cause adhesion of the NP to a much stiffer plasma membrane. Therefore, we can infer that the membrane surface charges are responsible for the enhancement of the adhesion

behavior.

5.3 Results

The first critical issue is the choice of the spreading parameter S (or the per unit area change of the surface energy) [see eqs.(2,4)] in our model. In the absence of any electrostatic effect, the change in the surface energy (dictated by S) provides the energy for the bending that results from the NSA. Considering $(\tilde{\kappa})_{\Delta W_{elec}=0} = \tilde{\kappa}_0 \sim A_0 S/(k_B T)$, we can have $S \sim 2B/R^2 \sim 40 k_B T/(30\ nm)^2 = 4.56 \times 10^{-6}\ N/m$ (considering the size of the 1-D NP of the order of 30 nm). Considering this value of S, we can obtain the ratio $\tilde{\kappa}/\tilde{\kappa}_0 = (\tilde{\kappa})_{\Delta W_{elec}\neq 0}/\tilde{\kappa}_0$ as a function of the salt concentration and the surface charge density of the plasma membrane [see Fig. 2(c)]. *Results demonstrate $\tilde{\kappa} > \tilde{\kappa}_0$ – therefore, the NP NSA triggered alteration of the electrostatic condition ensures a possibility of the NSA to a significantly stiffer plasma membrane.* It is useful to re-iterate here that $\tilde{\kappa}$ and $\tilde{\kappa}_0$ denote the maximum values of the stiffness of the PM to which NP NSA becomes possible in presence and absence of the surface charge effect consideration. Given that $\tilde{\kappa} > \tilde{\kappa}_0$ (see Fig. 2c later), we can infer that the surface charge effect ensure that the maximum value of the stiffness of the PM to which NP NSA becomes possible increases with the consideration of surface charge effect. This is same as writing that the surface charges promote NSA of NPs to stiffer PMs. This is the central result of this letter. Secondly, for the case with surface charges, adhesion to a membrane with bending modulus less than $\tilde{\kappa}$ will definitely occur and will cause a much larger membrane deformation. In order to calculate $\bar{\psi}$ and ΔW_{elec}, we use the following parameters: $\epsilon_0 = 8.8 \times 10^{-12}\ C/(Vm)$, $\epsilon_e = \epsilon_c = 79.8$, $\epsilon_m = 2$, $d_m = 4\ nm$, $d_c = d_e = 1\ \mu m$ (d_c is the distance between the membrane-cytosol-interface (MCI) and the cytosol centerline and d_e is the distance between the MEI and the cytosol

centerline (see [77])), $k_B = 1.38 \times 10^{-23}\ J/K$, $e = 1.6 \times 10^{-19}\ C$, and $T = 298\ K$

Fig. 2(a) depicts the transverse variation of $\bar{\psi}$ as a function of the salt concentration for both fully-permeable and semi-permeable (nature of semi-permeability has been discussed in the figure caption) membranes. We separately show the $\bar{\psi}$ variations before and after the NP adhesion. NP adhesion destroys the EDL developed in the ES for both the permeable and the semi-permeable membranes. The EDL in the CS remains; however, while for the permeable membrane $\bar{\psi}$ distribution in the CS is identical before and after the NP adhesion, for the semi-permeable membrane it is different before and after the adhesion. The adhesion of the NP at the MEI changes the boundary condition, which in turn changes the $\bar{\psi}$ distribution within the membrane for the semi-permeable case (see the case for $\sigma = -0.1\ e/nm^2$) and thereby affects the $\bar{\psi}$ distribution within the CS. We next use this ψ distribution before and after the NP adhesion to calculate ΔW_{elec} (see the SM for details). Fig. 2(b-i,ii) provide the variation of ΔW_{elec} with c_∞ for different σ values for both permeable and semi-permeable membranes. The formation of the EDL is a spontaneous process. Therefore, the energy associated with the EDL is typically negative [193, 194] and hence its destruction in the ES on the account of the NSA of a metallic NP on the membrane surface would lead to an increase in the energy, i.e., $\Delta W_{EDL} = W_{EDL,final} - W_{EDL,initial} = W_{no\ EDL} - W_{EDL} > 0$. On the other hand, we notice $\Delta W_{elec} < 0$. This stems from the fact that for the ES $(W_{elec})_{ES} = (W_{EDL})_{ES} + \left(W_{surface\ charge}\right)_{MEI}$, where $\left(W_{surface\ charge}\right)_{MEI} = \sigma\psi_{MEI}$ (ψ_{MEI} is the electrostatic potential at the MEI) denotes the energy per unit area associated directly with the presence of charges on the MEI (see the SM for details). $\left(W_{surface\ charge}\right)_{MEI}$ is invariably positive and is different from $(W_{EDL})_{ES}$, which refers to the energy associated with the EDL formed in the ES as a space-charge on the charged MEI. For our chosen set of

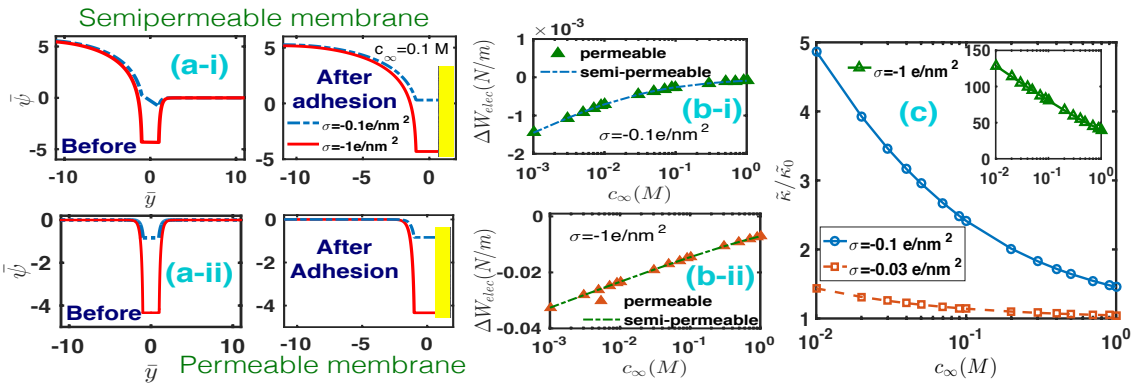

Figure 5.2: Variation of the dimensionless EDL electrostatic potential $\bar{\psi} = e\psi/(k_B T)$ with $\bar{y} = y/d_m$ (d_m is the thickness of the PM) before (left) and after (right) the NP adhesion to (a-i) semi-permeable plasma membrane and (a-ii) fully-permeable plasma membrane. Following the adhesion there is no EDL in the ES for either the permeable or the semi-permeable membrane. In both (a-i) and (a-ii), results are shown for $c_\infty = 0.1\ M$ (the typical physiological salt concentration) and $\sigma = -0.1\ e/nm^2,\ -1\ e/nm^2$ and $n_\infty = 6.023 \times 10^{26} \times c_\infty$ (where n_∞ is in $1/m^3$ and c_∞ is in M). (b) Variation of ΔW_{elec} with c_∞ for both permeable and semi-permeable membranes for (b-i) $\sigma = -0.1\ e/nm^2$ and (b-ii) $\sigma = -1\ e/nm^2$. We witness very little difference in ΔW_{elec} between the cases of permeable and semi-permeable membranes. (c) Variation of $\tilde{\kappa}/\tilde{\kappa}_0$ with c_∞ for different σ for the fully permeable membrane. There is a very little difference in $\tilde{\kappa}/\tilde{\kappa}_0 - vs - c_\infty$ variation between the cases of permeable and semi-permeable membranes. Hence we do not separately show the results $\tilde{\kappa}/\tilde{\kappa}_0 - vs - c_\infty$ variation for the case of semi-permeable membrane. Here the semi-permeable membrane is characterized as a membrane that allows the passage of only positive ions from the electrolyte to the cytosol side..

parameters, $|\left(W_{surface\ charge}\right)_{MEI}| > |\left(W_{EDL}\right)_{ES}|$. The NSA of the NP to the membrane not only destroys the EDL in the ES, but also nullifies the effect of the membrane surface charge at the MEI. Therefore, at the final adhesion state both $\left(W_{surface\ charge}\right)_{MEI} = 0$ and $\left(W_{EDL}\right)_{ES}$ and hence the condition of $|\left(W_{surface\ charge}\right)_{MEI}| > |\left(W_{EDL}\right)_{ES}|$ before the NP NSA ensures $\Delta W_{elec} = \Delta W_{EDL} + \Delta W_{surface\ charge} < 0$. This is true for both the permeable and the semi-permeable membranes, as evident in Figs. 2(b-i,ii).

An increase in the salt concentration (c_∞) reduces the ψ_{MEI} for a constant σ [77,121,195]. This can be justified from the scaling condition $d\psi/dy \propto \sigma \Rightarrow \psi_{MEI} \propto \lambda\sigma$ (with $y \sim \lambda$ and $\psi \sim \psi_{MEI}$ and λ being the EDL thickness) and the fact that $\lambda \sim c_\infty^{-1/2}$. As a consequence $\left(W_{surface\ charge}\right)_{MEI}$ before the NSA is smaller for a larger c_∞, ensuring a smaller $\left(\Delta W_{elec}\right)_{ES}$ for a larger c_∞. This is true for both permeable and semi-permeable membranes [see Fig 2(b-i,ii)]. On the other hand, an increase in σ will obviously increase $\left(W_{surface\ charge}\right)_{MEI} = \sigma\psi_{MEI}$. Moreover ψ_{MEI} also increases with an increase in σ with the increase being more pronounced at smaller c_∞ [77, 121, 195] – as a consequence, one witnesses a nonlinearly large increase in the ΔW_{elec} ratio with an increase in σ [compare Fig 2(b-i) and Fig 2(b-ii)].

The net change in the electrostatic energy (ΔW_{elec}) being negative (regardless of the nature of permeability of the membrane, salt concentration, and σ), it provides the additional energy for inducing the NP-NSA-induced bending of stiffer membranes, as evident from eq.(4). This is confirmed by noting $\tilde{\kappa}/\tilde{\kappa}_0 > 1$ for all values of c_∞ and σ [see Fig. 2(c)]. ΔW_{elec} is larger for a smaller c_∞ [see Fig 2(b-i,ii)]. This justifies why one witnesses a larger $\tilde{\kappa}/\tilde{\kappa}_0$ for a smaller c_∞. Furthermore the nonlinear increase in ΔW_{elec} with σ ensures that $\tilde{\kappa}$ may become almost two-orders of magnitude larger than $\tilde{\kappa}_0$ even for the most standard physiological salt concentration of 0.1 M [see the inset of Fig. 2(c)].

Chapter 6: Surface Charge Mediated Lipid Bilayer coated Nanoparticle Adhesion on Membranes

In this chapter we study the problem of attraction of a lipid bilayer coated NP towards the lipid bilayer. The EDL distribution plays a significant role in this process too. It causes a repulsion between the NP and the bilayer whereas van der Waal's causes attraction. The interplay of these two along with the thermal fluctuations causes the system to have a length scale defined here as a critical length for adhesion to happen. We do not find a zone for NSA here which was present in chapter 4. Thus NSA can be resisted by such coatings on NPs.[1]

Specific receptor-ligand (RL) mediated interactions between ligand-grafted nanoparticles (NPs) and receptor-bearing plasma membranes (PMs) of cells have been the basis of using NPs for targeted drug and gene delivery [196–199], imaging of cellular processes [200], etc. Despite the significant degree of specificity that has been achieved by improving the design of the ligands that are grafted on the NPs [196, 199], it is virtually impossible to avoid some finite extent of nonspecific adhesion (NSA) of the NPs to non-targeted, healthy cells. Such NSA and the subsequent endocytosis of the NPs within the healthy cells often lead to highly detrimental cytotoxicity effects [201, 202]. There-

[1] Contents of this chapter have been published as: *S. Sinha, H.S. Sachar, and S. Das, Electrostatically-motivated design of biomimetic nanoparticles: Promoting specific adhesion and preventing nonspecific adhesion simultaneously, Applied Physics Letters, 112, 243702 (2018)*

fore, there has been a sustained need to develop such ligand-grafted NPs that not only accomplish successful R-L mediated specific adhesion, but also ensure least cytotoxicity following the unavoidable NSA [203, 204].

In this chapter we consider biomimetic NPs (or NPs encapsulated in lipid bilayers derived from the PMs [205, 206]) and show that such NPs may undergo strong-enough electrostatic repulsion from the PMs, such that they will not get closer to the PM beyond a certain critical distance $d_{g,c,1}$ despite the presence of other opposing attractive influences such as the thermal fluctuations and van der Waals (vdW) interactions [207]. In other words, if the NP-PM separation distance d_g is less than $d_{g,c,1}$, the electrostatic repulsion will overcome the attractive influences and drive the NP away from the PM. Presence of a finite $d_{g,c,1}$, therefore, will ensure that the lipid bilayer encapsulated NPs (LBLENPs) will not undergo any NSA. Secondly, these coated NPs should be functionalized by grafting them with ligands [**?**, **?**] such that these ligands may specifically interact with the receptors of the targeted cells at $d_g \gg d_{g,c,1}$ triggering the onset of R-L mediated specific adhesion – the resulting receptor-ligand length (d_{RL}) should therefore be much larger than $d_{g,c,1}$. Hence our letter establishes that for LBLENPs with (a) a finite $d_{g,c,1}$ and (b) $d_{g,c,1} < d_{RL}$, one can indeed ascertain the most elusive condition where the specific adhesion is promoted and the NSA is prevented simultaneously under the physiological conditions (see Fig. 1B), which is never the case for bare-gold NPs (see Fig. 1A and [207]).

6.0.1 Theory

We consider a 1-D gold NP encapsulated within a lipid bilayer of thickness $2d_m$ (see Fig. 1B). The hydrophilic heads of this encapsulating LBL, in contact with the electrolyte solution, contains charges with a charge density σ. We consider the interaction

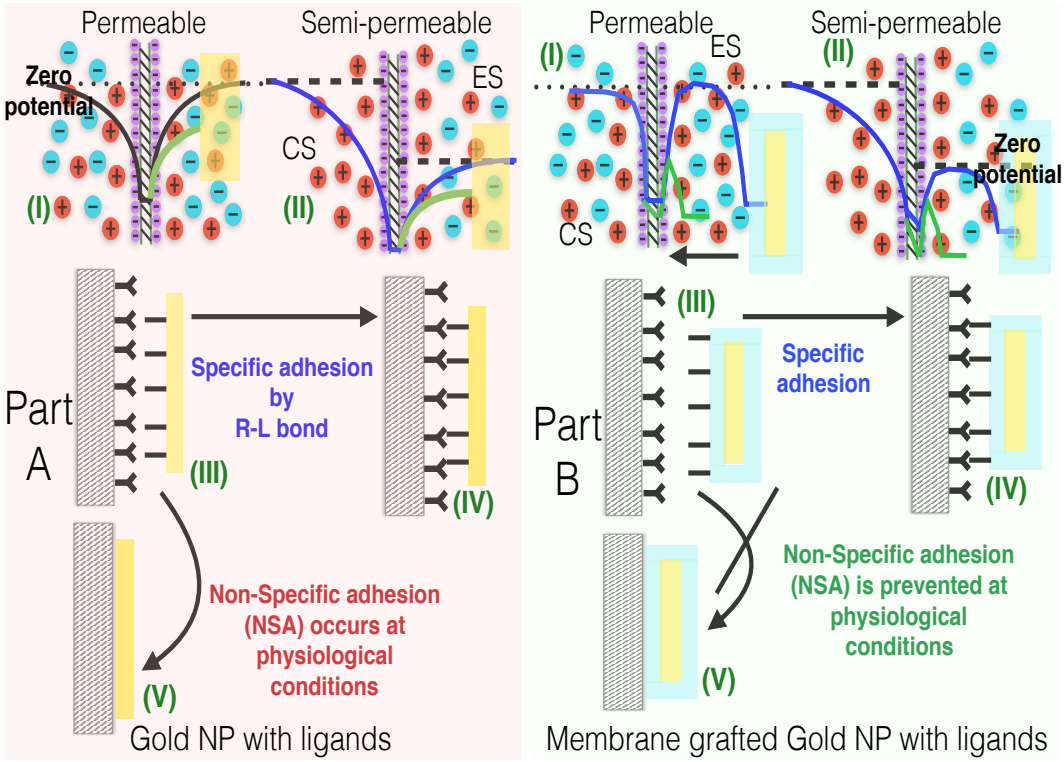

Figure 6.1: **Part A:** Description of the situation when a ligand-grafted bare Gold (Au) NP interacts with the plasma membrane (PM). (I,II) depicts the electrostatic potential (ψ) for the permeable and the semi-permeable membranes, respectively. For both the cases, ψ is shown with and without the NP. (III-IV) describes the typical problem of the *specific adhesion* of the NP to the membrane through the formation of a R-L complex. (V) represents how such bare gold NP will also undergo a NSA to the membrane of a healthy cell under physiological conditions. **Part B:** Description of the situation when a lipid-bilayer encapsulated NP (LBENP) interacts with the PM. The LBLENP bears ligands on the surface of the encapsulating LBL. (I,II) depicts the electrostatic potential (ψ) for the permeable and the semi-permeable membranes, respectively for two different distances of separation between the LBLENP and the PM. (III-IV) describes the typical problem of the *specific adhesion* of the NP to the membrane through the formation of a R-L complex. (V) depicts how under physiological conditions, NSA adhesion between the LBLENP and the PM of a healthy cell is prevented due to the electrostatic effects.

of such LBLENP with the charged PM, with the PM separating the electrolyte and the cytosol. We consider both permeable and semi-permeable PMs. Under these conditions, the equations governing the electrostatic potential ψ in the system can be expressed as:

$$\begin{aligned}
\frac{d^2\psi}{dy^2} &= -\frac{\rho_{e,c}}{\epsilon_0\epsilon_c} \quad for \quad -(d_m + d_c) \leq y \leq -d_m, \\
\frac{d^2\psi}{dy^2} &= 0 \quad for \quad -d_m \leq y \leq d_m, \\
\frac{d^2\psi}{dy^2} &= -\frac{\rho_{e,e}}{\epsilon_0\epsilon_e} \quad for \quad d_m \leq y \leq (d_m + d_g), \\
\frac{d^2\psi}{dy^2} &= 0 \quad for \quad (d_m + d_g) \leq y \leq (3d_m + d_g).
\end{aligned} \tag{6.1}$$

Here $\rho_{e,c}$ and $\rho_{e,e}$ are the EDL charge densities in the ES (electrolyte side) and the CS (cytosol side) of the PM, ϵ_c and ϵ_e are the relative permittivities of the cytosol and the electrolyte, ϵ_0 is the permittivity of free space, $2d_m$ is the membrane thickness, $y = -(d_m + d_c)$ is the location of the cytosol centerline, $y = -d_m$ and $y = +d_m$ are the locations of the membrane-cytosol-interface (MCI) and membrane-electrolyte-interface (MEI) of the PM, and $y = d_m + d_g$ and $y = 3d_m + d_g$ are the locations of the MEI and the membrane-NP interface of the NP. Of course, the NP being that of gold there is no net charge or net electrostatic potential for $3d_m + d_g < y < 3d_m + d_g + d_t$ (d_t is the thickness of the NP). On the other hand, there is indeed an EDL distribution on the side of the NP that is not facing the PM (i.e., $y > 5d_m + d_g + d_t$), but we consider that d_t is large enough to ensure that this partiuclar EDL does not affect the PM-NP interactions. For a PM that is fully permeable to a salt AB, $\rho_{e,c} = \rho_{e,e} = e\left(n_{A^+} - n_{B^-}\right) = 2n_\infty \sinh\left(\frac{e\psi}{k_BT}\right)$ [see eq.(1)]. On the other hand, for a PM that is semi-permeable to a salt AD allowing the passage of only cations (A^+) from the ES to the CS, $\rho_{e,c} = en_{A^+} = en_\infty \exp\left(-\frac{e\psi}{k_BT}\right)$ and $\rho_{e,e} = e(n_{A^+} - n_{D^-}) = 2n_\infty \sinh\left(\frac{e\psi}{k_BT}\right)$ [see eq.(1)]. Here in order to express the ion number density n_i, we always employ the Boltzmann distribution, so that $n_i = n_\infty \exp\left(-\frac{ez_i\psi}{k_BT}\right)$.

Here e is the electronic charge, k_BT is the thermal energy, n_∞ is the bulk ion number density, and z_i is the ion valence (here we always consider $|z_i| = 1$). Once $\rho_{e,c}$ and $\rho_{e,e}$ are known, ψ is obtained by solving eq.(1) in presence of the following boundary conditions (considering zero charge at the metal-NP-membrane interface):

$$\begin{aligned}
&\left(\epsilon_m \frac{d\psi}{dy}\right)_{y=-d_m^+} - \left(\epsilon_c \frac{d\psi}{dy}\right)_{y=-d_m^-} = -\frac{\sigma}{\epsilon_0}, \\
&\left(\epsilon_e \frac{d\psi}{dy}\right)_{y=d_m^+} - \left(\epsilon_m \frac{d\psi}{dy}\right)_{y=d_m^-} = -\frac{\sigma}{\epsilon_0}, \\
&\left(\frac{d\psi}{dy}\right)_{y=-(d_m+d_c)} = 0, \quad (\psi)_{y=-d_m^+} = (\psi)_{y=-d_m^-}, \\
&(\psi)_{y=d_m^+} = (\psi)_{y=d_m^-}, \quad (\psi)_{y=\left(d_m+d_g\right)^+} = (\psi)_{y=\left(d_m+d_g\right)^-}, \\
&\left(\epsilon_m \frac{d\psi}{dy}\right)_{y=\left(d_m+d_g\right)^+} - \left(\epsilon_e \frac{d\psi}{dy}\right)_{y=\left(d_m+d_g\right)^-} = -\frac{\sigma}{\epsilon_0}, \\
&\left(\frac{d\psi}{dy}\right)_{y=-(3d_m+d_g)} = 0.
\end{aligned} \tag{6.2}$$

In eq.(2), ϵ_m is the relative permittivity of the membrane, σ is the surface charge density at the membrane surfaces, i.e., MCI of the PM and the MEIs of the PM and the LBLENP. Once ψ has been obtained numerically, it can be used to obtain the ratio R of the repulsive (electrostatic or E_{elec}) to the attractive (thermal fluctuations or k_BT + vdW or E_{vdW}) influences as a function of PM-LBLENP separation distance d_g (see the supplementary material or SM of [207] for the detailed derivation):

$$R = \frac{E_{elec}}{E_{vdW} + k_BT} = \frac{A_{NP}\int_{d_m}^{d_m+d_g} \Pi dy}{\frac{A_{NP}A_{Ham}}{12\pi d_g^2} + k_BT}, \tag{6.3}$$

where A_{NP} is the cross sectional area of the NP, A_{Ham} is the Hamaker constant and k_BT is the thermal energy. Π is the electrostatic disjoining pressure in the electrolyte (i.e., $d_m \leq y \leq d_m + d_g$) and is expressed as (see the SM of [207] for the detailed derivation):

$$\Pi = -\frac{1}{2}\epsilon_0\epsilon_r \left(\frac{d\psi}{dy}\right)^2 + 2n_\infty k_BT \left[\cosh\left(\frac{e\psi}{k_BT}\right) - 1\right]. \tag{6.4}$$

The disjoining pressure in eq.(4) is space invariant (see the SM of [207]) in the region $d_m \leq y \leq d_m + d_g$, while the contribution of the vdW interaction appearing in R is computed considering "plate-plate"-type interaction between the PM and the LBLENP.

6.1 Results

Fig. 2(a-i,ii) shows the variation of the electrostatic potential distribution($\bar{\psi}$) in the entire system of a LBLENP approaching a PM membrane for the case of a fully-permeable PM. For a larger distance of separation (d_g) between the NP and the PM, the EDLs formed at these two MEIs don't interact with each other enforcing ψ to steeply decrease away from the MEI of both the interfaces leading to $\psi \approx 0$ at the centre of the electrolytic space between the PM and the LBLENP. When d_g is reduced, the two EDLs formed at the two MEIs overlap ensuring a less steeper decay of ψ away from the MEIs leading to a finite non-zero ψ at the centre of the electrolytic space. Such a weak decay of ψ (or equivalently, a small value of $d\psi/dy$) ensures a non-isopotential condition across the PM (i.e., there is a gradient of ψ within the PM) in order to maintain the electrostatic stress boundary condition at the MEI of the PM. Smaller the value of d_g, larger is the extent of the EDL overlap and hence larger is this gradient in ψ across the membrane. At a smaller c_∞ [see Fig. 2(a-ii)], the thickness of the EDLs formed at either of the MEIs is much larger [67, 77, 121] triggering an EDL overlap at a much larger d_g. As a consequence, the isopotential behavior of the PM breaks down at a much larger value of d_g, as compared to the case for a larger c_∞. Analogously, for a weaker c_∞, the steepness of ψ across the PM is much larger. Figs 2(a-i,ii) provide the most remarkable examples where the non-isopotential electrostatics of a fully-permeable PM have been identified. From this ψ distribution, we can employ eqs.(3,4) to compute the ratio R, see

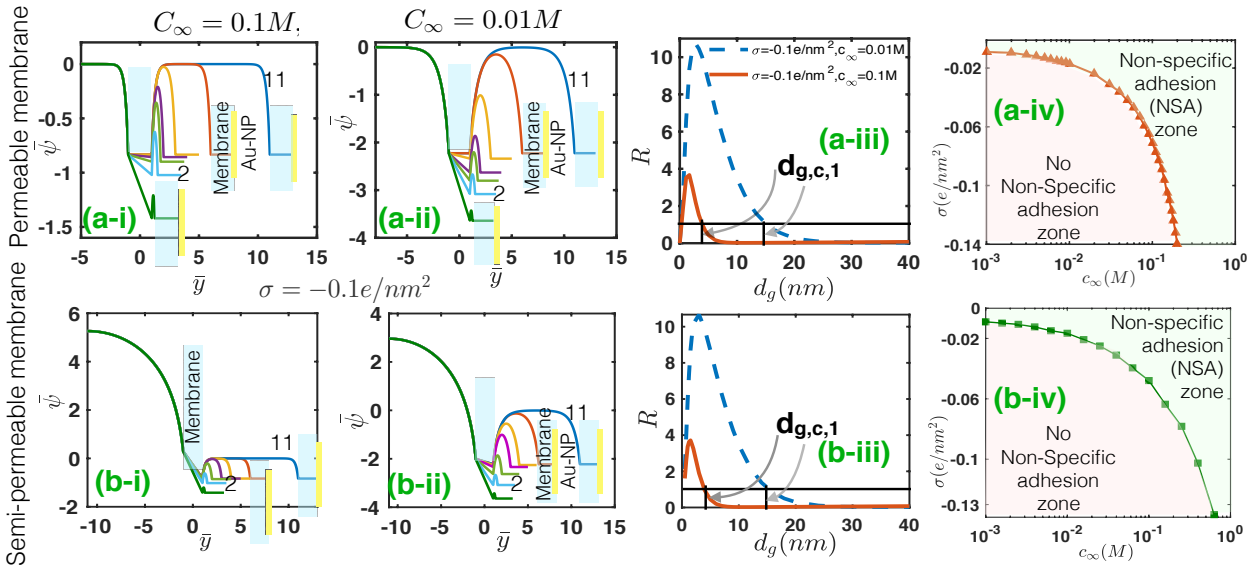

Figure 6.2: **Panel a:** Electrostatic interactions between the LBLENP and a fully-permeable PM. (a-i,ii) Variation of the dimensionless electrostatic potential $[\bar{\psi}]$ with $\bar{y}$ for different distance of separation (d_g/d_m) between PM and LBLENP. d_g is the distance between the MEIs of the PM and the LBLENP. Results are provided for (i) c_∞=0.1 M and (ii) $c_\infty = 0.01\ M$. For both (i) and (ii), we mark values of d_g/d_m (namely $d_g/d_m = 11, 2$) (a-iii) Variation of the dimensionless energy ratio R with d_g for two different values of c_∞. Presence of a finite $d_{g,c,1}$ for (i.e., $c_\infty = 0.1\ M$ and $\sigma = -0.1\ C/m^2$) implies the prevention of NSA at the physiological conditions. For a-i to a-iii, we consider $\sigma = -0.1\ C/m^2$. (a-iv) $\sigma - c_\infty$ phase space for $R = 1$ demarcating the $\sigma - c_\infty$ combinations that prevents or fails to prevent the NSA of the LBLENP to the PM. **Panel b:** Electrostatic interactions between the LBLENP and a semi-permeable PM, permeating only cations from ES to the CS. (b-i,ii) $\bar{\psi}$ with $\bar{y}$ for different values of d_g/d_m for (i) $c_\infty = 0.1\ M$ and $c_\infty = 0.01\ M$. (b-iii) Dimensionless energy ratio R with d_g for two values of c_∞. Presence of a finite $d_{g,c,1}$ for (i.e., $c_\infty = 0.1\ M$ and $\sigma = -0.1\ C/m^2$) implies the prevention of NSA. For b-i to b-iii, we consider $\sigma = -0.1\ C/m^2$. (b-iv) $\sigma - c_\infty$ phase space for $R = 1$. $A_{Ham} = A_{Ham,LBL-LBL} = 5 \times 10^{-21}\ J$ [208].

Fig. 2(a-iii). The non-monotonic variation in R has been reported by us previously [207]. As the LBLENP approaches the PM, the electrostatic repulsion gradually increases and overcomes the thermal fluctuations to ensure a progressive increase in R with a decrease in d_g. Eventually R exceeds unity implying that any further spontaneous (i.e., without any external drive) movement of the LBLENP towards the PM is resisted and the LBLENP will be electrostatically repelled and driven away from the PM. Of course, the very nature of the vdW interaction ensures that R does not vary with d_g monotonically; rather, for a significantly smaller d_g, vdW attraction overcomes the electrostatic repulsion ensuring a decrease in R with a decrease in d_g. Therefore, there can be two possible values of d_g where $R = 1$ – we denote them as $d_{g,c,1}$ and $d_{g,c,2}$ with $d_{g,c,1} \gg d_{g,c,2}$. In our previous paper [207], we have hypothesized that the R-L-mediated specific NP-membrane adhesion is feasible only if $d_{RL} > d_{g,c,1}$. In this paper, we probe if at all the presence of $d_{g,c,1}$ can enable us in designing such NPs that *do not undergo NSA*. NSA is possible only if the NPs can spontaneously approach and attach (i.e., without involving any R-L interactions) to the non-targeted cells. Presence of a finite $d_{g,c,1}$ would imply that the NPs can no longer spontaneously attach (without R-L interactions) to the cells, since electrostatic repulsion would forbid the NPs to come closer to the PM than $d_{g,c,1}$. In our previous paper [207], where we had considered bare-gold NPs, for realistic physiological conditions (i.e., $c_\infty = 0.1\ M$, $\sigma = 0.1\ e/nm^2$), the ratio R [see eq.(3)] was always less than unity and hence we never encountered a finite $d_{g,c,1}$. On the other hand, for the present case, the surface modification of the NPs, i.e., encapsulating them in LBLs, ensure a significantly large negative surface charge on the NP, which in turn enhances the LBLENP-PM electrostatic repulsion and ensures a finite $d_{g,c,1}$ even for the realistic physiological conditions (i.e., $c_\infty = 0.1\ M$, $\sigma = 0.1\ e/nm^2$) [see Fig. 2(a-iii)]. *Hence, we can infer that these LBLENPs,*

even for the most realistic physiological conditions, will support the R-L mediated specific adhesion (as we shall choose such ligands that ensure $d_{RL} > d_{g,c,1}$) and prevent the NSA (due to the very presence of a finite $d_{g,c,1}$), simultaneously. This is the central finding of this paper. Fig. 2(a-iv) provides the $\sigma - c_\infty$ phase-space for $R = 1$ for the fully-permeable PM, clearly identifying the $\sigma - c_\infty$ combinations that prevent or fails to prevent the NSA.

In Fig. 2(b-i) to 2(b-iv), we study the LBLENP-PM interactions for a semi-permeable PM. Very similar qualitative behavior is witnessed for the variation of ψ as a function of the PM-LBLENP separation distance d_g [see Fig. 2(b-i,ii)], namely (a) the EDLs from the two MEIs interact only when d_g is significantly small leading to a weak gradient in ψ, a finite ψ at the electrolyte centerline and a significantly large potential gradient across the membrane and (b) a weaker salt concentration enforces an EDL-EDL interaction over a much larger value of d_g. Fig. 2(b-iii) shows the $R - vs - d_g$ variation pinpointing the corresponding $d_{g,c,1}$, while Fig. 2(b-iv) provides $\sigma - c_\infty$ phase space for $R = 1$ demarcating the conditions that prevents or fails to prevent the NSA. Most intriguingly, we witness that the chosen semi-permeability conditions prevents NSA for even larger values of c_∞ (as large as $c_\infty \approx 0.3\ M$ for $\sigma = -0.1\ C/m^2$) and smaller values of σ (as small as $\sigma \approx -0.06\ C/m^2$ for $c_\infty = 0.1\ M$).

6.2 Discussions

Our theory points to the selection of an optimal combination of the negative charge on the NP (that ensures a finite $d_{g,c,1}$ even for a large physiological salt concentration of hundreds of milimolars) and the length of the engineered ligands (that ensure a d_{RL} which is greater that $d_{g,c,1}$). In the Supplementary Material, [**?**], we tabulate different negatively charged micro-nanocarriers for drug delivery and their approximate surface

charge densities – our theory is useful to test the potential application of simultaneous promotion of specific adhesion and prevention of NSA by all these micro-nanomoeities. In addition, other nanomoeities interacting with the PM through the R-L interactions (e.g., nanoscopic extracellular vesicle interacting with target cell membrane for pore formation and delivery of cargo inside the cell [168]) is also amenable to treatment by our theory.

Finally, the present theory considers a 1-D NP, while most of the existing analysis consider a spherical NP (bare or LBL-coated). Our choice of the 1-D NP is primarily motivated by recent findings that such 1-D NP (often referred to as discoidal NPs) can lead to a more efficient accumulation/internalization within cells and organs as compared to spherical NPs [210, 211]. Moreover, in a recent paper, where we specifically computed the EDL-mediated enhancement of NSA to stiffer membranes [195], we established that very often the model for a 1-D NP is sufficient to provide a gross insight on the interaction of a PM and a spherical NP.

To summarize, the chapter presents an idea on how electrostatics can be used to achieve the most elusive condition desired by all NP-based drug delivery mechanism: simultaneous accomplishment of R-L interaction mediated specific adhesion and prevention of NSA. As a representative example, we consider a biomimetic LBLENP, which is invariably negatively charged stemming from the negative charge density of the encapsulating bilayer derived from the PM [209] – however, we emphasize that the model is generic that can be employed for any negatively charged micro-nanocarrier.

Chapter 7: Future directions and further studies

This thesis significantly contributes towards the understanding of the process of adhesion and the role of EDL in that process. But of course there are numerous systems that get affected by the process of adhesion. This thesis only discusses and focuses on gold NP adhesion adhesions. There are other NP adhesion systems too.

One such system to consider is the system of Silica NPs which are also widely used for drug delivery. Silica is a dielectric substance and hence will support an electrostatic distribution across itself. It will be very different from gold as a metal NP does not support any potential on itself. Study of this silica system and understanding the physics of adhesion is one such very important domain to look into. Particularly there are reports of electroporation of membranes caused by silica NPs. Is there an electrostatic reason behind that? Such questions remain to be understood and can be ventured into using models present in this thesis.

Vesicles are small membrane bound components that enter and exit the cells. One which enters the cells are called extracellular vesicles. That is a system of membrane on membrane adhesion where the core of the vesicle is fluid filled. In the literature, researchers have engineered vesicles and have placed various drugs and commodities inside them. They have used them to deliver various chemicals and entities inside the the cell. Study of such vesicle adhesion can be directly performed using the models present in chapter

6. A fluid filled core has to be considered in all those cases. This added complexity will significantly change the overall electrostatic picture of the process of adhesion.

Intracellular vesicles are bags of vesicles released by the cell itself. They are considered as agents of communication between different cells. There are upcoming studies where they are considered as cancer biomarkers. This thesis strongly establishes the fact that EDL influences adhesion from the ES side. We do not talk about anything that can happen in the CS side. Extracellular vesicles come from the CS side, adhere to the membrane and then get released. Adhesion from the CS side will provide insights to such process.

The process of adhesion mentioned in this thesis restricts itself to only one mechanism of adhesion that is the one that occurs by R-L binding. There are other mechanisms of adhesion too. There are biphasic vesicles which adheres by a very specific kind of adhesion called the necking mechanism. The plasma membrane in those cases forms alternative shapes that causes the system to adhere to its body and then by a chemical mechanism fuses the two membranes together without the R-L bonding. There are other kinds of bonding that happens in those cases.

NPs are widely used for imaging of various tissues. Thus sometimes they have fluorescent proteins on them which can behave in a different fashion that typical R-L type fluorescence. The energy of adhesion process significantly changes there. The R-L binding in thesis leads to a free energy release from the system that favors adhesion. It has been found out that in such cases of specialized fluorescent proteins R-L binding might not be energy favorable but there can be no energy penalty at all. These complex systems have remained beyond the scope of this thesis and we hope to study them in the future.

Bibliography

[1] F. G. Donnan, Chem. Rev. **73**, 1 (1924).

[2] R. Collander, Annu. Rev. Biochem. **6**, 1 (1937).

[3] R. S. Lillie, Biol. Bull. **17**, 188 (1909).

[4] D. A. T. Dick, J. Theor. Biol. **7**, 504 (1964).

[5] D. E. Discher and A. Eisenberg, Science **297**, 967 (2002).

[6] B. E. Sumpio, J. T. Riley, and A. Dardik, Int. J. Biochem. Cell Biol. **34**, 1508 (2002).

[7] R. Roodbeen and J. C. M. van Hest, BioEssays, **31**, 1299 (2009).

[8] P. L. Steponkus, Annu. Rev. Plant Physiol. **35**, 543 (1984).

[9] J. de Jong , R. G. H. Lammertink, and M. Wessling, Lab Chip **6**, 1125 (2006).

[10] F. A. Esteve-Turrillas, A. Pastor, V. Yusa, and M. de la Guardia, Tr. Anal. Chem. **26**, 703 (2007).

[11] R. W. Tsien, Annu. Rev. Physiol. **45**, 341 (1983).

[12] H. Reuter, Annu. Rev. Physiol. **46**, 473 (1984).

[13] W. A. Catterall, Science **242**, 4875 (1988).

[14] F. Sachs, Molecul. Cell Biochem. **104**, 57 (1991).

[15] A. L. Hodgkin and P. Horowicz, J. Physiol. **104**, 148 (127).

[16] G. Scatchard, J. Am. Chem. Soc. **68**, 2315 (1946).

[17] O. I. Vinogradova, L. Bocquet, A. N. Bogdanov, R. Tsekov, and V. Lobaskin, J. Chem. Phys. **136**, 034902 (2012).

[18] P. Mitchell, Science **206**, 48 (1979).

[19] H. J. Knot and M. T. Nelson, J. Physiol. **508**, 199 (1998).

[20] P. Gilon and J. C. Henquin, J. Biol. Chem. **267**, 20713 (1992).

[21] D. R. Green and G. Kroemer, Science **305**, 626 (2004).

[22] J. H. Lakey and M. Ptak, Biochem. **27**, 4639 (1988).

[23] M. L. Fishman and F. R. Eirich, J. Phys. Chem. **75**, 3135 (1971).

[24] M. Elimelech and W. A. Phillip, Science **333**, 712 (2011).

[25] B. E. Logan and M. Elimelech, Nature **313**, 488 (2012).

[26] Q. Li, J. O. Jensen, R. F. Savinell, and N. J. Bjerrum, Prog. Polymer Sci. **34**, 449 (2009).

[27] G. Orive et al., Nat. Med. **9**, 104 (2003).

[28] B. Neumcke and P. Läuger, Biophys. J. **9**, 1160 (1969).

[29] B. Neumcke, D. Walz, P. Läuger, Biophys. J. **10**, 172 (1970).

[30] H. Ohshima and S. Ohki, Biophys. J. **47**, 673 (1985).

[31] B. H. Honig, W. L. Hubbell, and R. F. Flewelling, Ann. Rev. Biophys. Biophy. Chem. **15**, 163 (1986).

[32] S. McLaughlin, Ann. Rev. Biophys. Biophy. Chem. **18**, 113 (1989).

[33] K. E. Forsten, R. E. Kozack, D. A. Lauffenburger, and S. Subramaniam, J. Phys. Chem. **98**, 5580 (1994).

[34] S. R. Maduar and O. I. Vinogradova, J. Chem. Phys. **141**, 074902 (2014).

[35] A. Wasserman and A. R. Felmy, Appl. Env. Microbiol. **64**, 2295 (1998).

[36] S. R. Maduar, V. Lobaskin, and O. I. Vinogradova, Farad. Discus. **166**, 317 (2013).

[37] J. P. Novak, J. Theor. Biol. **185**, 173 (1997).

[38] R. Chein, H. Chen, and C. Liao, J. Mem. Sci. **342**, 121 (2009).

[39] K. Dähnert and D. Huster, J. Colloid Interface Sci. **215**, 131 (1999).

[40] R. Tsekov and O. I. Vinogradova, J. Chem. Phys. **126**, 094901 (2007).

[41] H. Maeda and F. Oosawa, Biophys. Chem. **12**, 215 (1980).

[42] V. Lobaskin, A. N. Bogdanov and O. I. Vinogradova, Soft Matt. **12**, 9428 (2012).

[43] Y. Zhou and G. Stell, J. Chem. Phys. **89**, 7010 (1988).

[44] F. Calabro and P. Zunino, Math. Model. Meth. Appl. Sci. **16**, 479 (2006).

[45] G. Stell and C. G. Joslin, Biophys. J. **50**, 855 (1986).

[46] S-T. Hwang, Kor. J. Chem. Eng. **28**, 1 (2010).

[47] V. S. Vaidyanathan, J. Electroanal. Chem. **6**, 599 (1979).

[48] O. S. Andersen, S. Feldberg, H. Nakadomari, S. Levy, and S. McLaughlin, Biophys. J. **21**, 35 (1978).

[49] V. S. Vaidyanathan, Colloid. Surf. **6**, 291 (1983).

[50] R. M. Peitzsch, M. Eisenberg, K. A. Sharp, and S. McLaughlin, Biophys. J. **68**, 729 (1995).

[51] S. Carnie and S. McLaughlin, Biophys. J. **44**, 325 (1983).

[52] N. S. V. Barbosa, E. R. A. Lima, M. Boström, and F. W. Tavares, J. Phys. Chem. B **119**, 6379 (2015).

[53] D. T. Warshaviak, M. J. Muellner, and M. Chachisvilis, Biochim. Biophys. Acta **1808**, 2608 (2011).

[54] J. Gumbart, F. Khalili-Araghi, M. Sotomayor, and B. Roux, Biochim. Biophys. Acta **1818**, 294 (2012).

[55] J. N. Sachs, P. S. Crozier, and T. B. Woolf, J. Chem. Phys. **121**, 10847 (2004).

[56] A. A. Gurtovenko and I. Vattulainen, J. Chem. Phys. **130**, 215107 (2009).

[57] A. A. Gurtovenko and I. Vattulainen, J. Am. Chem. Soc. **127**, 17570 (2005).

[58] Q. Shi, S. Izvekov, and G. A. Voth, J. Phys. Chem. B **110**, 15045 (2006).

[59] M. Patra, M. Karttunen, M. T. Hyvönen, E. Falck, P. Lindqvist, and I. Vattulainen, Biophys. J. **84**, 3636 (2003).

[60] S. E. Feller, Curr. Opin. Colloid Interface Sci. **5**, 217 (2000).

[61] K. M. Merz, Curr. Opin. Struct. Biol. **7**, 511 (1997).

[62] A. Y. Grosberg, T. T. Nguyen, and B. I. Shklovskii, Rev. Mod. Phys. **74**, 329 (2002).

[63] J. Pittler, W. Bu, D. Vaknin, A. Travesset, D. J. McGillivray, M. Lösche, J. Phys. Cond. Matt. **17**, S2943 (2006).

[64] K. Besteman, M. A. G. Zevenbergen, H. A. Heering, and S. G. Lemay, Phys. Rev. Lett. **93**, 170802 (2004).

[65] Q. Tan, G. Zhao, Y. Qiu, Y. Kan, Z. Ni, and Y. Chen, Langmuir **30**, 10845 (2014).

[66] H. Greberg and R. Kjellander, J. Chem. Phys. **108**, 2940 (1998).

[67] S. R. Maduar and O. I. Vinogradova, J. Chem. Phys. **145**, 164703 (2016).

[68] I. Langmuir, J. Chem. Phys. **6**, 873 (1938).

[69] E. D. Korn, Science **153**, 1491 (1966).

[70] E. D. Korn, J. Gen. Physiol. **52**, 257 (1968).

[71] R. S. Weinstein, New Engl. J. Med. **281**, 86 (1969).

[72] F. A. Vandenheuvel, Adv. Lipid Res. **9**, 161 (1971).

[73] J. M. Besterman and R. B. Low, Biochem. J. **210**, 1 (1983).

[74] N. W. Andrews, P. E. Almeida, and M. Corrotte, Trend. Cell Biol. **24**, 734 (2014).

[75] J. Grove and M. Marsh, J. Cell Biol. **195**, 1071 (2011).

[76] C. A. Lamb, H. C. Dooley and S. A. Tooze, Bioessays **35**, 34 (2012).

[77] S. Sinha, H. Jing, and S. Das, J. Mem. Sci. **533**, 364 (2017).

[78] D. E. Clapham, Cell **80**, 259 (1995).

[79] W. Y. Cheung, Science **207**, 19 (1980).

[80] G. S. B. Williams, L. Boyman, A. C. Chikando, R. J. Khairallah, and W. J. Lederer, Proc. Natl. Acad. Sci. USA **110**, 10479 (2013).

[81] J. H. Lakey and M. Ptak, Biochemistry **27**, 4639 (1988).

[82] M. G. Shapiro, K. Homma, S. Villarreal, C-P. Richter, and F. Bezanilla, Nature Comm. **3**, 736 (2012).

[83] P. Wang, D. Zhou, T. B. Kinraide, X. Luo, L. Li, D. Li, and H. Zhang, Plant Physiol. **148**, 2134 (2008).

[84] P. Wang, T. B. Kinraide, D. Zhou, P. M. Kopittke, and W. J. G. M. Peijnenburg, Plant Physiol. **155**, 808 (2011).

[85] N. Ben-Tal, B. Honig, C. Miller, and S. McLaughlin, Biophys. J. **73**, 1717 (1997).

[86] W. D. Heo, T. Inoue, W. S. Park, M. L. Kim, B. O. Park, T. J. Wandless, and T. Meyer, Science **314**, 1458 (2006).

[87] Z. Guo, H. Peng, J. Kang, and D. Sun, Biomed. Rep. **4**, 528 (2016).

[88] M. Zorkoa and U. Langel, Adv. Drug Delivery Rev. **57**, 529 (2005).

[89] M. L. A. Simon, M. P. Platre, M. M. Marqus-Bueno, L. Armengot, T. Stanislas, V. Bayle, M-C. Caillaud, and Y. Jaillais, Nature Plants **2**, 16089 (2016).

[90] R. R. Arvizo, O. R. Miranda, M. A. Thompson, C. M. Pabelick, R. Bhattacharya, J. D. Robertson, V. M. Rotello, Y. S. Prakash, and P. Mukherjee, Nano Lett. **10**, 2543 (2010).

[91] S. H. Behrens and D.G. Grier, J. Chem. Phys. **115**, 6716 (2001).

[92] L. H. Klausen, T. Fuhs, and M. Dong, Nature Comm. **7**, 12447 (2016).

[93] T. B. Kinraide and P. Wang, J. Exp. Bot. **61**, 2507 (2010).

[94] R. A. Böckmann, A. Hac, T. Heimburg, and H. Grubmüller, Biophys. J. **85**, 1647 (2003).

[95] C. C. Logisz and J. S. Hovis, Biochim. Biophys. Acta **1717**, 104 (2005).

[96] I. Martn, M. Teixid, and E. Giralt, Chembiochem. **12**, 896 (2011).

[97] T. Yamada, T. K. Das Gupta, and C. W. Beattie, Mol. Pharmaceutics, **10**, 3375 (2013).

[98] T. Yamada, S. Signorelli, S. Cannistraro, C. W. Beattie, and A. R. Bizzarri, Mol. Pharmaceutics, **12**, 140 (2015).

[99] H. M. Khan, T. He, E. Fuglebakk, C. Grauffel, B. Yang, M. F. Roberts, A. Gershenson, and N. Reuter, Biophys. J. **110**, 1367 (2016).

[100] B. Yang, M. Pu, H. M. Khan, L. Friedman, N. Reuter, M. F. Roberts, and A. Gershenson, J. Am. Chem. Soc. **137**, 14 (2015).

[101] R. E. Dalby and A. Kuhn, FEMS Microbiol. Rev. **36**, 1023 (2012).

[102] S. A. Pandit, David Bostick, and M. L. Berkowitz, Biophys. J. **85**, 3120 (2003).

[103] E. Chibowsk and A. Szczes, Adhesion **22**, 755 (2016).

[104] W. Choi, J-E. Gu, S-H. Park, S. Kim, J. Bang, K-Y. Baek, B. Park, J. S. Lee, E. P. Chan, and J-H. Lee, ACS Nano **9**, 345 (2015).

[105] C. E. Ashley, E. C. Carnes, G. K. Phillips, D. Padilla, P.

[106] K. S. Butler, P. N. Dufree, C. Theron, C. E. Ashley, E.

[107] J. Liu, A. Stace-Naughton, C. J. Brinker, Chem. Commun.

[108] K. S. Ramamurthi, S. Lecuyer, H. A. Stone, and R. Losick, Science **323**, 1354 (2009).

[109] R. L. Gill Jr., J-P. Castaing, J. Hsin, I. S. Tan, X. Wang, K. C. Huang, F. Tiana, and K. S. Ramamurthi, Proc. Natl. Acad. Sci. USA **112**, E1908 (2015).

[110] L. A. Jaffe and L. C. Schlichter, J Physiol. **358**, 299-319 (1985)

[111] D. H. McCulloh and E. L. Chambers, J. Gen. Physiol., **99**, 137-175 (1991)

[112] S. C.Lee, R. A.Fissore and R. Nuccitell, Developmental Biology, **232**, 127-148 (2001)

[113] E. Neher and A. Marty, Proc. Natl. Acad. Sci. USA **79**, 6712 (1982).

[114] B. Rituper,A. Gucek, J. Jorgacevski, A. Flasker, M. Kreft, and R. Zorec, Nature Protocols **8**, 1169 (2013).

[115] A. F. Oberhauser, l. M. Robinson, and J. M. Fernandez, Biophys. J. **71**, 1131 (1996).

[116] H. B. Zhao and J. Santos-Sacchi, Nature **399** 359 (1999).

[117] F. Rieke and E. A. Schwartz, Neuron **13** 863 (1994).

[118] T. M. Bartoletti, N. Babai, and W. B. Thoreson, J Neurophysiol. **103**, 419 (2010).

[119] A. L. Firth, C. V. Remillard, O. Platoshyn, I. Fantozzi, E. A. Ko, and J. X.-J. Yuan, Pulm. Circ. **1**, 48 (2011).

[120] J. M. Fernandez, F. Bezanilla, and R. E. Taylor, J. Gen. Physiol. **79**, 41 (1982).

[121] S. Sinha, H. Jing, and S. Das, Appl. Phys. Lett. **111**, 063702 (2017).

[122] S. Genet, R. Costalat, and J. Burger, Acta Biotheoretica **48**, 273 (2000).

[123] S. Genet, R. Costalat, and J. Burger, Biophys. J. **81**, 2442 (2001).

[124] J. M. Troiano, L. L. Olenick, T. R. Kuech, E. S. Melby, D. Hu, S. E. Lohse, A. C. Mensch, M. Dogangun, A. M. Vartanian, M. D. Torelli, E. Ehimiaghe, S. R. Walter, L. Fu, C. R. Anderton, Z. Zhu, H. Wang, G. Orr, C. J. Murphy, R. J. Hamers, J. A. Pedersen, and F. M. Geiger, J. Phys. Chem. C, **119**, 534-536 (2015).

[125] H. Wang, J. Drazenovic, Z. Luo, J. Zhang, H. Zhou, and S. L. Wunder, RSC Adv., **2**, 11336-11348 (2012).

[126] A. Negoda, K-J. Kim, E. D. Crandall, and R. M.Worden, Biochim. Biophys. Acta, **1828**, 2215-2222 (2013).

[127] E. Blanco, H. Shen, and M. Ferrari, Nat. Biotech. **33**, 941 (2015).

[128] T. Sun, Y. S. Zhang, B. Pang, D. C. Hyun, M. Yang, and Y. Xia, Angew. Chem. **53**, 12320 (2014).

[129] K. Ulbrich, K. Hola, V. Subr, A. Bakandritsos, J.Tucek, and R. Zboril, Chem. Rev. **116**, 5338 (2016).

[130] R. Singh and J. W. Lillard, Jr., Exp. Mol. Pathol. **86**, 215 (2009).

[131] D. F. Emerich and C. G. Thanos, J. Drug Target. **15**, 163 (2007).

[132] S. K. Nune, P. Gunda, P. K Thallapally, Y-Y. Lin, M. L. Forrest, and C. J Berkland, Expert Opin. Drug Deliver. **6**, 1175 (2009).

[133] N. Erathodiyil and J. Y. Ying, Acc. Chem. Res. **44**, 925 (2011).

[134] S. T. Selvan, T. T. Tan, D. K. Yi, and N. R. Jana, Langmuir **26**, 11631 (2010).

[135] B. Korzeniowska, R. Nooney, D. Wencel, C. McDonagh, Nanotech. **24**, 442002 (2013).

[136] D. K. Chatterjee, P. Diagaradjane, and S. Krishnan, Ther, Deliv. **2**, 1001 (2011).

[137] P. Kaur, M. L. Aliru, A. S. Chadha, A. Asea, and S. Krishnan, Int. J. Hyperthermia **32**, 76 (2016).

[138] R. Ivkov, Int. J. Hyperthermia **29**, 703 (2013).

[139] K. Niikura, K. Nagakawa, N. Ohtake, T. Suzuki, Y. Matsuo, H. Sawa, and K, Ijiro, Bioconjugate Chem. **20**, 1848 (2009).

[140] S. Zhang, J. Li, G. Lykotrafitis, G. Bao, and S. Suresh, Adv. Mater. **21**, 419 (2009).

[141] H. Yuan and S. Zhang, Appl. Phys. Lett. **96**, 033704 (2010).

[142] H. Yuan, C. Huang, and S. Zhang, Plos One **5**, e13495 (2010).

[143] H. Yuan, J. Li, G. Bao, and S. Zhang, Phys. Rev. Lett. **105**, 138101 (2010).

[144] C. Huang, P. J. Butler, S. Tong, H. S. Muddana, G. Bao, and S. Zhang, Nano Lett. **13**, 1611 (2013).

[145] S. Zhang, H. Gao, and G. Bao, ACS Nano **9**, 8655 (2015).

[146] C. Huang, Y. Zhang, H. Yuan, H. Gao, and S. Zhang, Nano Lett. **13**, 4546 (2013).

[147] H. Zhang, Q. Ji, C. Huang, S. Zhang, B. Yuan, K. Yang, Y-Q. Ma, Sci. Rep. **5**, 10525 (2015).

[148] V. V. Ginzburg and S. Balijepalli, Nano Lett. **7**, 3716 (2007).

[149] M. Deserno and W. M. Gelbart, J. Phys. Chem. B **7**, 3716 (2007).

[150] M. Deserno, Phys. Rev. E **69**, 031903 (2004).

[151] J. Agudo-Canalejo and R. Lipowsky, Nano Lett. **15**, 7168 (2015).

[152] A. H. Bahrami, M. Raatz, J. Agudo-Canalejo, R. Michel, E. M. Curtis, C. K. Hall, M. Gradzielski, R. Lipowsky, T. R. Weik, Adv. Colloid Interface Sci. **208**, 214 (2014).

[153] J. Agudo-Canalejo and R. Lipowsky, ACS Nano **9**, 3704 (2015).

[154] A. H. Bahrami, R. Lipowsky and T. R. Weikl, Soft Matt. **12**, 581 (2016).

[155] Xin Yi and H. Gao, Nanoscale **9**, 454 (2017).

[156] R. R. Arvizo, O. R. Miranda, M. A. Thompson, C. M. Pabelick, R. Bhattacharya, J. D. Robertson, V. M. Rotello, Y. S. Prakash, and P. Mukherjee, Nano Lett. **10**, 2543 (2010).

[157] E. C. Cho, J. W. Xie, P. A. Wurm, Y. N. Xia, Nano Lett. **9**, 1080 (2009).

[158] A. Verma and F. Stellacci, Small **6**, 12 (2010).

[159] E. A. L. Biessen, H. F. Bakkeren, D. M. Beuting, J. Kuiper, and T. J. C. van Berkel, Biochem. J. **299**, 291 (1994).

[160] K. Köhler, S. Xiong, J. Brzostek, M. Mehrabi, P. Eissmann, A. Harrison, S-P. Cordoba, S. Oddos, V. Miloserdov, K. Gould, N. J. Burroughs, P. A. van der Merwe, and D. M. Davis, Plos One **5**, e15374 (2010).

[161] P. H. Yang, X. Sun, J. F. Chiu, H. Sun, and Q. Y. He, Bioconjugate Chem. **16**, 494 (2005).

[162] J. F. Allard, O. Dushek, D. Coombs, and P. A. van der Merwe, Biophys. J. **102**, 1265 (2012).

[163] M. L. Dustin and J. A. Cooper, Nat. Immunol. **1**, 23 (2000).

[164] S. Amara, M. T. Ivy, E. L. Myles, and V. Tiriveedhi, Cell Immunol. **302**, 1 (2016).

[165] I. Dobrzynska, E. Skrzydlewska, and Z. A. Figaszewski, J. Membr. Biol. **246**, 161 (2013).

[166] A. Lundgren, B. Agnarsson, R. Zirbs, V. P. Zhdanov, E. Reimhult, and F. Höök, ACS Nano **10**, 9974 (2016).

[167] C. Thery, L. Zitvogel, and S. Amigorena, Nature Rev. Immunol. **2**, 569 (2002).

[168] I. Prada and J. Meldolesi, Int. J. Mol. Sci. **17**, 1296 (2016).

[169] S. Batzri and E. D. Korn, J. Cell. Biol. **66**, 621 (1975).

[170] B. Westermann, Curr. Opin. Cell Biol. **35**, 1 (2015).

[171] M. Lebiedzinska, G. Szabadkai, A. W. Jones, J. Duszynski, and M. R. Wieckowski, Int. J. Biochem. Cell Biol. **41**, 1805 (2009).

[172] K. L. Chen and G. D. Bothun, Environ. Sci. Technol. **48**, 873 (2014).

[173] M. I. Setyawati, C. Y. Tay, D. Docter, R. H. Stauber and D. T. Leong, Chem. Soc. Rev. **44**, 8174 (2015).

[174] N. Lewinski, V. Colvin, and R. Drezek, Small **4**, 26 (2008).

[175] Z. Liu, Y. Wu, Z. Guo, Y. Liu, Y. Shen, P. Zhou, and X. Lu, Plos One **9**, e99175 (2014).

[176] M. Yin, Y. Yin, Y. Han, H. Dai, and S. Li, J. Nanomater. *doi* : 10.1155/2014/731897 (2014).

[177] R. de Lima, A. B. Seabra, and N. Duran, J. Appl. Toxicol. **32**, 867 (2012).

[178] S. Naahidi, M. Jafari, F. Edalat, K. Raymond, A. Khademhosseini, P. Chen, J. Control. Rel. **166**, 182 (2013).

[179] F. Tang, L. Li, and D. Chen, Adv. Mater. **24**, 1504 (2012).

[180] M. Rai, A. Yadav, and A. Gade, Biotechnol. Adv. **27**, 76 (2009).

[181] C. Marambio-Jones and E. M. V. Hoek, J. Nanoparticle Res. **12**, 1531 (2010).

[182] J. W. Rasmussen, E. Martinez, P. Louka, and D. G. Wingett, Expert Opin. Drug Del. **7**, 1063 (2010).

[183] Y. Yue, R. Behra, L. Sigg, and K. Schirmer, Nanotoxicology **10**, 1075 (2016).

[184] B. Ghosh, A. Singh, M. Li, A. V. Vlassov, C. Burnett, N. Puri, and K. Roy, Oligonucleotides **20**, 163 (2010).

[185] O. C. Farokhzad, Nature **526**, 47 (2015).

[186] A. M. Carmona-Ribeiro, Int. J. Nanomedicine **5**, 249 (2010).

[187] Y. Gong and F. M. Winnik, Nanoscale **4**, 360 (2012).

[188] S. Zhang, H. Gao, and G. Bao, ACS Nano **9**, 8655 (2015).

[189] A. Xu, M. Yao, G. Xu, J. Ying, W. Ma, B. Li, and Y. Jin, Int. J. Nanomedicine **7**, 3547 (2012).

[190] H. Yuan and S. Zhang, Appl. Phys. Lett. **96**, 033704 (2010).

[191] L. Lai, X. Xu, C. T. Lim, and J. Cao, Biophys. J. **109**, 2287 (2015).

[192] K. M. McMahon, L. Foit, N. L. Angeloni, F. J. Gilesx, L. I. Gordony, and C. S. Thaxton, Cancer Treat Res. **166**, 129 (2015).

[193] H. Jing, S. Sinha, and S. Das, Soft Matt. **13**, 553 (2017).

[194] S. Sinha, K. I. Bae, and S. Das, Colloid. Surf. A **489**, 216 (2016).

[195] S. Sinha, H. Jing, H. S. Sachar, and S. Das, Appl. Phys. Lett. **111**, 263702 (2017).

[196] M. Srinivasarao and P. S. Low, Chem. Rev. **117**, 12133 (2017).

[197] L. M. Bareford and P. W. Swaan, Adv. Drug. Deliver. Rev. **59**, 748 (2007).

[198] P-W. Cheng, Human Gene Ther. **7**, 275 (2008).

[199] R. A. Petros and J. M. DeSimone, Nature Rev. Drug Discov. **9**, 615 (2010).

[200] K. T. Thurn et al., Nanoscale Res Lett. **2**, 430 (2007).

[201] C. Kirchner et al., Nano Lett. **5**, 331 (2005).

[202] N. Lewinski, V. Colvin, and R. Drezek, Small **4**, 26 (2008).

[203] R.Shukla, V. Bansal, M. Chaudhary, A. Basu, R. R. Bhonde, and M. Sastry, Langmuir **21**, 10644 (2005).

[204] B. Ankamwar, T. C. Lai, J. H. Huang, R. S. Liu, M. Hsiao, C. H. Chen, and Y. K. Hwu, Nanotechnology **21**, 075102 (2010).

[205] S. C. Balmert and S. R. Little, Adv. Mater. **24**, 3757 (2012).

[206] J. Guo, M. R. Cahill, S. L. McKenna, C. M. O'Driscoll, Biotech. Adv. **32**, 1396 (2014).

[207] S. Sinha, H. Jing, H. S. Sachar, and S. Das, Appl. Phys. Lett. **111**, 263702 (2017).

[208] P. A. Attard, D. J. Mitchell, and B. W. Ninham, Biophys. J. **53**, 457 (1988).

[209] C-M. J. Hu, L. Zhang, S. Aryal, C. Cheung, R. H. Fang, and L. Zhang, Proc. Natl. Acad. Sci. **108**, 10980 (2011).

[210] E. Blanco, H. Shen, and M. Ferrari, Nat. Biotechnol. **33**, 941 (2015).

[211] K. C. L. Black, Y. Wang, H. P. Luehmann, X. Cai, W. Xing, B. Pang, Y. Zhao, C. S. Cutler, L. V. Wang, Y. Liu, and Y. Xia, ACS Nano **8**, 4385 378 (2014).